Western Graduate&PostdoctoralStudies

Western University
Scholarship@Western

Electronic Thesis and Dissertation Repository

January 2020

The role of Heat Shock Protein 90 in the Keap1/Nrf2 Mediated Oxidative-Stress Response

Zheng Song, *The University of Western Ontario*

Supervisor: Choy, James W.Y., *The University of Western Ontario*
Joint Supervisor: Prado, Marco, *The University of Western Ontario*
A thesis submitted in partial fulfillment of the requirements for the Master of Science degree in Biochemistry
© Zheng Song 2020

Follow this and additional works at: https://ir.lib.uwo.ca/etd

Part of the Biochemistry Commons, Biophysics Commons, and the Molecular Biology Commons

Recommended Citation

Song, Zheng, "The role of Heat Shock Protein 90 in the Keap1/Nrf2 Mediated Oxidative-Stress Response" (2020). *Electronic Thesis and Dissertation Repository*. 6761.
https://ir.lib.uwo.ca/etd/6761

This Dissertation/Thesis is brought to you for free and open access by Scholarship@Western. It has been accepted for inclusion in Electronic Thesis and Dissertation Repository by an authorized administrator of Scholarship@Western. For more information, please contact wlswadmin@uwo.ca.

ABSTRACT

Oxidative and proteotoxic stress are common hallmarks of Neurodegenerative diseases (NDs). Cellular proteostasis is maintained through Heat shock protein (Hsp) 90 and Stress-inducible protein 1 (STIP1) modulating the stability of their substrates (clients). Hsp90/heat shock factor (HSF)1 pathway activation attenuates proteotoxicity. Meanwhile, activating the Kelch-like ECH associated protein 1 (Keap1)/ nuclear factor (erythroid-derived 2)-like 2 (Nrf2) pathway combats oxidative stress. Numerous studies attempted to individually manipulate the expression of Hsp90 or Nrf2 to treat NDs.

Novel interactions of Hsp90 with Nrf2 and Keap1 were discovered via yeast-2-hybrid screening (unpublished data). We analyzed their interactions through NMR spectroscopy, ITC, protein-binding assay, Western blotting, and RT-qPCR. We demonstrated that Hsp90 and STIP1 are modulators of both Nrf2 and Keap1's protein stability. Keap1 directly binds with STIP1 and Hsp90. Keap1 interacts Hsp90 via the Kelch domain. Our study revealed potential crosstalk between Keap1/Nrf2 and Hsp90/HSF1 cytoprotective pathways and the possibility of co-modulating them.

Key Words: Neurodegenerative disease, Nrf2, Keap1, Hsp90, HSF1, STIP1, Molecular chaperones, Co-chaperones, Clients, Oxidative Stress, Proteotoxic Stress, NMR spectroscopy

Summary for Lay Audience

This work addresses the biophysical and biological analysis of Nrf2 and Keap1 as client proteins of Hsp90 chaperone machinery, which can provide valuable insights into treatment designs towards neurodegenerative diseases (ND). Heat shock protein (Hsp) 90, one of the most abundant and evolutionary conserved molecular chaperones, modulates protein folding, proteostasis maintenance, and proteotoxicity clearance. Substrate proteins that interact with Hsp90 are called clients. The proper folding and functionality of Hsp90 clients are maintained through the chaperone networks and co-chaperones, such as Stress-inducible protein 1 (STIP1). This network and the clients of Hsp90 are found to play important roles in neurodegenerative diseases. The inhibition of Hsp90 activates the heat shock factor (HSF)1- mediated heat shock response (HSR), which attenuates the harmful aggregated protein Amyloid-β (Aβ) and tau-related toxicity in Alzheimer's disease. Meanwhile, Nuclear Factor Erythroid 2-Related Factor 2 (Nrf2), a master regulator of antioxidative response, combats oxidative stress and the proteotoxicity, such as the neuronal Aβ oligomer toxicity. Numerous studies are devoted to separately manipulating the level of Hsp90 or Nrf2 in treating ND. Here we provide insights into the crosstalk of the Nrf2- and Hsp90-mediated cytoprotective pathways implying the potential in co-modulating their levels.

Novel interactions of Hsp90 with Nrf2 and Kelch-like ECH associated protein 1 (Keap1), the negative regulator of Nrf2, were discovered via yeast-two-hybrid screening by our

collaborator, Dr. Duennawald. Following this result, we analyzed their interactions through NMR spectroscopy, ITC, protein-binding assay, Western blotting, and RT-qPCR. Our findings showed that both Hsp90 and STIP1 interacts with Nrf2 and Keap1. Specifically, Keap1 interacted with Hsp90 via the Kelch domain. In addition, by using the genetically modified mouse models recently developed by Dr. Prado's lab, we investigated the functional consequences of these interactions *in vivo.* Our data indicated that STIP1 plays a critical role in Hsp90's ability to modulate the protein stability of Keap1 and Nrf2. The interactions of Hsp90 with Keap1 and Nrf2 reveal exciting underlying crosstalk in Keap1/Nrf2 and Hsp90/HSF1 cytoprotective pathways and the potential in co-modulating these pathways. Further characterizing their interacting mechanisms and cellular functions may provide valuable insights in treating neurodegenerative diseases.

Co-Authorship Statement

Chapter 2

Section 2.1 Protein overexpression and purification

This section of the chapter contains work from previously established efforts of Anne Brickenden, Andrew Maciejewski, Halema Khan, Marco Antonio Maximo Prado, and James Wing-Yiu Choy. Maciejewski, A., Prado, M. A., and Choy, W. Y. (1)H, (1)(5)N and (1)(3)C backbone resonance assignments of the TPR1 and TPR2A domains of mouse STIP1. Biomol NMR Assign. **7**, 305-310, (2012).

Khan, H., Cino A.E, Brickenden, A., Fan, J., Yang, D. Choy W.Y., Fuzzy Complex Formation between the Intrinsically Disordered Prothymosin α and the Kelch domain of Keap1 involved in the oxidative stress response. JMB 425(6), 1011-1027 (2013).

Section 2.6 Animal Model & Section 2.7 Cell Tissue Culture

This section of the chapter contains unpublished work from Rachel Lackie, Abdul Razzaq, Marco Antonio Maximo Prado, which included generating the WT & △TPR1 mice line and the SN56-WT & SN56-STIP1-KO cell line.

Chapter 3

Section 3.6 Preliminary NMR data on the interaction of Nrf2 with Hsp90β

This section of the chapter contains work from Nadun Chanaka Karunatilleke, which includes providing the purified Nrf2 protein for the NMR spectroscopy experiment.

Acknowledgments

I would like to thank my supervisor Dr. James Wing-Yiu Choy and Dr. Marco Antonio Maximo Prado, for providing me the opportunity to conduct research and complete my master's degree in their laboratories. I sincerely appreciate the continuous support and amazing guidance in the past two years. I am incredibly grateful for the tremendous resource and expertise I received from both supervisors.

I am tremendously thankful for Dr. Martin Duennwald for his support in my project. I would also love to acknowledge my appreciation for the time and suggestions provided by my advisory committee members, Dr. Ilka Heinemann, and Dr. Peter Stahopulos.

I am more than gratified for the help provided by Anne Brickenden and Nadun Chanaka Karunatilleke in the Choy lab, as well as Jue Fan and Sanda Raulic in Prado lab. Thank you for supporting me and teaching me skills throughout my Master's program. I would also like to send my appreciation to Rachel Lackie, Abdul Razzaq, and Vy Ngo for guiding me in my project and providing me materials from their research studies. I am also thankful for all the other members in the Choy lab and Prado lab for providing me help and time whenever they get the chance.

Finally, I would like to thank my family members for supporting me throughout the last two years. All of you are my heroes who help me to accomplish what I have.

Table of Contents

ABSTRACT ii

Summary for Lay Audience iii

Co-Authorship Statement v

Acknowledgments vi

List of Figures x

CHAPTER 1: INTRODUCTION 1

1.1 Neurodegenerative Diseases 1

1.2 Molecular Chaperone 3

1.3 Heat Shock Protein (Hsp) 90 5

1.3.1 Hsp90 Chaperone Mechanism 5

1.3.2 Hsp90/HSF1 - Mediated Heat Shock Response 8

1.4 Co-chaperone Stress-Inducible Phosphoprotein 1 (STIP1) 11

1.4.1 The study of modulation of client stability by Hsp70/Hsp90/STIP1 chaperone machinery 12

1.4.1.1 Homozygous mutant STIP1 mice (△TPR1 mice) 13

1.5 Keap1/Nrf2-Mediated Oxidative Stress Response 16

1.5.1 Nrf2 as a Transcription Factor in the pathway 16

1.5.2 Keap1 as the Major Negative Regulator of Nrf2 19

1.5.3 Keap1/Nrf2 - Mediated Pathway & Neurodegenerative Diseases 23

1.6 Crosstalk Between the Keap1/Nrf2 and Hsp90/HSF1 Cytoprotective Pathways 25

1.7 The Scope of the Thesis 26

CHAPTER 2: MATERIALS&METHODS 28

2.1 Protein overexpression and purification 28

2.1.1 Preparation of recombinant Kelch domain of human Keap1 28

2.1.2 Preparation of recombinant Human Keap1 31

2.1.3 Preparation of recombinant Human Hsp90β 34

2.1.4 Preparation of recombinant Mouse STIP1 37

2.2 Nuclear Magnetic Resonance (NMR) Spectroscopy 40
2.3 Isothermal Titration Calorimetry 40
2.4 Fluorescently labeling proteins 41
2.5 Protein – Binding Assay 42
2.6 Animal Model 45
2.6.1 WT & △TPR1 Mice 45
2.7 Cell tissue culture 45
2.7.1 SN56 Cell Line 45
2.8 Western Blotting 46
2.9 Quantitative Real-Time Polymerase Chain Reaction 47
2.10 Statistical Analysis 48
CHAPTER 3: RESULTS 49
3.1 Preparation of recombinant protein samples 49
3.1.1 The Kelch Domain of Human Keap1 49
3.1.2 Full-length Human Keap1 53
3.1.3 Full-length Human Hsp90β 55
3.1.4 Full-length mouse STIP1 59
3.2 Hsp90β binds the Kelch domain of Keap1 61
3.2.1 NMR titrations show that Hsp90β interact with the Kelch domain of Keap1 61
3.2.2 Hsp90β binds to Kelch domain of Keap1 with a weak affinity 68
3.2.3 Estimation of the binding affinity between Hsp90β and Kelch domain of Keap1 using the protein-binding assay 70
3.3 Keap1 as a potential client of Hsp90β 75
3.3.1 Endogenous Keap1 protein expression showed patterns like Hsp90 client protein levels 75
3.3.2 Endogenous Keap1 requires functional co-chaperone STIP1 to maintain protein stability 78
3.4 Keap1 interacting with both Hsp90β and STIP1 80
3.4.1 Recombinant Human Keap1 interacts to recombinant Human Hsp90β 80

3.4.2 Estimation of the binding affinity between Keap1 and fluorescently labeled STIP1 using the protein-binding assay 82
3.5 Nrf2 as a potential client of Hsp90β 85
3.5.1 Endogenous Nrf2 protein expression showed patterns like Hsp90 client protein levels 85
3.5.2 Endogenous Nrf2 requires functional endogenous co-chaperone STIP1 to maintain protein stability 87
3.6 Preliminary NMR data on the interaction of Nrf2 with Hsp90β 89
CHAPTER 4: DISCUSSION 91
4.1 Keap1 as a client of Hsp90 92
4.1.1 Keap1 interacts with Hsp90 through the Kelch domain 96
4.1.2 Keap1 might bind with Hsp90 through other domains 98
4.2 Nrf2 as a client of Hsp90 99
4.3 STIP1 is critical for modulating Keap1 and Nrf2 protein stability 101
4.4 Significance 103
CHAPTER 5: CONCLUSION 104
5.1 Conclusion 104
5.2 Limitation & Future Directions 105
5.2.1 Molecular mechanism of Keap1-Hsp90 and Nrf2-Hsp90 interaction 105
5.2.2 The role of STIP1 in transferring Keap1 and Nrf2 to Hsp90 107
SUPPLEMENTARY 108
BIBLIOGRAPHY 111

List of Figures

Figure 1 Model of the Hsp90-HSF1 Heat Shock Response Pathway 10

Figure 2 Model of the Keap1-Nrf2 Antioxidative Response Pathway 22

Figure 3 The Purification of the Kelch domain of Keap1 51

Figure 4 The Protein stability of the Kelch domain of human Keap1 52

Figure 5 The Purification of recombinant human Keap1 54

Figure 6 The Purification of recombinant human Hsp90β 57

Figure 7 The Protein stability of recombinant human Hsp90β 58

Figure 8 The Purification of recombinant mouse STIP1 60

Figure 9 The two-dimensional ^{1}H-^{15}N HSQC spectrum of ^{15}N-labeled Kelch domain of Keap1 64

Figure 10 The signal intensity of ^{15}N-labeled Kelch domain gradually reduces as an increasing amount of Hsp90β is added to the solution 66

Figure 11 Kelch domain of Keap1 binds to Hsp90β weakly 69

Figure 12 Plate binding assay of fluorescently labeled Kelch binds to Hsp90β weakly 72

Figure 13 Plate binding assay of fluorescently labeled Kelch at low concentration binds to Hsp90β weakly 73

Figure 14 Plate binding assay of fluorescently labeled Kelch at high concentration binds to Hsp90β 74

Figure 15 Protein expression of Keap1 in *STIP1*$^{\Delta TPR1}$ mouse line & STIP1-SN56-OK ells ..77

Figure 16 mRNA expression of Keap1 in *STIP1*$^{\Delta TPR1}$ mouse line & STIP1 SN56 KO cells .79

Figure 17 Plate binding assay of fluorescently labeled Keap1 binds to Hsp90β weakly 81

Figure 18 Plate binding assay of fluorescently labeled STIP1 binds to Keap1 with high affinity 83

Figure 19 Plate binding assay of fluorescently labeled STIP1 at high concentration binds to Keap1 84

Figure 20 Protein expression of Nrf2 in *STIP1*$^{\Delta TPR1}$ mouse line & STIP1 SN56 KO cells....86

Figure 21 mRNA expression of Nrf2 in *STIP1*$^{\Delta TPR1}$ mouse line & STIP1 SN56 KO cells....88

Figure 22 The signal intensity of ^{15}N-labeled Nrf2 showed mild residue chemical shift as Hsp90β is added to the solution 90

Figure 23 The overexpression of Middle domain (MD) and C-terminal domain (CTD) of recombinant human Hsp90β.....108

Figure 24 The purification of the Middle domain (MD) of recombinant human Hsp90β....109

Figure 25 The purification of the C-terminal domain (CTD) of recombinant human Hsp90β 110

CHAPTER 1: INTRODUCTION

1.1 Neurodegenerative Diseases

Neurodegenerative disease is an umbrella term encompassing disorders such as Alzheimer's disease (AD), Parkinson's disease (PD), Huntington's diseases (HD), Amyotrophic Lateral Sclerosis (ALS) (Dinkova-Kostova & Kazantsev, 2017). Many of these diseases show pathological symptoms such as problems with movements or deterioration in mental functioning, called dementia (Neurodegenerative Disease Research, JPND). Dementia causes enormous burdens towards the Canadian health care system with more than 419,000 Canadians diagnosed with such conditions in 2016, and about 76,000 new cases per year (Canadian institutes of health research, CCNA). The fast-growing prevalence of neurodegenerative diseases leads to socioeconomic impacts such as burden in private household caregiving, government-provided long-term residential care facilities, and national financial costs up to $22.7 billion annually (NeuroScience Canada 2006). Moreover, the world health organization estimates that neurodegenerative diseases will become the second leading cause of death in Canada by 2040 (NeuroScience Canada 2006).

Neurodegenerative disorders are diseases of the central nervous system that cause debilitating effects to neurons. These disorders share neuropathological symptoms encompassing aberrant protein disrupting protein-related homeostasis, oxidative stress, and free radical formation, the dysfunctionality of mitochondria and neuroinflammatory responses (Jellinger, 2003; 2010). The sequence of these

pathological events is not determined, therefore, the cause of the neurodegenerative disorders remained a mystery. Numerous efforts have been devoted to developing effective drugs for treating such harmful cellular events (Dinkova-Kostova & Kazantsev, 2017; Neef et al., 2010; Patel & Mandal, 2018; Youdim & Buccafusco, 2005). In brief, contemporary therapeutic approaches towards treating neurodegenerative disease are separated into categories such as mitochondrial-direct therapies, stem cell therapies, epigenetic modulator-related therapies, and mitochondrial dynamics modulator-related therapies (Patel & Mandal, 2018). Yet the currently available treatments of neurodegenerative diseases remain incapable of modifying the disease resulting in incomplete and transient benefits in treating patients (Patel & Mandal, 2018).

Two major common pathological hallmarks found in neurodegenerative diseases are the excessive amount of reactive oxygen species creating oxidative stress (OS) and impairments of protein homeostasis (proteostasis), folding, trafficking and degradation (Dinkova-Kostova & Kazantsev, 2017; Khanam et al., 2016; Neef et al., 2010; Pajares et al., 2017; Patel & Mandal, 2018). Targeting these underlying factors represents a possibility in counteracting neurodegeneration. Two cytoprotective pathways, Keap1/Nrf2 pathway and Hsp90/HSF1 pathway play essential roles in combating OS and loss of proteostasis, respectively. The results of my study provide evidence of possible cross-talks between these pathways, which could shed valuable insights into developing therapeutic drugs that target them to treat neurodegenerative diseases.

1.2 Molecular Chaperone

Protein misfolding is one of the critical pathological factors in numerous neurodegenerative diseases such as Parkinson's, Huntington's, ALS, Frontotemporal lobar degeneration (FTLD) and Alzheimer's Disease (Koh et al., 1990; Pike et al., 1992; Yanker et al., 1989). Misfolded proteins tend to expose large hydrophobic surfaces leading to the formation of protein aggregates. These aggregates could cause deleterious effects in cells due to their inability to maintain their native structure for proper functionalities (Chiti & Dobson, 2006; Walsh & Selkoe, 2007).

Molecular chaperones are the major proteins that govern the proper folding of other proteins. The term "molecular chaperone" was first used by Ron Laskey to describe nucleoplasmin, a protein that binds and transport histones into the nuclear compartment (Laskey et al., 1978). Molecular chaperones are considered as proteins that assist the folding, stabilizing, translocating, or degrading of other proteins. Many proteins require the aids of the cellular chaperone machinery to fold into the functional three-dimensional conformation (Hartl & Hayer-Hartl, 2009). For instance, essential proteins such as actins and tubulins have low intrinsic folding efficiencies and cannot fold without chaperones (Hartl & Hayer-Hartl, 2009). Chaperones also play critical roles in activities that maintain proteostasis such as *s*tabilizing non-native proteins, refolding of stress-denatured protein, oligomeric assembly, intracellular protein transport, and proteolytic degradation (Hartl & Hayer-Hartl, 2009). Many chaperones are stress protein or heat-shock protein (Hsp) that are upregulated during proteolytic stress

caused by an increased amount of aggregating unfolded proteins. They are often named after their molecular weight, for instance, Hsp40, Hsp60, Hsp70, and Hsp90. Together they form complex intracellular chaperone networks (Balch, 2008). Chaperones, such as Hsp70 and Hsp90, mainly bind exposed hydrophobic amino acid sidechains on misfolded proteins, thus inhibit their aggregation tendency and promote the refolding process via ATP-regulated cycles (Balch, 2008; Hartl & Hayer-Hartl, 2009).

Neurodegenerative disorders such as Alzheimer's, Parkinson's, Huntington's and prion diseases share pathological states in which deposition of fibrillar aggregates and aberrantly folded proteins cause neuronal cytotoxicity (Chiti & Dobson, 2017; Muchowski et al., 2000; Reis et al., 2017). Recent advances in understanding the aging process indicate that protein quality declines as the functional capacity of chaperones decreases (Balch, 2008; Sittler et al., 2001). Studies using cell culture, fruit fly, and mouse models showed enhancing the protein-folding ability of cells through elevating chaperone protein expression provides positive benefits in modifying the neurodisorder pathology caused by misfolded protein (Neef et al., 2012). Therefore, further investigation of the cellular chaperone machinery network and their roles in helping protein fold is of utmost importance.

1.3 Heat Shock Protein (Hsp) 90

1.3.1 Hsp90 Chaperone Mechanism

Hsp90 is conserved in bacteria and all eukaryotes, indicating its importance to a large number of organisms and the long history in evolution (Dinkova-Kostova & Kazantsev, 2017; Genest et al., 2019: Radii et al., 2017; Prodromou, 2017). Hsp90 protein found in *Escherichia coli* is called HtpG (Li & Buchner, 2012). In yeast, two isoforms of Hsp90 existed in the cytosol, Hsc82, and Hsp82 (Li & Buchner, 2012). In mammalian cells., two major isoforms of Hsp90, Hsp90α (inducible and major form) and Hsp90β (constitutive and minor form) exist in the cytoplasm (Li & Buchner, 2012). In particular, Hsp90β was required for early embryonic development and long-term cellular adaptation (Li & Buchner, 2012; Sreedhar et al., 2004).

Hsp90 interacts with a large (> 2000) and diverse pool of substrate proteins (which are often referred to as clients) that perform essential cellular functions, such as signaling proteins (i.e., HSF1), kinases (i.e., cyclin-dependent kinase), steroid hormone receptors (i.e., glucocorticoid receptor) and disease-related proteins (i.e., tumor suppressor p53, the microtubule-binding protein Tau) (Pearl & Prodromous, 2016; Taipale et al., 2010). Among these clients, many of them are oncogenic proteins that are crucial for cancer progression, making Hsp90 a therapeutic target for cancer treatments (Genest et al., 2019). Moreover, the Hsp90 also modulates the quality of essential proteins and the

degradation of aberrant proteins that tend to aggregate in neurodegenerative diseases, making it a possible target in treating neurological disorders. Interestingly, the client proteins of Hsp90 vary in structure as well as sequence, implying that the specificity of Hsp90 in interacting with its clients remains to be understood.

Hsp90 also forms machinery with Hsp70/Hsp40 chaperones to support protein folding, oligomeric assembly, damaged protein repair, and degradation (Kim et al., 2013; Saibil, 2012; Winkler et al., 2012). This system involves the cochaperone STIP1 that allows clients to be transferred from Hsp70 to Hsp90 during the protein folding process (Pratt et al., 2015). Specifically, STIP1 interacts with both Hsp70 and Hsp90 to stabilize their interactions with clients (Sung et al., 2016). Many studies sought better understandings towards the client - chaperone interactions and their involvement in biological processes for their essential roles in cellular survival and neurodisorder-related treatments. Therefore, the manipulation of Hsp70/Hsp90 machinery in studies not only facilitates the understanding of their clients but also help validates similar experimental methods and the litany of studies which it depends on (Alvira S et al., 2014; Genest et al., 2019; Kirschke et al., 2014; Verba et al., 2016).

At the native cytosolic state, Hsp90 exists as a homodimer. The protein is composed of three domains: The N-terminal domain (NTD), the middle domain (MD), and the C-terminal domain (CTD). Both the NTD and MD of Hsp90 participate in ATP-hydrolysis, whereas the CTD is

responsible for the dimerization. The MD is also involved in interacting with Hsp70, whereas the MEEVD motif in CTD mediates the binding with many co-chaperones containing tetratricopeptide repeat (TPR) domains, including STIP1 (Florian et al., 2017; Lackie et al., 2017; Zuehlke et al., 2017). Besides, the long, flexible, and the charged linker between NTD and MD has also been shown to modulate the conformation and co-chaperone interaction of Hsp90 (Hainzl, 2009; Jahn, 2014; 2018; Tsutsumi, 2009; 2012).

All three domains of Hsp90 are involved in recruiting different sets of clients. In addition, the ATP hydrolysis function of Hsp90 plays an essential role in the binding and release of some of its clients. Hsp90 is highly dynamic in structure. It cycles through different conformation states, such as apo state, ATP-bound state, and the ADP-bound state, during the ATP hydrolysis process (Krukenberg et al., 2008; Southworth & Agard, 2008). Hsp90 ATP chaperone conformational cycle starts with the open apo conformation. The binding of ATP to the NTD of Hsp90 causes the protein to change into a closed conformation where the NTD and MD promote the ATP hydrolysis. When the ATP is hydrolyzed, Hsp90 releases the ADP product and returns to the apo-state (Ali et al., 2006; Lavery, 2014; Shiau et al., 2006; Tsutsumi, 2009). The ATP hydrolysis mechanism is conserved among eukaryotic Hsp90 species implying the importance of ATP hydrolysis in Hsp90's *in vivo* functions (Richter et al., 2008).

1.3.2 Hsp90/HSF1 - Mediated Heat Shock Response

Heat Shock Factor 1 (HSF1), a client of Hsp90, is a master regulator of heat shock response (HSR) (Akerfelt et al., 2010; Neef et al., 2012). HSF1 belongs to the vertebrate family of HSF proteins and is conserved in its protein structure across yeast, fruit fly, and mammalian cells (Akerfelt et al., 2010). It mediates the transcriptional activation of the HSR, which can be triggered by cytoplasmic proteotoxic stimuli, including increased temperature, oxidative stress, bacterial and viral infection (Lackie RE et al., 2017; Neef et al., 2012). The activation of HSR primarily promotes the expression of genes encoding multiple chaperones to combat cellular stress and other essential cellular events, including protein degradation, ion transportation, signal transduction, energy generation, carbohydrate metabolism and cytoskeleton formation (Akerfelt et al., 2010; Gonsalves et al., 2011; Hahn et al., 2004; Trinklein et al., 2004).

The regulation of HSF is stress-dependent and controlled through multiple chaperones and co-chaperone regulatory mechanisms (Neef et al., 2012) (Figure 1). Under basal homeostasis conditions, HSF1 is repressed through the activity of chaperone proteins, including Hsp90, Hsp70, Hsp40 and other co-chaperones (Ali et al., 1998; Bharadwaj et al., 1999; Guo et al., 2001; Neef et al., 2012). The role of Hsp70 and Hsp40 focuses on binding to the transcriptional activation domain of HSF1 to repress its activation (Neef et al., 2012). Meanwhile, Hsp90 and co-chaperone 23 with other proteins together bind with the regulatory domain of HSF1 (Ali et al., 1998; Bharadwaj et al., 1999; Guo et

al., 2001; Neef et al., 2012).

When entering cellular proteotoxic-related stress, HSF1 gets released from the protein complex formed by the multiple chaperones and co-chaperones previously mentioned (Lackie et al., 2017; Neef et al., 2012). This allows HSF1 to translocate into the nucleus (Lackie et al., 2017). After translocation into the nucleus, HSF1 homotrimerizes and binds to the cis-acting heat shock elements in the stress responding genes to upregulate the expression of many essential chaperones and co-chaperones, such as Hsp90, Hsp70, Hsp27 and Hsp40 (Neef et al., 2012). The upregulation of such cytoprotective proteins can support protein integrity and disposal (Lackie et al., 2017). The phosphorylation of HSF1 at specific serine residues further promotes its transcriptional activity. However, the mechanism of phosphorylation events remains undetermined (Neef et al., 2010). Moreover, the fate of HSF1 after dissociation from DNA also remains to be determined (Yang et al., 2008). Knock-down of HSF1 expression has been shown to enhance the neuropathological effects of toxic misfolded proteins, implying the potential of upregulating HSR in treating ND (Karam et al., 2017; Kraemer et al., 2006; Nollen et al., 2004; Wang et al., 2009).

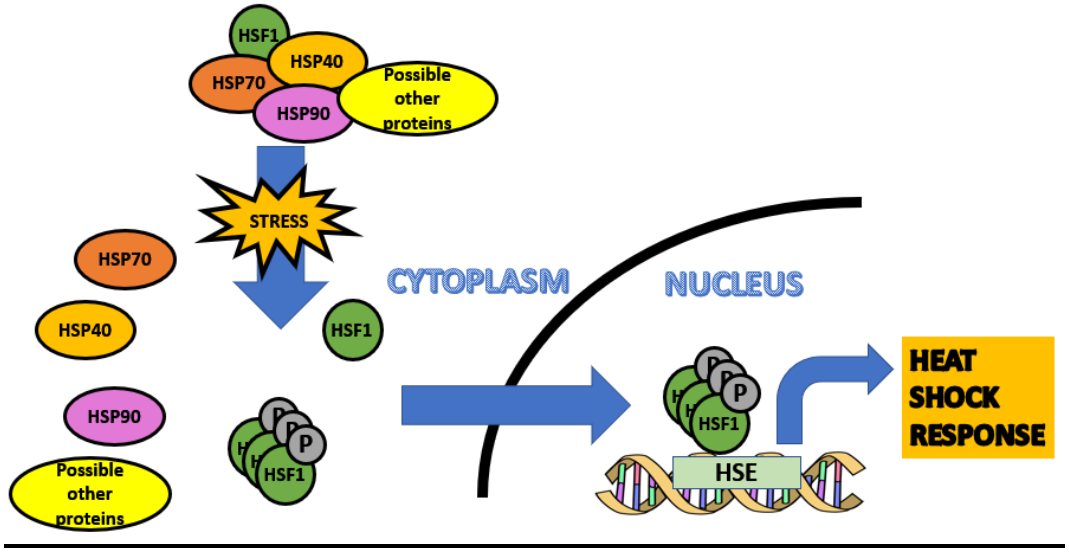

Figure 1

Figure 1. Model of the Hsp90-HSF1 Heat Shock Response Pathway. HSF1 is believed to reside in a complex with Hsp90, Hsp70, and Hsp40 in the cytosol. When the cell is under proteotoxic stress or heat stress, the unfolded or misfolded proteins competed with HSF1 to bind with Hsp90 chaperones and co-chaperones. The unbound HSF1 monomers trimerize as they translocate into the nucleus, which leads to the upregulation of more chaperones and co-chaperones to combat against proteotoxic stress.

1.4 Co-chaperone Stress-Inducible Phosphoprotein 1 (STIP1)

Hop/STI1/STIP1 is a co-chaperone of the Hsp70/Hsp90 machinery (Röhl et al., 2015; Scheufler et al., 2000). It resides in the cytosol but can also shuttle between the nucleus and cytoplasm (Longshaw et al., 2004). STIP1 consists of three TPR domains (TPR1, TPR2A, and TPR2B) and two domains rich in aspartate and proline residues (DP1 and DP2). During the chaperone-assisted client folding, Hsp70 first interacts with the TPR1 and TPR2B domains of STIP1 (Pratt et al., 2015). Hsp90 then binds to the TPR2A domain, which interferes with the interaction between Hsp70 and the TPR2B domain (Pratt et al., 2015). The binding of Hsp90 and STIP1 reorganizes the ternary Hsp70-client-STIP1 complex, allowing the client to be transferred to Hsp90 (Pratt et al., 2015). The role of the DP domains of STIP1 remains unclear currently (Pratt et al., 2015). In addition, TPR2A-TPR2B-DP2 is the minimal fragment of STIP1 that is required for the client transfer implying the essential functionalities of these domains (Pratt et al., 2015; Schmid et al., 2012).

The deletion of the TPR1 domain hampers the client transfer from Hsp70 to Hsp90, which leads to a decline in the client protein level (Karam et al., 2017). The deletion of STIP1 leads to decreases of various Hsp90 client's protein levels, implying its vital role in maintaining cellular proteostasis (Beraldo et al., 2013; Lackie et al., in preparation; Longshaw, 2004; Nollen et al., 2004). The deletion of STIP1 in mice is shown to be lethal, indicating its essential cellular functions towards organism survival (Beraldo et al., 2013).

1.4.1 The study of modulation of client stability by Hsp70/Hsp90/STIP1 chaperone machinery

As previously mentioned, the folding of client proteins starts with forming a complex with Hsp70 and its co-chaperone Hsp40 and then gets transferred to Hsp90 through the assistance of co-chaperone STIP1 (Lackie et al., in preparation). This chaperone machinery plays a crucial role in protein quality control, which is important to neurodegenerative disorder studies (Fontaine et al., 2016; Lackie et al., in preparation). However, the role of STIP1 and Hsp70/Hsp90 in maintaining proteostasis in mammals is not well understood. Dr. Marco Prado's lab addressed this question through generating a mouse line with STIP1 hypomorphic allele in mice to observe the effects of reducing STIP1 gene expression on the client proteins as well as the survival of these mice. Moreover, a CRISPR–Cas9 STIP1 knockout neuronal cell line was developed as well to further investigate the importance of STIP1 in the functionality of Hsp70/Hsp90 chaperone machinery (Lackie et al., in preparation). These studies revealed the importance of STIP1 in maintaining the neuronal resilience during aging and the functionality of the chaperone network, especially in neurodegeneration conditions (Lackie et al., in preparation).

1.4.1.1 Homozygous mutant STIP1 mice (△TPR1 mice)

The hypomorphic TPR1-deprived STIP1 mice were generated by removing the exons 2 and 3 of the STIP1 gene using the Cre/lox system (Lackie et al., in preparation). These homozygous mutant STIP1 mice (△TPR1 mice) are an excellent tool in understanding the importance of the TPR1 domain of STIP1 in assisting the client transfer between Hsp70 and Hsp90.

The △TPR1 mice were found to be viable but had a significantly lower birth rate than Mendelian distribution (Lackie et al., in preparation). Lackie's results showed that the △TPR1 mice had a high mortality rate during an early age, which suggested that the reduction of STIP1 protein level caused by deleting the TPR1 domain caused an increased mortality rate. This indicated that STIP1 plays an essential role in mammalian development. More interestingly, many proteins that were involved in Hsp70/Hsp90 network functionality and protein folding presented a decrease in the protein expression but without a significant change in gene expression. For example, a peptidyl-prolyl cis/trans isomerase (PPIase) called Pin1, which coordinates with the Hsp90 chaperone complex and regulates the phosphorylation of tau protein, showed 50% reduction in protein expression (Dickey et al., 2007; Lackie et al., in preparation). The reduction of these protein levels in △TPR1 mice indicates that the TPR1 domain of STIP1 is vital for maintaining the proteostasis and it plays a crucial role in STIP1's ability to regulate the stability of Hsp90 and co-chaperones involved in Hsp70/Hsp90 chaperone machinery (Lackie et al., in preparation).

Many client proteins of the Hsp70/Hsp90 chaperone machinery also showed a reduction in protein levels in the △TPR1 mice (Lackie et al., in preparation). Specifically, glucocorticoid receptor (Gr), Tau protein, and G protein-coupled receptor kinase 2 (GRK2), which are all Hsp90 client proteins, all showed a significant reduction in protein expression but without gene-level changes (Lackie et al., in preparation). These results showed that the client proteins of Hsp90 could largely depend on the functionality of the TPR1 domain of STIP1 to become fully folded or stable.

1.4.1.2 SN56 – STIP1 KO Cell Line

The SN56 – STIP1 Knockout cell line (SN56-STIP1 KO) was developed by using optimized CRISPR Design (http://crispr.mit.edu/) to design the guide RNAs for the *Stip1* gene. The construct was sequenced and used to transfect SN56 cells using Lipofectamine 2000 (Invitrogen, Carlsbad, CA, USA). The resultant clones that showed complete elimination of STIP1 protein expression were used to investigate further the importance of STIP1 in regulating Hsp90 client protein and co-chaperone as well as protecting neuronal cells from environment stress (Lackie et al., in preparation).

The SN56 -STIP1 KO cells showed an increase in the cell death levels compared to the SN56 wild-type (WT) cells (Razzaq, 2018; Lackie lead, in preparation). This indicated that STIP1 was crucial for the survival of neurons, and deleting STIP1 compromises the neuron's ability to combat environmental stresses. Moreover, co-chaperones and client proteins of Hsp90, such as FK506 binding protein 51 kDa (FKBP51), CypA, Pin1, Glucocorticoid Receptors, all showed a reduction in

protein expression level (Razzaq et al., 2018). The decrease of client protein levels indicated that a loss of proteostasis is related to the loss of STIP1 in neurons. These results together suggest that STIP1 is a critical co-chaperone that regulates the Hsp70/Hsp90 machinery and is required for the recruitment and stabilization of Hsp90 client proteins (Beraldo et al., 2013; Lackie et al., in preparation).

1.5 Keap1/Nrf2-Mediated Oxidative Stress Response

1.5.1 Nrf2 as a Transcription Factor in the pathway

Reactive oxygen species (ROS) are oxygen metabolism by-products that play essential roles in cell signaling (Deshmukh et al., 2017). The excessive accumulation of oxidative stress (OS) and ROS production can disrupt the cellular antioxidative mechanism. Distrupting the redox homeostasis leads to proteostasis imbalance, DNA modification, inflammations (Browne & Beal, 2006; Johnson & Johnson, 2015; Kerr et al., 2017). These harmful effects contribute to the progression of many neurodegenerative diseases (Browne & Beal, 2006; Johnson & Johnson, 2015; Kerr et al., 2017). Also, common pathological features such as aggregating aberrant proteins, microglial activation, and mitochondrial dysfunction could generate more ROS and OS that cause more damages to the central nervous system (Deshmukh et al., 2016). The critical pathway that combat the OS/ROS damages and degradation of misfolded aggregated proteins is mediated by transcription factor; nuclear factor (erythroid-derived 2)-like 2 (Nrf2) (Pajares et al., 2017).

Nrf2 is considered as a master regulator of cellular redox homeostasis and removal of damaged proteins under OS/ROS conditions (Johnson & Johnson, 2015; Kerr, 2017; Pajares M. et al., 2017). It belongs to the Cap 'n' Collar (CNC) family of the basic leucine zipper regulatory proteins (Deshmukh et al., 2017). The CNC family proteins contain CNC domains that heterodimerize with

small Maf proteins to bind with DNA to regulate gene expressions (Derjuga et al., 2004; Deshmukh et al., 2017). This protein family also includes other transcription factors such as NF-E2, Nrf1, Nrf3, Bach1, and Bach2 (Motohashi et al., 2002). Amongst these proteins, Nrf2 is the most intensively studied due to its essential function in cellular redox metabolism (Chan et al., 1993). Human Nrf2 has 605 amino acids and is composed of seven well-conserved functional domains, Nrf2-ECH homology (Neh) 1-7 (Baird L & Dinkova-Kostova, 2011; Wang et al., 2013). Each domain plays an essential role in the function of Nrf2, but herein, the relevant domains would be briefly introduced. The Neh1 domain is involved in CNC and DNA binding, which dimerizes with Maf small protein (Deshmukh et al., 2017; Johnson & Johnson, 2015). The Neh2 domain, containing lysine residues that can be ubiquitinated by CUL3-dependent E3-ubiquitin ligases, is required for the negative regulation of Nrf2 (Johnson & Johnson, 2015; Sekhar et al., 2002). The Neh3 domain plays an essential role in promoting the transcription of cytoprotective genes (Nioi et al., 2005).

Nrf2 mediates the basal and stress-inducible expression of cytoprotective antioxidative genes participating in the phase I, II and III detoxifying metabolism, glutathione and peroxiredoxin/thioredoxin metabolism and NADPH production, i.e., the detoxifying and oxidative stress enzyme, xenobiotic-metabolizing, and other cytoprotective genes (Kobayashi et al., 2006; Itoh, 1999; Pajares et al., 2017; Zhang et al., 2013). Nrf2 induces these cytoprotective genes expression by targeting the antioxidative responsive element (ARE). ARE (which is called electrophile response

elements (EpREs)) is a cis-regulatory element found in the upstream promoter regions of many phase II metabolic genes (Rushmore et al., 1990; 1991). The phase II metabolic genes encode enzymes, such as glutathione-transferase (GST), quinone oxidoreductase 1 (NQO1) and NAD(P)H, that are critical in detoxifying xenobiotics and combating oxidative stress in response to electrophiles and oxidants (Zhang et al., 2013). The cytoprotective importance of Nrf2 has been shown through the phenotype of the Nrf2 null mice which experiences higher sensitivity towards xenobiotics such as benzo(a)pyrene, butylated hydroxytoluene, acetaminophen, and etc (Aoki et al. 2001; Calkins et al. 2005; Chan & Kan, 1999; Enomoto et al. 2001; Khor et al. 2006; 2008; Xu et al. 2006).

The Nrf2-mediated antioxidative pathway plays a preventative and cytoprotective role in combating oxidative stress (Kobayashi et al., 2006; Itoh, 1999; Pajares et al., 2017; Zhang et al., 2013). Targeting the activation of Nrf2 for upregulating various enzymes has been the center of research themes, including detoxifying carcinogens, chemotherapeutic and radiotherapies (Kensler & Wakabayashi, 2010; Lau et al., 2008; Takahashi et al., 2015). Recent studies showed that the expression of phase II enzymes also provided neuroprotection to the central nervous system (Deshmukh et al., 2016; Zhang et al., 2013). This is because the pathophysiological events found in neurodegenerative diseases often cause the accumulation of OS and ROS, leading to damages to lipids, proteins, and DNA (Deshmukh et al., 2016). Therefore, it is crucial to study the role of the Nrf2-mediated pathway in order to provide helpful guidance to therapeutic development for treating

neurological disorders.

1.5.2 Keap1 as the Major Negative Regulator of Nrf2

Kelch-like ECH associated protein 1 (Keap1) is a major negative regulator of the Keap1/Nrf2 pathway (Zhang et al., 2013). It functions as a substrate adaptor of a CUL3-dependent E3-ubiquitin ligase complex that targets Nrf2 for ubiquitination-dependent degradation (Bryan et al., 2013; McMahon et al., 2004; Ogura et al., 2010). The 624-amino acid human Keap1 consists of four domains: The Broad complex Tramtrack and Bric-a-Brac (BTB) domain, the intervening region (IVR), the double glycine repeat (DGR) and the C-terminal region (CTR) (Ogura et al., 2010). The Keap1 is found to be highly conserved among eukaryotes such as mice and humans (Deshmukh et al., 2017; Li et al., 2007). Keap1 exists as a homodimer primarily in the cytoplasm that also shuttles to the nucleus (Sun et al., 2011; Zhang et al., 2013). The BTB domain plays the role of dimerizing Keap1 as well as stress sensing through the cysteines in its structure (Deshmukh et al., 2017; Ogura et al., 2010). The IVR domain is crucial for sensing electrophilic and oxidative stress due to the two critical cysteine residues, Cys273, and Cys288 (Deshmukh et al., 2017; Ogura et al., 2010). Moreover, the BTB domain and the IVR domain together are important for the polyubiquitination and 26S proteasomal mediated degradation for Nrf2 (Deshmukh et al., 2017). The functions of DGR and CTR regions, which is called Kelch domain together, are mainly focusing on repressing Nrf2 activity (Canning et al., 2015; Deshmukh et al., 2017; Ogura et al., 2010).

The binding of Keap1 to Nrf2 triggers the clearance of excessively produced Nrf2 through CUL3-dependent E3-ubiquitin ligase-mediated ubiquitination (Kobayashi et al., 2004). Under the basal homeostatic condition, Keap1 binds Nrf2 through the Kelch domain to send it for degradation by the proteasome (Ogura et al., 2010). The Kelch domain of Keap1 contains six Kelch repeats that form a six-bladed β-propeller structure (Canning et al., 2015). This β-propeller structure form electrostatic interactions with the Neh2 domain of Nrf2 through two sites: the weak affinity binding site called the DLG motif (residues 24-31); and the strong affinity binding site called the ETGE motif (residues 78 – 82) (Zhang et al., 2013). This combination forms a strong and weak affinity "hinge-and-latch" model that inhibits the activation of Nrf2 in the cytosol (Canning et al., 2015; Zhang et al., 2013). Previous studies have shown that the DLG binds to Kelch 100-fold weaker compared to the affinity of ETGE binding to Kelch (Tong et al., 2006).

Electrophilic/oxidative stress leads to structural modifications of the Keap1 homodimer (Deshmukh et al., 2016). Notably, Keap1 is structurally abundant in cysteine residues, with 25 cysteines found in mouse and 27 cysteines in human homologs (Johnson & Johnson, 2017). Previous studies revealed that amongst all the cysteines that existed in Keap1, Cys273, and Cys288 are the two most crucial ones in causing the conformational changes of Keap1 (Deshmukh et al., 2016; Ogura et al., 2010). Under stress conditions, these cysteine residues are covalently modified, causing the structural changes of Keap1. This leads to the dissociation of Keap1 from the DLG motif of Nrf2

(Taguchi et al., 2011). The high levels of newly synthesized Nrf2 proteins quickly accumulate and translocate into the nucleus. Eventually, Nrf2 binds to the ARE and promotes the expression of a large group of cytoprotective genes that are responsible for combating detoxifications, antioxidant, and proteostasis restoring genes (Figure 2) (Baird et al., 2014; Furukawa et al., 2005; Joshi et al., 2015; Khan et al., 2015; Kang et al., 2004; Kobayashi et al., 2004; Zipper et al., 2002).

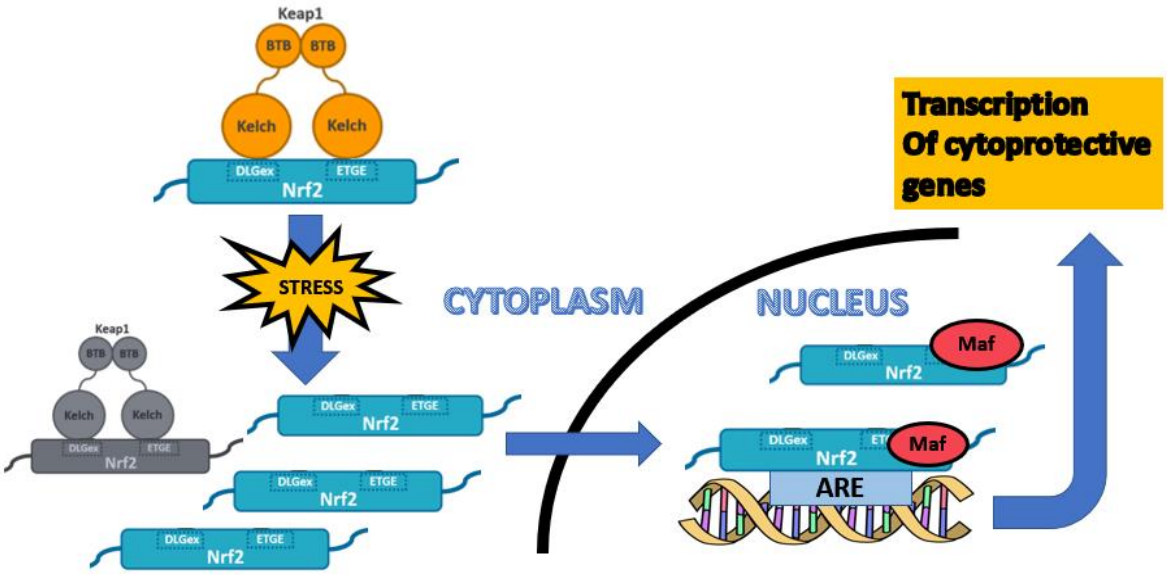

Figure 2

Figure 2. Model of the Keap1-Nrf2 Antioxidative Response Pathway. At basal state, Keap1 represses Nrf2 by promoting its degradation. And under oxidative stress, Nrf2 disassociates from Keap1 and activates the transcription of antioxidative elements.

1.5.3 Keap1 / Nrf2 - Mediated Pathway & Neurodegenerative Diseases

The Keap1/Nrf2 pathway plays an essential role in protecting against many neurological diseases (Zhang et al., 2013). In the following content, various neurodegenerative diseases and the importance of the Keap1/Nrf2 pathway towards treating these disorders would be discussed.

Parkinson's disease is characterized by the loss of dopaminergic neurons and the deposition of Lewy bodies in many regions of the brain (Tufekci et al., 2011). Previous studies have shown that Nrf2 exists with higher expression in PD patients, which may be due to neurons' attempt to combat oxidative toxicity (Ramsey et al., 2007).

Alzheimer's disease is a neurodegenerative disease associated with loss of neurons, the formation of intracellular neurofibrillary tangles and the deposition of amyloid-beta (Ramsey et al., 2007). Researchers have found that Nrf2 expression is extremely low in AD patients. The decline of Keap1/Nrf2 related proteins are associated with a significant amount of amyloid-beta deposition, and over-expressing Nrf2 through Nrf2-activator could provide neuroprotection against AD pathological symptoms (Kanninen et al., 2008; Ramsey et al., 2007).

Multiple sclerosis (MS) is an autoimmune and inflammatory disease that is believed to be initiated by the toxicity caused by abnormal activation of CD4+ T cells which led them to cross the blood-brain barrier inappropriately (Benedict & Zivadinov, 2011). Increasing evidence has shown that Nrf2 is essential for the proper functioning of CD4+ T cells. For instance, Nrf2 knockout mice showed

increased expression of inflammatory enzymes and enhanced immune cell (CD4+ T cells) activation (Johnson et al., 2010). Moreover, promoting the Nrf2 activation via modifying Keap1 structure or inducing Nrf2 expression have been shown to suppress neuroinflammation, which is beneficial in treating MS (Linker et al., 2011; Pareek et al., 2011).

Huntington's Disease (HD) is an autosomal dominantly inherited neurodegenerative disease caused by the genetic condition that leads to abnormal body movements, cognitive impairments, and personality changes (Kumar et al., 2010). Evidence suggested that elevation of Nrf2 expression can reduce the pathological symptoms in HDs such as striatal atrophy, mitochondrial impairment and the neuron lesions (Calkins et al., 2005; Stack et al., 2010). ALS is a neurodegenerative disease caused by loss and degeneration of neurons among the spinal cord, brain stem, and motor cortex. The elevated level of Nrf2 triggered by Nrf2-inducers significantly reduces the progression of ALS in-mouse models and protects motor neurons against toxicity caused by mutated proteins found in ALS (Pehar et al., 2007; Neymotin et al., 2011).

In conclusion, the Keap1/Nrf2-mediated cytoprotective pathway is significant in protecting neurons from various neurodegenerative diseases as well as in treating neurological diseases previously mentioned (Zhang et al., 2013).

1.6 Crosstalk Between the Keap1/Nrf2 and Hsp90/HSF1 Cytoprotective Pathways

Both Keap1/Nrf2 and Hsp90/HSF1 cytoprotective pathways that play crucial roles in neuronal survival and neuroprotection against oxidative and proteotoxic stress. Multiple previous studies indicated connections between these two pathways, which were previously believed to be independent of each other. However, the molecular mechanism of their connection remained unclear. For example, Satoh et al. (2011) found that both pathways can be activated by the same pro-electrophilic toxic to provide neuroprotection against oxidative stress and endoplasmic reticulum stress (Dinkova-Kostova & Kazantsev, 2017). Zhang et al. (2014) found that an inhibitor of Hsp90, electrophilic sulphoxythiocarbamate, can also inhibit Keap1, leading to the activation of both Keap1/Nrf2 and Hsp90/HSF1 pathways. Naidu et al. (2015) demonstrated that Keap1/Nrf2 and Hsp90/HSF1 pathways crosstalk by sharing transcription targets such as Hsp70, heme oxygenase 1, p62, activating transcription factor 3, and they compensate each other when either one of the pathways is compromised (Naidu et al., 2015). Miller and Ramos (2005) identified that Nrf2 and Hsp90β (a constitutively expressed homolog of Hsp90) are components of the heterocomplex that interacts with ARE/EpREs, which implied that Hsp90β might interact with Nrf2. These studies illustrate the possibility of co-modulating both pathways to develop effective therapeutic drugs.

1.7 The Scope of the Thesis

Typical pathological hallmarks, such as oxidative stress and proteotoxicity, found in NDs, are closely related to the Hsp90/HSF1 and Keap1/Nrf2 cytoprotective pathways. Interestingly, our collaborator, Dr. Martin Duennwald (Western University) has recently identified the interactions of Hsp90 with Nrf2 and Keap1 via yeast-two-hybrid screening (unpublished data). The interactions between these proteins may imply the crosstalk between the Keap1/Nrf2 and Hsp90/HSF1 pathways. However, the molecular mechanisms of these interactions are unclear.

Following these findings, we investigated the molecular basis and functionality of the interactions of Hsp90 with Keap1 and Nrf2. Our study revealed the underlying crosstalk between the Keap1/Nrf2 and Hsp90/HSF1 cytoprotective pathways and the potential in co-modulating them. Further characterizing their interacting mechanisms and cellular functions will provide valuable insights in treating NDs.

<u>HYPOTHESIS</u>: We hypothesize that Keap1 and Nrf2 are clients of Hsp90, and Hsp90 together with STIP1 modulates their protein stability.

We aim to understand the role of Hsp90 in mediating the Keap1-Nrf2 pathway through both *in vitro* and *in vivo* approaches. *In vitro* studies include using protein-ligand binding assay (a

modification of ELISA assay), isothermal titration calorimetry, and nuclear magnetic resonance spectroscopy to characterize the interactions of Hsp90 with Keap1, STIP1 with Keap1, and the interactions of Hsp90 with Nrf2.

In vivo studies utilize *STIP1*$^{\Delta TPR1}$ mouse line and SN56 wild type (WT) /SN56-STIP1-KO cell line to study the gene and protein expression of Keap1 and Nrf2 as clients to STIP1/Hsp90 machinery using Real-time quantitative Polymerase Chain Reaction (RT - qPCR), Western Blotting.

Our objectives include:

I. Identify the interactions of Human Hsp90 with Keap1 and Nrf2 *in vitro*

II. Determine whether Keap1 and Nrf2 are clients of Hsp90 *in vivo*

III. Determine whether the interactions of Keap1 and Nrf2 with Hsp90 modulate their protein stability *in vivo*

CHAPTER 2: MATERIALS&METHODS

2.1 Protein overexpression and purification

2.1.1 Preparation of recombinant Kelch domain of human Keap1

2.1.1.1 Overexpression of recombinant Kelch domain of human Keap1

The expression and purification of recombinant Kelch domain of Keap1 were reported previously (Khan et al. 2013). A brief description of the process of overexpressing and purifying Kelch will be provided. The pET15b plasmid carrying the Kelch cDNA was introduced into *Escherichia coli* (*E. coli*) BL21 (DE3) cells (Novagen) by the standard method (Sambrook & Russell, 2006). Bacteria were plated onto Luria-Bertani (LB) agar media containing 50 µg/mL Carbenicillin (US biological) and were incubated overnight at 37 ℃. A single colony was inoculated 2 mL of LB media with 50 µg/mL Carbenicillin overnight at 37 ℃. After overnight growth, the bacteria culture was collected and stored away with 300 µL/mL glycerol at -80 ℃.

When overexpressing Kelch, 20 µL of the media containing pET15b Kelch plasmid was taken out of the stock and resuspended in 2 mL of LB media containing 50 µg/mL Carbenicillin as a starter culture. The starter culture was incubated at 37 ℃ overnight. Then the 2 mL culture was directly added to 200 mL LB media with 50 µg/mL Carbenicillin per 1 L LB growth of bacteria. The 200 mL LB was grown

overnight at 37 °C. After the overnight growth, the bacterial cells were pelleted by centrifugation (6, 000 xg, 15 mins, room temperature, Avanti rotor JLA-16, 250) and were resuspended into 1 L of LB media containing 50 µg/mL Carbenicillin to reach a starting OD_{600} of 0.09-0.12. The cell culture was incubated at 37 °C until the OD_{600} reach 0.8-0.9. The Kelch overexpression was induced overnight with 1 mM isopropyl-beta-D-thiogalactopyranoside (IPTG, BioShop) at 15 °C. The cells were later harvested after 18 hrs of growth with $OD_{600} > 2.0$. The bacterial cells were pelleted by centrifugation at 6,000 xg for 20 mins in a Beckman JLA-9.1000 rotor. The pellets were washed with 1 x Dulbecco's Phosphate Buffered Saline, then with lipopolysaccharide (LPS) solution 1 (5 mM $CaCl_2$, 20 mM Trisaminomethane/Tris buffer pH8.0) and finally with LPS solution 2 (10 mM Ethylenediamineteraacetic/EDTA acid, 20 mM Tris buffer pH 8.0). The pellet was collected by centrifugation at 6, 000 xg for 20 mins in a Beckman JA 30.50 rotor, then stored at -20 °C until needed.

2.1.1.2 Purification of recombinant Kelch domain of human Keap1

Bacterial cells were thawed in 37 °C water bath and resuspended in 20 mL/g of Lysis buffer (20 mM Tris-HCl, 150 mM NaCl, 1 mM EDTA, pH 8.0 – 9.0). The suspension was mixed with 2 scoops of human lysozyme and incubated in 37 °C water bath for up to 30 mins. The suspension was then subjected to lysis by Avastin Homogenizer. The product after lysis was mixed with protease inhibitor, 100 µL phenylmethylsulfonyl fluoride (PMSF) per 10 mL of suspension and was adjusted with imidazole stock (1 M) as well as NaCl stock (5 M) to binding buffer (20 mM Tris-HCl, 500 mM NaCl,

10 mM Imidazole, 1 mM EDTA, pH 7.8) concentrations. Cellular debris and protein precipitation were removed by centrifugation at 40, 000 xg in JA 30.5 rotor at 4 °C for 30 mins. The resulting supernatant was adjusted to 7.8 pH using 1 N HCl stock and was then combined with 10 mL of binding buffer equilibrated Ni-Sepharose beads and incubated at room temperature (22 °C) for about 2 hrs. The Ni-sepharose beads were poured back into a 50 mL column and washed by gravity using 100 mL of binding buffer (20 mM Tris-HCl, 1 mM EDTA, 10 mM Imidazole and 500 mM NaCl at pH 7.8) followed by 500 mL wash buffer A (20 mM Tris-HCl, 500 mM NaCl, 20 mM Imidazole at pH 7.8) and 500 mL wash buffer B (20 mM Tris-HCl, 500 mM NaCl, 40 mM Imidazole at pH 7.8). The bound Kelch was eluted over a 30 mins duration with 5 mL fractions by gravity flow with elution buffer (20 mM Tris-HCl, 500 mM NaCl, 750 mM Imidazole at pH 7.8). Protein containing fractions were determined by qualitative BioRad assay and pooled together. The eluted protein solution was desalted through being dialyzed in 2 L dialysis buffer (20 mM 4-(2-hydroxyethyl)-1-piperazineethanesulfonic acid/Hepes, 100 mM NaCl, 1 mM Dithiothreitol/DTT at pH 7.5) using a Spectra/Por 6 dialysis tubing with a molecular weight cut-off (MWCO) of 30 kDa overnight and then another 4 hrs.

The dialyzed protein sample was centrifugated to remove precipitation (40, 000 xg, 15 mins, at 4 °C). Then the protein sample was filtered through a 0.20 µm low protein binding membrane filter (Pall) before further purification process. Every 20 mg of the Kelch protein was combined with 10 µL of 21.2 U/µL thrombin stock and was incubated overnight at 4 °C. The next day, the cleaved Kelch protein

sample was loaded to the dialysis buffer equilibrated HiLoad S75 Column and was eluted with 1 mL fractions. The collected fractions were analyzed by sodium dodecyl sulphate polyacrylamide gel electrophoresis (SDS-PAGE) using 12 % gels with Coomassie Brilliant Blue R-250 staining. Fractions that contained the pure Kelch protein were pooled and subjected to a BioRad assay to determine the protein concentration. The final pure Kelch sample was used for further experiments.

2.1.2 Preparation of recombinant Human Keap1

2.1.2.1 Overexpression of recombinant Human Keap1

The pET1b plasmid carrying the Keap1 cDNA was introduced into *Rosetta* 2 (DE3) pLysS cells (Novagen) by the standard method (Sambrook & Russell, 2006). The Bacteria were stored at -80 °C (Eggler, 2005; Ogura, 2010).

When overexpressing Keap1, 20 µL of the media containing pET1b Keap1 plasmid was taken out of the stock and resuspended in 2 mL of 2x YT media containing 50 µg/mL Carbenicillin as a starter culture. The starter culture was incubated at 37 ℃ overnight. Then the 2 mL culture was directly added to 200 mL LB media with 50 µg/mL Carbenicillin per 1-litre LB growth of bacteria. The 200 mL LB was grown overnight at 37 ℃. After the overnight growth, the bacterial cells were pelleted by centrifugation (6, 000 xg, 15 mins, room temperature, Avanti rotor JLA-16, 250) and were resuspended into 1 L of LB media containing 50 µg/mL Carbenicillin to reach a starting OD_{600} of 0.10 - 0.15. The cell culture was incubated at 37 ℃ until the OD_{600} reach 0.8-0.9. The Keap1 overexpression was induced overnight with 1 mM IPTG (BioShop) at 22 ℃. The cells were later harvested after 18 hrs of growth with $OD_{600} > 2.0$. The bacterial cells were pelleted by centrifugation at 6,000 xg for 20 mins in a Beckman JLA-9.1000 rotor. The pellets were washed with 1 x Dulbecco's Phosphate Buffered Saline (PBS) and collected by centrifugation at 6, 000 xg for 20 mins in a Beckman JA 30.50 rotor, then stored at -20 ℃ until needed.

2.1.2.2 Purification of recombinant Human Keap1

Bacterial cells were thawed in 37 ℃ water bath and resuspended in 30 mL/g of Lysis buffer (50 mM Tris-HCl, 150 mM NaCl, 5 mM $MgSO_4$, pH 8.0 – 9.0). The suspension was mixed with 2 scoops of human lysozyme and incubated in 37 ℃ water bath for up to 30 mins. The suspension was then subjected to lysis by Avastin Homogenizer. The product after lysis was mixed with protease inhibitor,

100 µL PMSF per 10 mL of suspension and was adjusted with imidazole stock (1 M) as well as NaCl stock (5 M) to binding buffer (50 mM Tris-HCl, 500 mM NaCl, 10 mM Imidazole, pH 7.8) concentrations. Cellular debris and protein precipitation were removed by centrifugation at 40, 000 xg in JA 30.5 rotor at 4 °C for 30 mins. The resulting supernatant was adjusted to pH 7.8 using 1 N HCl stock and was then combined with 15 mL of binding buffer equilibrated Ni-Sepharose beads and incubated at 4 °C for about 2 hrs. The Ni-sepharose beads were poured back into a 50 mL column and washed by gravity using 150 mL of binding buffer followed by 500 mL wash buffer (50 mM Tris-HCl, 500 mM NaCl, 20 mM Imidazole at pH 7.8). The bound Keap1 was eluted over a 30 mins duration with 5 mL fractions by gravity flow with elution buffer (50 mM Tris-HCl, 500 mM NaCl, 750 mM Imidazole at pH 7.8). Protein containing fractions were determined by qualitative BioRad assay and pooled together. The eluted protein solution was desalted through being dialyzed in 2 L dialysis buffer (20 mM Hepes, 100 mM NaCl, 1 mM tris(2-carboxyethyl)phosphine/TCEP at pH 7.5) using a Spectra/Por 6 dialysis tubing with a molecular weight cut-off (MWCO) of 30 kDa overnight and then another 4 hrs.

The dialyzed protein sample was centrifugated to remove precipitation (40, 000 xg, 15 mins, at 4 °C). Then the protein sample was filtered through a 0.20 µm low protein binding membrane filter (Pall) before further purification process. The purified Keap1 protein sample fractions were analyzed by SDS-PAGE using 8 % gels with Coomassie Brilliant Blue R-250 staining. The purified Keap1 protein sample

was subjected to a BioRad assay to determine the protein concentration and was used for further experiments.

2.1.3 Preparation of recombinant Human Hsp90β

2.1.3.1 Overexpression of recombinant Human Hsp90β

The pET28a hHSP90β was transformed into Escherichia coli BL21 (DE3) cells (Novagen) and stored at -80 ℃. When doing a 1 L growth, bacteria were resuspended in 2 mL of 2x YT media containing 35 µg/mL Kanamycin as a starter culture. The starter culture was incubated at 37 ℃ for 5 hrs. Then the 2 mL culture was directly added to 200 mL LB media with 35 µg/mL Kanamycin per 1 L LB growth of bacteria. The 200 mL LB was grown overnight at 37 ℃. After the overnight growth, the bacterial cells were pelleted by centrifugation (6, 000 xg, 15 mins, room temperature, Avanti rotor JLA-

16, 250) and were resuspended into 1 L of LB media containing 50 µg/mL Carbenicillin to reach a starting OD_{600} of 0.09 - 0.12. The cell culture was incubated at 37 °C until the OD_{600} reach 0.8-0.9. The Hsp90β overexpression was induced overnight with 0.5 mM IPTG (BioShop) at 22 °C. The cells were later harvested after 18 hrs of growth with OD_{600} > 2.0. The bacterial cells were pelleted by centrifugation at 6,000 xg for 20 mins in a Beckman JLA-9.1000 rotor. The pellets were washed with 1 x Dulbecco's Phosphate Buffered Saline (D-PBS) and collected by centrifugation at 6, 000 xg for 20 mins in a Beckman JA 30.50 rotor, then stored at -20 °C until needed.

2.1.3.2 Purification of recombinant Human Hsp90β

Bacterial cells were thawed in 37 °C water bath and resuspended in 30 mL/g of Lysis buffer (50 mM NaH_2PO_4/Na_2HPO_4, pH 8.0 – 9.0). The suspension was mixed with 2 scoops of human lysozyme and incubated in 37 °C water bath for up to 30 mins. The suspension was then subjected to lysis by Avastin Homogenizer. The product after lysis was mixed with protease inhibitor, 100 µL PMSF per 10 mL of suspension and was adjusted with imidazole stock (1 M) as well as NaCl stock (5 M) to binding buffer (50 mM NaH_2PO_4/Na_2HPO_4, 400 mM NaCl, 6 mM Imidazole, pH 7.8) concentrations. Cellular debris and protein precipitation were removed by centrifugation at 40, 000 xg in JA 30.5 rotor at 4 °C for 30 mins. The resulting supernatant was adjusted to pH 7.8 using 1 N HCl stock and was then combined with 10 mL of binding buffer equilibrated Ni-Sepharose beads and incubated at 4 °C for

about 2 hrs. The Ni-sepharose beads were poured back into a 50 mL column and washed by gravity using 150 mL of binding buffer followed by 500 mL wash buffer (50 mM NaH_2PO_4/Na_2HPO_4, 400 mM NaCl, 20 mM Imidazole at pH 7.8). The bound Hsp90β was eluted over a 30 mins duration with 5 mL fractions by gravity flow with elution buffer (50 mM NaH_2PO_4/Na_2HPO_4, 400 mM NaCl, 300 mM Imidazole at pH 7.8). Protein containing fractions were determined by qualitative BioRad assay and pooled together. The eluted protein solution was desalted through being dialyzed in 2 L dialysis buffer (20 mM Hepes, 100 mM NaCl, 1 mM DTT at pH 7.5) using a Spectra/Por 6 dialysis tubing with a molecular weight cut-off (MWCO) of 30 kDa overnight and then another 4 hrs.

The dialyzed protein sample was centrifugated to remove precipitation (40, 000 xg, 15 mins, at 4 °C). Then the protein sample was filtered through a 0.20 μm low protein binding membrane filter (Pall) before further purification process. The His-tag of Hsp90β was not cleaved because it becomes unstable after the cleavage. The eluted protein was passed through the Superdex 10/300 GL 200 column (GE Healthcare) while being exchanged into 20 mM Hepes, 100 mM NaCl, 1 mM DTT at pH 7.5. The purified Hsp90β protein sample fractions were analyzed by SDS-PAGE using 8 % gels with Coomassie Brilliant Blue R-250 staining. The purified Hsp90β protein sample was subjected to a BioRad assay to determine the protein concentration and was used for further experiments.

2.1.4 Preparation of recombinant mouse STIP1

2.1.4.1 Overexpression of recombinant mouse STIP1

The pDEST17 plasmid (Invitrogen) TEV-STI in *E. coli* BL21 pLysS was added to 2 mL of 2x Yeast Extract Tryptone (2x YT) with 50 ug/mL Carbenicillin and 34 µg/mL Chloramphenicol as starting culture. The starting culture was grown, shaking at 37 °C for 5 hrs. 500 mL of LB (with 1 mL Micronutrients and 1.5 mM $MgCl_2$) was inoculated with 4 mL of the starter cultures and grown overnight at 37 °C. The next morning, the overnight culture was centrifuged and resuspended in fresh LB media (with 1.5 mM $MgCl_2$, 1 mM Micronutrients, 50 ug/mL Carbenicillin, 17 ug/mL Chloramphenicol) and set up 1 L LB at starting OD_{600} of 0.18. When the OD_{600} reached above 1.0, 4 hs later, the temperature was decreased to 22 °C, and 1 mM of IPTG was added. The cultures were incubated overnight for 20 hrs before they were harvested by centrifugation. Pellets were washed with PBS then stored at -20 °C yielding a total of 6.4g wet weight from 2 L.

2.1.4.2 Purification of recombinant mouse STIP1

Typically, 3 g of bacteria, representing 1 L were resuspended in steps with 30 mL of Lysis Buffer (50 mM Tris, 100 mM NaCl, 1 mM EDTA pH 8.2) and incubated at 37 °C for 15 mins. The Dounce homogenizer was used to assist complete resuspension and shearing of DNA. ½ of a Protease Inhibitor tablet (w/o EDTA) was added before lysis with the Avastin homogenizer. Following three passes through the Avastin homogenizer, the lysate was adjusted with Imidazole stock (1 M) and NaCl stock (5 M) to 10 mM and 300 mM final concentrations respectively, followed by pH adjustment to 7.6 with 1 N HCl. The lysate was clarified by centrifugation at 32,000 xg for 30 mins at 4 °C. The supernatant was combined with 10 mL of equilibrated Ni-Sepharose beads (Binding buffer) and incubated at room temperature (22 °C) for ~ 2 hrs. The Ni-sepharose was poured back into a large column and washed by gravity with 150 mL of Binding Buffer (25 mM Tris, 300 mM NaCl, 10 mM Imidazole, pH 7.8), followed by 200 mL of Wash Buffer (25 mM Tris, 300 mM NaCl, 20 mM Imidazole, pH 7.8). Bound protein was eluted over a 30 mins duration with 5 mL fractions by gravity flow with Elution buffer (25 mM Tris, 300 mM NaCl, 1 M Imidazole pH 7.8). Protein containing fractions determined by Qualitative BioRad assay were pooled together and dialyzed at 4 °C in 12 K MWCO

Spectra Por 2 overnight against Dialysis Buffer I (20 mM Hepes, 100 mM NaCl, 1 mM DTT at pH 7.5). The dialysis buffer was changed the next morning and continued for 3 hrs. After removing the sample from dialysis, the protein concentration was determined (BioRad Assay: 100 mg). 5 mg of His-tagged Tobacco Etch Virus (TEV) protease was added to remove the Histidine tag overnight at 22 ℃. And the proteins were analyzed by SDS-PAGE (8 %).

The following day, the protein sample was filtered (0.8 µm), and the Imidazole concentration was adjusted to 10 mM final with 1 M Stock and 300 mM NaCl with 5 M stock. To remove un-cleaved protein and Histidine tag, the sample was cycled three times through 5 mL of equilibrated Ni-sepharose beads (Binding buffer) over a 30-minute duration. The unbound protein was dialyzed into 20 mM Hepes pH 7.4, 150 mM NaCl for 6 hours, refreshed and then overnight. After dialysis, the protein sample was filtered with 0.8 µm and 0.45 µm filters, and a BioRad assay revealed a typical final concentration to be 2.5 mg/mL with a yield of ~70 mg for a 1-liter LB media growth.

2.2 Nuclear Magnetic Resonance (NMR) Spectroscopy

All NMR experiments were performed on Varian Inova 600-MHz spectrometers (UWO Biomolecular NMR Facility) at 25 °C in 50 mM sodium phosphate, 100 mM NaCl, 1 mM DTT, and 10 % (v/v) D_2O (Cambridge Isotope Laboratories). All NMR data were processed with NMRpipe (Delaglio et al., 1995), and the spectra were analyzed with NMRviewJ (Johnson, 2004). For the NMR experiments, 650 μL of 50 μM ^{15}N-labelled Kelch was combined with 650 μL of 0 μM, 25 μM, 50 μM, and 100 μM Hsp90β at 1:0, 1:0.5, 1:1 and 1:2 molar ratio (Kelch: Hsp90β) point was reached. ^{1}H-^{15}N HSQC spectra were collected for each sample combination.

2.3 Isothermal Titration Calorimetry

The ITC experiments were performed on a MicroCal™ VP-ITC. The protein samples were dialyzed into 50 mM sodium phosphate, 100 mM NaCl, and 1 mM DTT at pH 7.0 or 20 mM Hepes buffer. For the titrations, purified degased Kelch and Hsp90β were prepared to 600 μM and 25 μM, respectively. Kelch was loaded into the 1.36 - mL cell and Hsp90β was loaded into the syringe (600 μL). Titrations were performed at 4 °C starting with an initial injection of 3 μL, followed by 29 injections of 5 μL, with a spacing of 200 s. The sample cell was stirred at 300 rpm throughout the experiment. The buffer blank was performed under the same condition and showed negligible heats of binding. All protein concentrations were determined using Bradford assays.

2.4 Fluorescently labeling proteins

Purified Proteins such as STIP1, Keap1, Hsp90β, Kelch were subjected to fluorescein labeling according to the experiment design. About 0.5 mg of Fluorescein-5-Maleimide dye Invitrogen F150 (Thermo Fisher Scientific) was dissolved in 100 µL DMSO as dye stock for the protein fluorescence labeling process. Protein samples were mixed with TCEP at 100 µM and incubated for about 15 mins at room temperature (22 °C) to reduce the intra- and inter-cellular disulfide bonds. Then per 1 mL of the 100 µM reduced protein sample was mixed with 3 µL of the 100 µM fluorescein dye stock to reach a dye concentration of 0.3 µM. The mixture of protein sample was incubated for up to 2 hrs at room temperature (22 °C) in the dark. After incubation, the labeling reaction was quenched with 23.8 mM 2-Mercaptoethanol/β -Me and transferred into 12-14 kDa MWCO dialysis tubing to be dialyzed against 2 L Hepes buffer (20 mM Hepes, 100 mM NaCl, 23.8 mM β -Me, pH 7.4) for overnight and refreshed buffer for another 4 hrs in the dark.

The next day, the dialyzed protein sample was collected and loaded to the PD10 column to complete the removal of unreacted dye. 0.5 -1 mL fractions were collected and subjected to readings at the absorbance of 280 nm to check the protein amount. And the protein concentration and dye labeling efficiency were calculated according to Thermo scientific dye manual:

$$\text{Protein Concentration (M)} = \frac{\text{Absorbance at 280nm} - (\text{Absorbance at 495nm x CF})}{\varepsilon}$$

CF = Correction factor $= \frac{\text{Absorbance at 280nm}}{\text{Asorbance at 495nm}}$ = 0.3000

ε = protein molar extinction coefficient = 68,000 M^{-1} cm^{-1}

Moles fluorescein per mole protein $= \frac{\text{Absorbance at 495nm}}{\varepsilon \text{ x protein concentration (M)}}$

The final labeled protein concentration was also determined with Bio-Rad protein assay to double-check the calculation. And the fluorescently labeled protein samples were used for protein-binding assay for fluorescein readings.

2.5 Protein – Binding Assay

All protein-binding assay was performed using Falcon 96-well black polystyrene plates. All purified protein samples were in 20 mM Hepes, 100 mM NaCl, and 1mM $MgCl_2$ at pH 7.4. The 96-well black polystyrene plates were treated with 100 µL poly-L-lysine per well to pre-coat the wells for 30 mins at 37 °C to ensure the protein can be better immobilized onto the wells. Prepared unlabeled protein (usually at 2 µM or 20-25 µg in 100 µL volume) were incubated in the wells overnight at 4 °C or for 30 mins at 37 °C. After the unlabeled protein was immobilized, the excessive protein was flicked off into the sink. The non-specific sites on the wells that were blocked with blocking solution (1 % gelatin, 100 mM glycine in 1 x PBS) for 1 hr at room temperature (22 °C). After blocking, the wells were subjected to 1 x T-PBS (0.05 % Tween) wash for three times. And then the plate was incubated with increasing concentrations of fluorescently labeled proteins (for example, STIP1, Hsp90β, Kelch and

Keap1) for 1 hr at room temperature (22 °C). Then the plate was subsequently washed extensively with 1 x T-PBS (0.05 % Tween). Following the wash, the fluorescence signal was measured at excitation and emission wavelengths of 485/535 nm, respectively.

Upon analyzing the data, we use the following method to estimate the binding affinity of protein-protein interaction. Referencing the analysis of binding of proteins proposed by Scatchard (1949) and literature about protein-protein interactions (Berson & Yalow, 1959; Feldman, 1972; Rosenthal, 1967) Binding between a receptor (R) and a ligand (L) could be represented as:

$$L + R \underset{k_{off}}{\overset{k_{on}}{\leftrightharpoons}} LR$$

The kinetics of binding between the ligand and receptor are often described by two rate constants, the estimate association rate constant of ligands binding to the receptor (k_{on}), and the disassociation rate constant of ligand disassociating from the receptor (k_{off}) (units are M^{-1} s^{-1} and s^{-1}). Moreover, K_d is defined as k_{off}/k_{on}. (Guldber & Waage, 1864; Hulme & Treventhick, 2010; Hunter & Cochran, 2016).

$$k_{on}[L][R] = k_{off}[LR]$$

$$K_a = \frac{kon}{koff} = \frac{[LR]}{[L][R]}$$

$$\frac{1}{Ka} = \frac{koff}{kon} = \frac{[L][R]}{[LR]} = K_d$$

Since the total receptor concentration equals the sum of the concentration of free receptor [R] and the concentration of bound state [LR] complex,

$$[R]_{total} = [R] + [LR]$$

Through rearrange the equations, we can derive the following equation:

$$[R]_{total} = \frac{[LR]Kd}{[L]} + [LR]$$

$$\frac{[LR]}{[R]\ total} = \frac{[L]}{[L]+Kd}$$

Since $[L]_{total} = [L]_{free} + [LR]$, we have $[L]_{free} = [L]_{total} - [LR]$. If we have $[R]_{total} << [L]_{total}$, then we have $[LR] << [L]_{total}$. Therefore, we can estimate that $[L]_{total} \approx [L]_{free}$. Under this circumstance, when the fraction bound [LR] and $[R]_{total}$ reach 1/2, which is the midpoint before saturating the binding between ligand and receptor, K_d equals to the $[L]_{total}$ at this point.

2.6 Animal Model

2.6.1 WT & ⊿TPR1 Mice

Our collaborator Dr. Marco Prado generously provided both the mouse models generated by the Prado lab. The *STIP1*$^{\Delta TPR1}$ mouse line (Lackie et al., in preparation; Razzaq, 2018) expresses hypomorphic STIP1 lacking the TPR1 domain (Lackie et al., in preparation). This mouse model was initially developed to investigate the function of the TPR1 domain in molecular chaperone networks, which can provide better insights into co-chaperone STIP1 in mammals. The STIP1 with the deletion of the TPR1 domain led to a significant reduction in levels of several Hsp90 co-chaperones and STIP1/Hsp90 client-proteins (Lackie et al., in preparation; Razzaq, 2018).

2.7 Cell tissue culture

2.7.1 SN56 Cell Line

And the murine Septal Neuronal cell (SN56) provided by Bruce Wainer, Emory University was used to generate STIP1 knockouts (Lackie et al., in preparation). STIP1 expression was eliminated with CRISPR-Cas 9 (Clustered Regularly Interspaced Short Palindromic Repeats) editing system. The optimized CRISPR Design Software (Http://crispr.mitedu/) was used to design guide RNAs for the mouse STIP1 gene to transfect SN56 cells. Specifically, the gene sequence was STIP1 Top 1:

5’CACCGGTAGTCTCCTTTCTTGGCGT 3’ and STIP1 Bottom 1 5’AAACACGCCAAGAAAGGAGACTACC 3’. The guide The SN56 cells were incubated in a complete median containing 1 mM of dbc AMP (Sigma-Aldrich), a cAMP analog, for 48 hrs.

2.8 Western Blotting

Mice were decapitated, and brains were rapidly excised on ice. The brains were dissected into the cortex on ice and flash frozen on dry ice before transfer to -80 °C. Protein extraction and western blot were carried out as previously described (Beraldo et al. 2013; Martins-Silva et al., 2011).

Western Blot was done by standard technique after peptide separation on 12 % Tris-tricine SDS-PAGE and electrotransfer to polyvinyl difluoride membrane (Beraldo et al., 2013). Protein from mouse brain tissue, SN56 cells were extracted using RIPA buffer (50 mM Tris, 150 mM NaCl, 1 % Triton X-100, 0.5 % Sodium Deoxycholate, 0.1 % SDS, pH 8.0) including protease inhibitors (Protease Inhibitor Cocktail Set 3-EMD Millimore, Burlington, MA) and phosphatase inhibitors (Phosphatase Inhibitor Cocktail Set 5-EMD Millimore, Burlington, MA), on ice for 15 mins. Protein extracts were centrifuged at 12, 000 xg at 4 °C for 20 mins and the supernatant was collected and quantified with BioRad protein assay methods. 5 – 30 µg of total proteins were loaded onto Bolt 4 – 12 % Bis-Tris gel. The antibodies used were anti-STIP1 (rabbit polyclonal 1:5000, in-house antibody), anti-Keap1 (1:500, ab218815, Abcam, Cambridge, UK), anti-Actin (1: 10,000, Chemicon, CA) anti-Nrf2 (rabbit polyclonal 1: 1,000,

PA1828, Boster, Pleasanton, CA). Images were acquired using the FluorChem Q system from Alpha Innotech and analyzed using the ChemiDoc XRS system software (BioRad).

2.9 Quantitative Real-Time Polymerase Chain Reaction

For Real-Time quantitative PCR (RT-qPCR), the RNA was isolated from the brain tissues of the *STIP1*$^{\Delta TPR1}$ and WT mouse line using Aurum Total RNA kit for fatty and fibrous tissue (Bio-Rad, Hercules, CA, USA). The same method was used to isolate RNA from the tissue culture of SN56-WT and SN56-STIP1-KO cell line. Quantification and quality analysis of RNA in the extracted samples was done by microfluidic analysis (Agilent Technologies' Bioanalyzer). First-strand cDNA was synthesized using the iSCRIPT cDNA SYNTHESIS KIT from BioRad. cDNA was subsequently subjected to RT-qPCR on a CFX-96 Real-Time System (Bio-Rad) using the iQ SYBR Green Supermix (Bio-Rad). For each experiment, a non-template reaction was used as a negative control. The gene sequence used for Keap1 was Top 1: 5’ GGATGGCAACACTGACTCCA 3’ and Keap1 Bottom 1 5’ GTCCCGCTCTGGCTCATATC 3’. The melting temperature for the Keap1 primer was 87.5 ℃. The gene sequence used for Nrf2 was Top 1: 5’ GGACATGGAGCAAGTTTGGC 3’ and Nrf2 Bottom 1 5’ CCAGCGAGGAGATCGATGAG 3’. The melting temperature for the Nrf2 primer was 82 ℃. Also, the absence of DNA contaminants was assessed in reverse transcription-negative samples and by melting-

curve analysis. Relative quantification of gene expression was done with the $\Delta\Delta CT$ method using β-actin gene expression to normalize the data.

2.10 Statistical Analysis

Statistical analysis for all Western blots, RT-qPCR, and Protein-binding assay was performed using GraphPad Prism 5 Software (Version 5.0 for Windows, La Jolla California USA). All results were expressed as mean +/- standard error (SEM) and analyzed with unpaired t-tests, one-way ANOVA or two-way ANOVA (when comparing control and experimental conditions in the various immunoblots and protein-binding assays). Significance levels are indicated using asterisks, where **** is $p<0.0001$, *** is $p<0.001$, ** is $p<0.01$, * is $p<0.05$.

CHAPTER 3: RESULTS

3.1 Preparation of recombinant protein samples

3.1.1 The Kelch Domain of Human Keap1

The protocol to overexpress the Kelch domain of Human Keap1 was established previously in the Choy lab (Khan, 2014). The growth conditions were optimized in both LB media and M9 minimal media to achieve the optimal protein expression level. The yield of the bacterial pellet was typically 4 - 5g (wet-weight) from a 1-liter LB culture and 3 - 4 g from a 1-liter M9 media culture. By using the purification procedures described in section 2.1.1.2 in Chapter 2, ~30 mg of Kelch protein could be obtained from a 1-liter LB growth and ~ 25 mg of ^{15}N-labeled Kelch could be obtained from a 1-liter M9 minimal media culture typically. The result of the SDS-PAGE analysis and the FPLC elution profile shown in Figure 3 demonstrated a single peak representing the pure Kelch protein as the final product.

According to multiple pieces of literature, Hsp90β was often stored in Hepes buffer, which ensured protein to remain more stable (Kundrat & Regan, 2014; Lorenz et al., 2014; Radli et al., 2017). Therefore, we decided to dialyze Kelch protein into Hepes buffer for storage at 4 °C for future experiments. The protein stability was also monitored over time. As shown in Figure 4, the Kelch sample remained stable for at least 7 days at 4 °C in Hepes buffer.

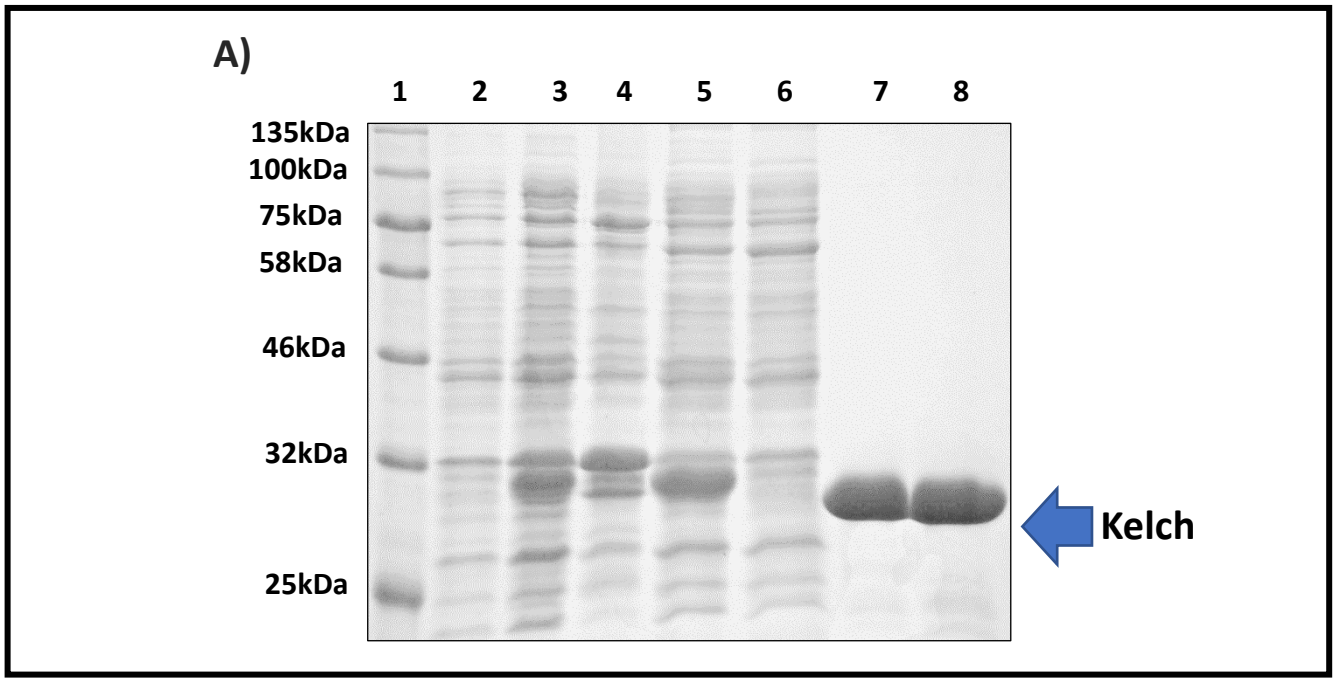
A)
1
2
3
4
5
6
7
8
135kDa
100kDa
75kDa
58kDa
46kDa
32kDa
25kDa
Kelch

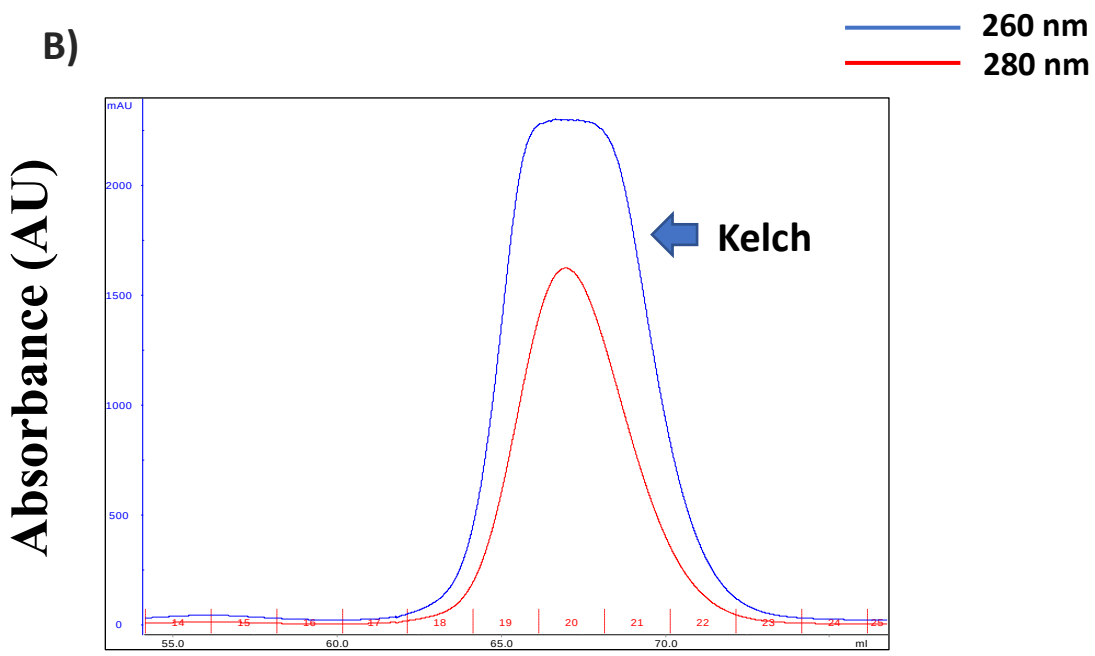

Figure 3

Figure 3. The Purification of the Kelch domain of Keap1. A) 12 % SDS-PAGE Analysis of the process purification of Kelch following the previously established protocol. Kelch domain of Human Keap1 was expressed from the plasmid pET15b in *E. coli* BL21 (DE3) cells with M9 minimal media. Lane 1- Protein molecular weight ladder; Lane 2- total protein of *E. coli* collected before overexpressing Kelch; Lane 3- total protein of *E. coli* collected after overexpressing Kelch; Lane 4-total protein from insoluble *E. coli*; Lane 5-total protein from soluble *E. coli*; Lane 6- total proteins that were not bound to Ni-sepharose beads; Lane 7- total protein size exclusion chromatography; Lane 8-the final purified Kelch. **B)** Elution profile from Size exclusion chromatography (HiLoad Superdex75) Slow Flow column (1 mL). Absorbance at 260 nm, 280 nm are shown. One major peak indicated the pure Kelch protein.

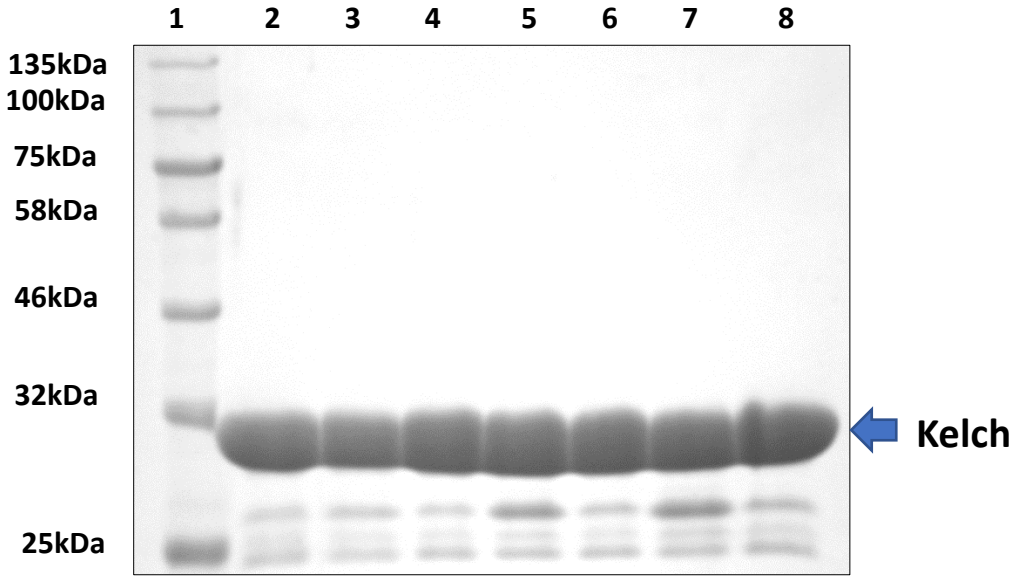

Figure 4

Figure 4. The Protein stability of the Kelch domain of Human Keap1. 12 % SDS-PAGE Analysis of Kelch domain of Human Keap1 in Hepes buffer (20 mM Hepes, 100 mM NaCl, 1 mM DTT at pH 7.5) which was used in most of the experiments. Lane 1- Protein molecular weight ladder; Lane 2- purified Kelch stored at 4 ℃ for 1 day; Lane 3- purified Kelch stored at 4 ℃ for 2 days; Lane 4- purified Kelch stored at 4 ℃ for 3 days; Lane 5- purified Kelch stored at 4 ℃ for 4 days; Lane 6- purified Kelch stored at 4 ℃ for 5 days; Lane 7- purified Kelch stored at 4 ℃ for 6 days; Lane 8- purified Kelch stored at 4 ℃ for 7 days.

3.1.2 Full-length Human Keap1

The procedures used to overexpress and purify human Keap1 was adapted from the published protocols in the literature (Eggler, 2005; Ogura, 2010). The growth conditions in LB media were optimized to achieve a higher protein expression level. Using the expression protocol outlined in section 2.1.2.2 in Chapter 2, the yield of the bacterial pellet was typically 6 - 7 g (wet weight) from a 1-liter LB culture.

Even though the full-length Keap1 could be overexpressed successfully in *E. coli*, the solubility of the protein is low. This may be because human Keap1 is a cysteine-rich protein, which contains 27 cysteines. Therefore, the protein is sensitive to oxidation, making it highly unstable and prone to precipitation (Saito, 2016). This property of Keap1 made the protein challenging to be kept in soluble form during and after the purification process. The typical yield of Keap1 was ~5.0 mg from 1-liter LB media growth, and the purified protein was immediately used for experimental purposes due to its limited stability.

Figure 5 showed the product of purification at each step, and the final product of Keap1 has two molecular weight indicating two different proteins. We sent the SDS-PAGE gel to MALDI mass spectrometry analysis to identify these two proteins (MALDI Mass Spectrometry Facility, London Regional Proteomics Centre, Western University). The result showed that the lower molecular weight band was the purified Keap1 while the higher molecular weight band was a contaminant. Further

optimization of the purification protocol is required to reduce the contamination.

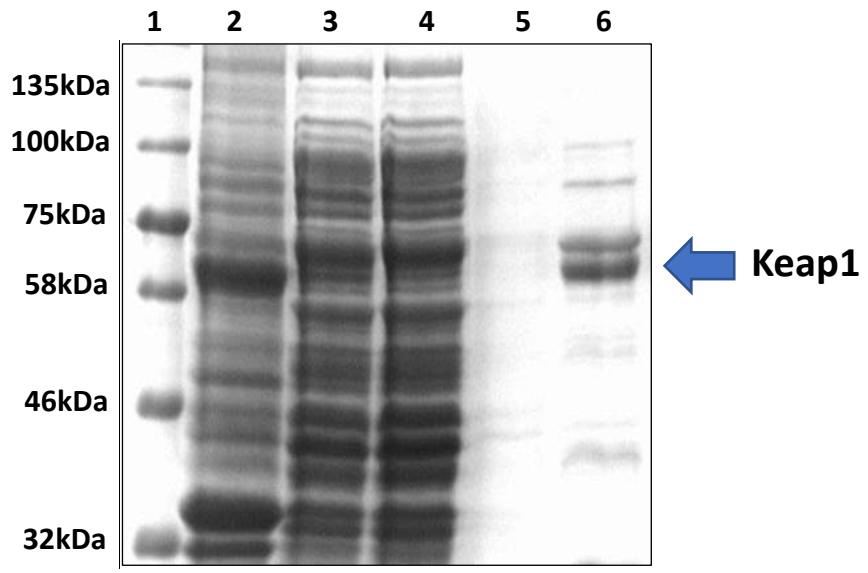

Figure 5

Figure 5. The Purification of recombinant human Keap1. 8 % SDS-PAGE Analysis of purified Keap1: Lane 1 - Protein molecular weight ladder; Lane 2 - total protein from insoluble *E. coli*; Lane 3 - total protein from soluble *E. coli*; Lane 4 - total protein collected from flow-through after washing beads; Lane 5- total protein collected from first wash of the beads; Lane 6 - the final purified Keap1 (the lower band).

3.1.3 Full-length Human Hsp90β

The protocols for overexpressing and purifying recombinant full-length Human Hsp90β was established in the Choy lab and literature (Maciejewski, 2017; Radli et al., 2017). The yield of the bacterial pellet was typically 4 - 5 g (wet weight) from a 1-liter LB culture.

As shown in Figure 6, Hsp90β was overexpressed in *E. coli* after IPTG induction. The protein remained soluble during the purification process. The wash buffer used was effective in removing contaminated proteins non-specifically bound to the Ni - sepharose beads. As the His-tagged Hsp90β was eluted off the beads, it was rather pure already. Then the protein was dialyzed to the proper buffer (20 mM Hepes, 150 mM NaCl, 1 mM $MgCl_2$, pH 7.4) in which Hsp90β was relatively stable. The his-tag was then removed from Hsp90β by the addition of thrombin.

The final step of purification included passing Hsp90β through a size exclusion column. Figure 6 B shows the FPLC elution profile. Peak #1 corresponded to ~ 400 - 700 kDa protein, which was likely to be the aggregated form of Hsp90β as it was prone to aggregation. Peak #2 represented a protein species of molecular weight ~ 160 - 170 kDa, which matched with the molecular weight of Hsp90β dimer. Peaks #3 and 4 were proteins species of molecular weight ~ 13 - 35 kDa, which were likely to be the degraded version of Hsp90β without C-terminal. The SDS-PAGE shown in Figure 6 A shows that after this final purification step, the Hsp90β was purified to near homogeneity. The typical yield of Hsp90β was about 6 - 8 mg from a 1-liter LB media culture.

Hsp90β as a chaperone was prone to aggregation because structurally, it contains a significant amount of hydrophobic surface areas. Figure 7 showed that Hsp90 becomes significantly degraded after a 3~5-day period. Because of this, we usually utilize freshly purified Hsp90β that was no more than 3-days old for our experiments.

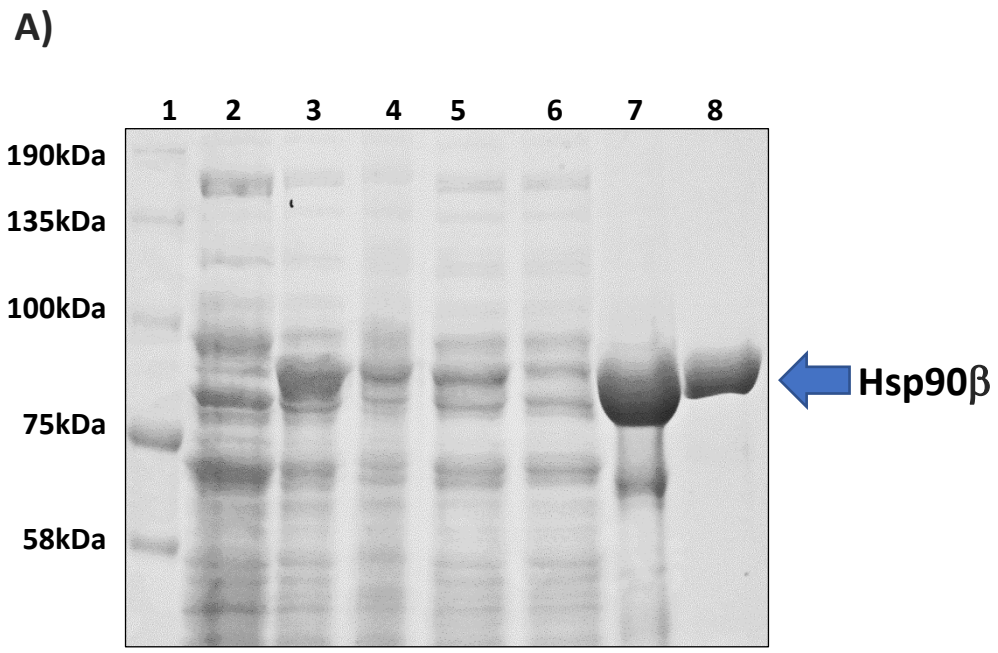

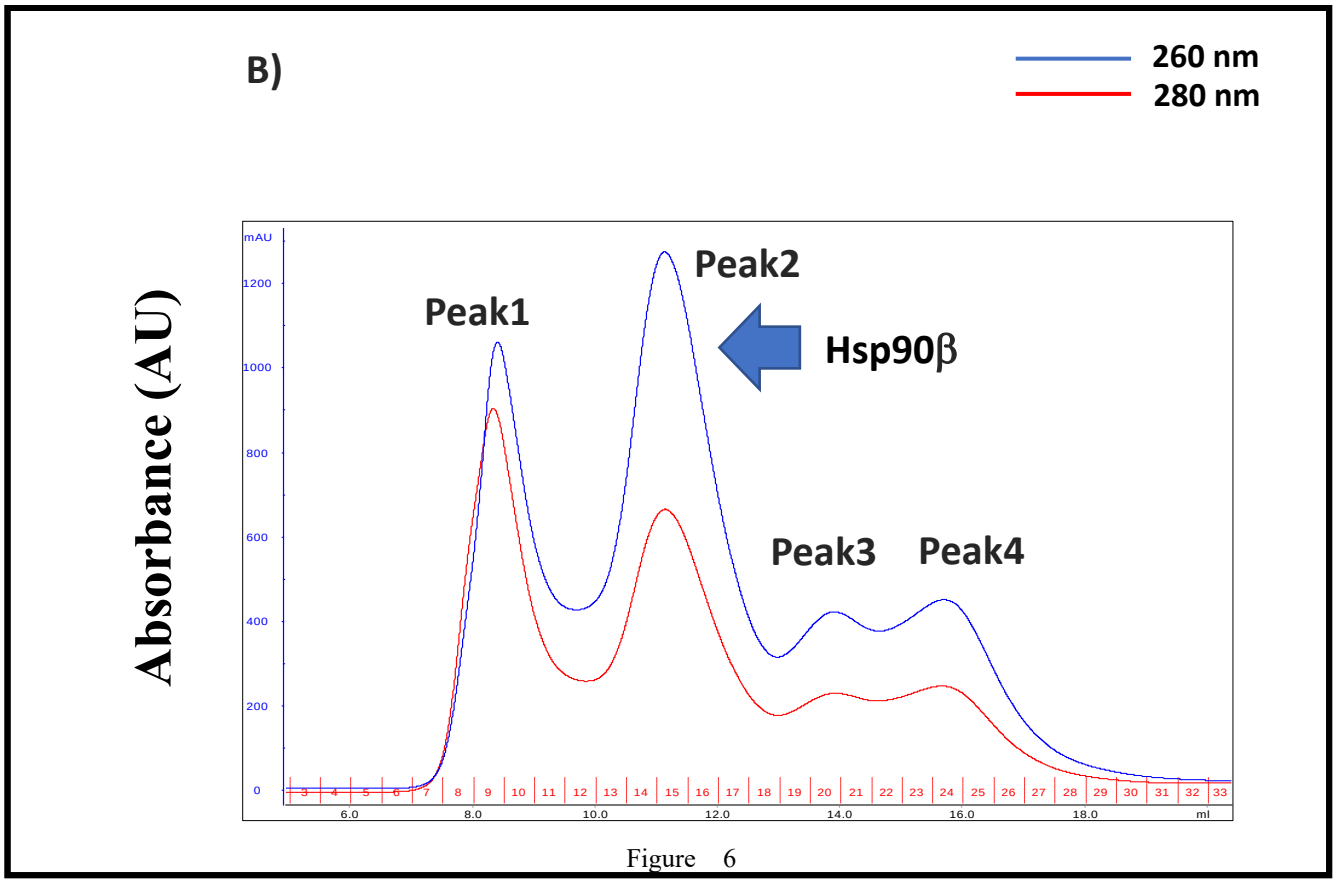

Figure 6. The Purification of recombinant human Hsp90β. A) 8 % SDS-PAGE gel of purified Hsp90β: 1- Protein molecular weight ladder; 2- total protein of *E. coli* collected before overexpressing Hsp90β; 3- total protein of *E. coli* collected after overexpressing Hsp90β; 4-total protein from insoluble *E. coli*; 5- total protein from soluble *E. coli*; 6- total proteins that were not bound to Ni-sepharose beads; 7- total protein size exclusion chromatography; 8-the final purified Hsp90β. **B)** Size exclusion chromatography (Superdex 200) of Hsp90β.

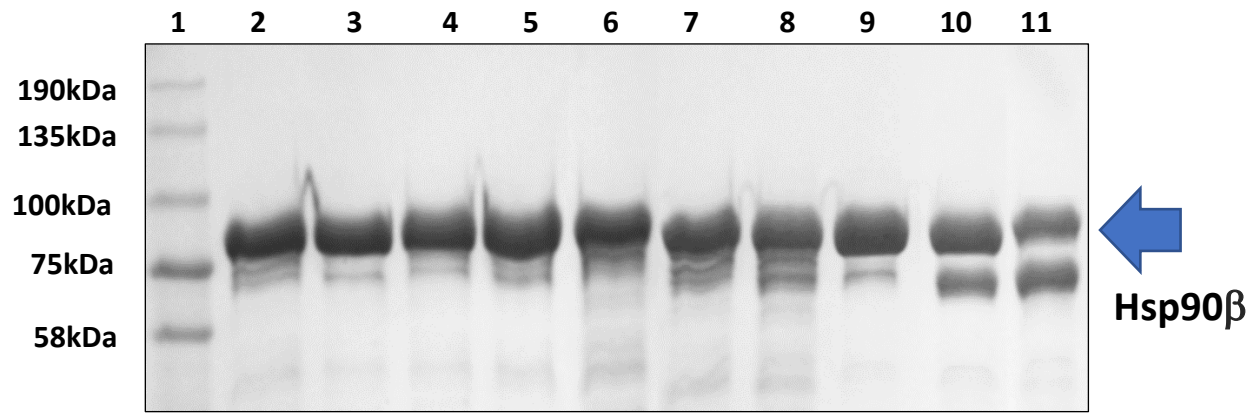

Figure 7

Figure 7. The Protein stability of recombinant human Hsp90β. 8 % SDS-PAGE Analysis of recombinant human Hsp90β in Hepes buffer (20 mM Hepes, 100 mM NaCl, 1 mM DTT at pH 7.4) which was used in most of the experiments. The profile shows that Hsp90β degrades much more significantly starting from the fourth day of being stored at 4 ℃. Lane 1- Protein molecular weight ladder; Lane 2- purified Hsp90β stored at 4 ℃ for 1 day; Lane 3- purified Hsp90β stored at 4 ℃ for 2 days; Lane 4- purified Hsp90β stored at 4 ℃ for 3 days; Lane 5- purified Hsp90β stored at 4 ℃ for 4 days; Lane 6- purified Hsp90β stored at 4 ℃ for 5 days; Lane 7- purified Hsp90β stored at 4 ℃ for 6 days; Lane 8- purified Hsp90β stored at 4 ℃ for 7 days; Lane 9- purified Hsp90β stored at 4 ℃ for 8 days; Lane 10- purified Hsp90β stored at 4 ℃ for 9 days; Lane 11- purified Hsp90β stored at 4 ℃ for 10 days.

3.1.4 Full-length mouse STIP1

The overexpression and purification protocols of recombinant full-length mouse STIP1 established in the Choy lab (Maciejewski, 2017) were used to prepare the STIP1 samples. Using the expression protocols outlined in Section 2.1.4.2 in Chapter 2, the yield of the bacterial pellet was typically 3 - 4 g (wet weight) from a 1-liter LB culture.

As it was shown in Figure 8, STIP1 was well overexpressed in *E. coli*. And the protein remains soluble during the purification process. Results of the SDS-PAGE analysis (Figure 8) shows that after the final purification step, STIP1 was purified to near homogeneity. The typical yield of STIP1 was about 70 mg from a 1-liter LB media culture.

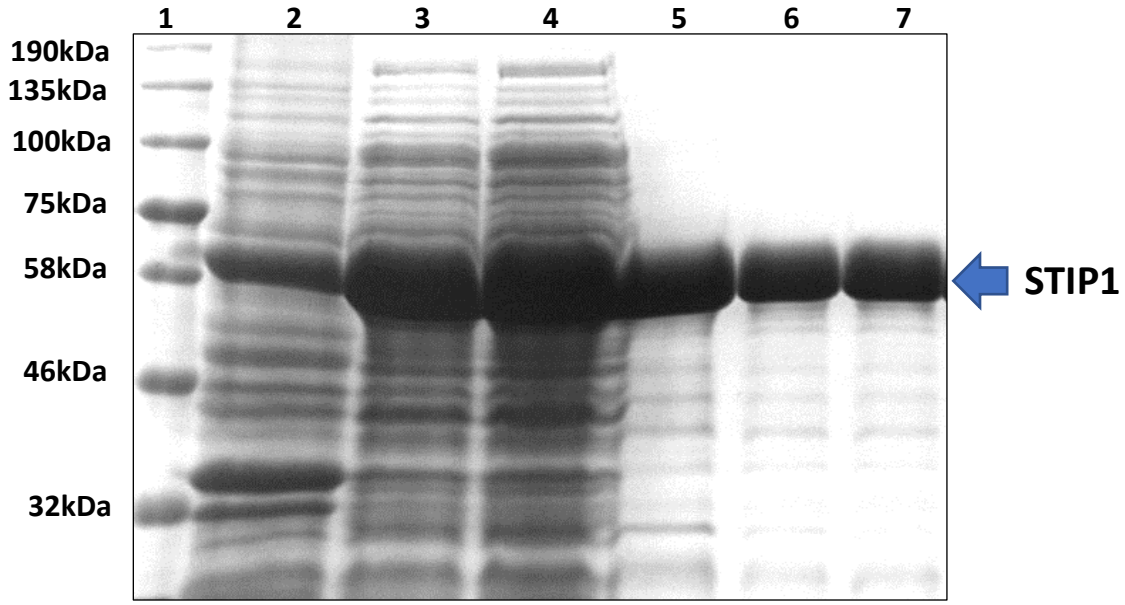

Figure 8

Figure 8. The Purification of recombinant mouse STIP1. 8 % SDS-PAGE Analysis of purified STIP1: Lane 1- Protein molecular weight ladder; Lane 2-total protein from insoluble *E. coli*; Lane 3-total protein from soluble *E. coli*; Lane 4-total protein from unbound; Lane 5-total protein eluted; Lane 6- STIP1 after cleavage of His-tag by TEV protease; Lane 7- the final purified STIP1.

3.2 Hsp90β binds the Kelch domain of Keap1

3.2.1 NMR titrations show that Hsp90β interact with the Kelch domain of Keap1

In a recent high throughput study of the chaperone-cochaperone-client interaction network in human cells, Taipale et al. uncovered that many proteins with Kelch domains could associate with the Hsp90β chaperone complexes. For instance, protein KLHL38 (Kelch-like Family Member 38), which contains a Kelch domain like Keap1, was found to co-immunoprecipitate with Hsp90β (Taipale et al., 2014). This finding suggested that proteins belonging to the Kelch-Like family could be a new pool of clients of Hsp90β. This information also led us to speculate that the Kelch domain of human Keap1 protein is responsible for interacting with Hsp90β. Therefore, we started determining whether Keap1 is a client of protein of Hsp90β through investigating the interaction between the Kelch domain and Hsp90β.

NMR spectroscopy is a powerful tool for investigating protein structure and interactions. To probe the interaction between Hsp90β and the Kelch domain of Keap1, we have performed ^{1}H-^{15}N Heteronuclear Single Quantum Coherence (HSQC) NMR experiments on ^{15}N-labeled Kelch domain of Keap1 in the presence of different molar ratios of Hsp90β. ^{1}H-^{15}N HSQC spectrum is frequently referred

to as the ‘fingerprint’ of a protein. Each peak in the HSQC spectrum represents the backbone amide moiety of an amino acid in the protein. The chemical shifts and intensity of a peak are highly dependent on the chemical environment and mobility of that particular residue. Therefore, comparing the HSQC spectrum of a protein in the absence and presence of a binding partner will allow us to identify the binding interface with residue-specific resolution (Cala et al., 2014; Meyer & Peters, 2003).

We first started with acquiring the HSQC spectra of the ^{15}N-labeled Kelch domain of Keap1. This served the purpose of ensuring the Kelch protein we purified was pure and well-folded. Figure 9A) shows a representative ^{1}H-^{15}N HSQC spectrum of ^{15}N-labeled Kelch. The spectrum contains well-dispersed peaks and matches with the spectra of Kelch previously collected by the lab under the same conditions, indicating that the purified Kelch sample was pure, and the protein adopted a well-folded conformation (Khan, 2014).

We then proceeded to perform the HSQC experiments on different mixtures of ^{15}N-labeled Kelch and unlabeled Hsp90. Even though the Kelch domain of Keap1 is relatively soluble, Hsp90□ protein is prone to precipitation. In order to obtain high-quality NMR data of the Kelch-Hsp90□ complex, we have performed the HSQC experiments using different protein concentrations, buffer conditions, and molar ratios of the two proteins. What we found was that Hsp90β could only remain soluble at a concentration lower than 100 μM in Hepes buffer. Thus, we went further to acquire the HSQC spectra of ^{15}N-labeled Kelch in the presence of unlabeled Hsp90β at 1:0 (50 μM: 0 μM), 1: 0.5

(50 μM: 25 μM), 1:1 (50 μM: 50 μM) and 1:2 (50 μM: 100 μM) molar ratios (Figure 10). Notably, since Hsp90β was not ^{15}N-labeled, it was not visible in the HSQC spectra we collected.

Figure 10 shows that many HSQC peaks of ^{15}N-labeled Kelch diminished significantly as more and more unlabeled Hsp90β was added. It is noteworthy that the NMR signal intensities a protein decrease with increasing molecular tumbling time (Frueh et al., 2014; Gell, 2002; Jiang et al., 2017). Because of this, the NMR signals of a low molecular weight protein are much stronger in intensity compared to the signals of a high molecular weight protein or complex with the same concentration. Since Hsp90β exists as a dimer in the native state with a molecular weight of 164 kDa, when a 32 - kDa Kelch molecule binds to an Hsp90 dimer, it becomes part of a large molecular complex with molecular weight about 200 kDa. At this molecular weight, the signals coming from the ^{15}N-labeled Kelch become too weak to be observed. Therefore, the significant reduction in peak intensities of Kelch upon the addition of Hsp90 indicates the interaction of these two proteins. We should point out that there were peaks of ^{15}N-labeled Kelch that remained observable even in the presence of two molar ratios of Hsp90. Based on the chemical shift assignments of Kelch published by the lab previously (Khan, 2013), it seems that many of these signals were originated from the amino acids in the flexible loops of the Kelch structure. These loops may remain flexible upon binding Hsp90□.

In principle, we could also perform HSQC experiments with ^{15}N-labeled Hsp90 and unlabeled Kelch. However, since Hsp90β exists as a dimer in the native state with a molecular weight of 164 kDa, it is too large to give NMR spectra with good quality.

^{1}H-^{15}N HSQC Spectra of ^{15}N-labelled Kelch domain of Keap1

A)

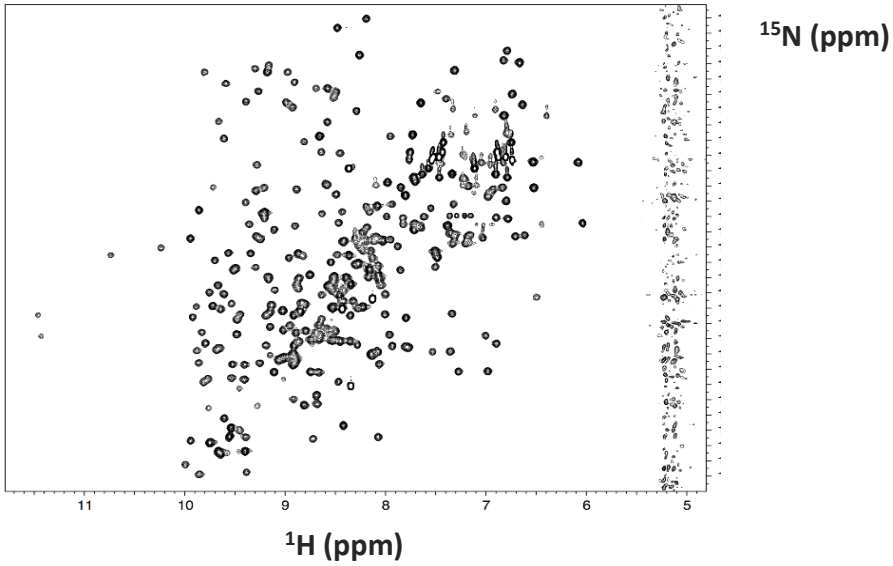

B)

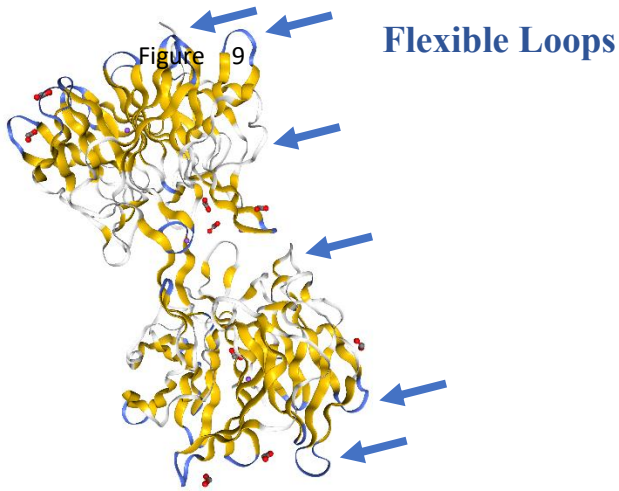

Figure 9

Figure 9. The Kelch Structure. A) The two-dimensional ^{1}H-^{15}N HSQC spectrum of ^{15}N-labeled Kelch domain of Keap1 (250 µM ^{15}N-Kelch, 50 mM Sodium phosphate, 100 mM NaCl, 1 mM DTT, pH 7.0 at 25 °C). **B) Structure of the Kelch domain of human Keap1** (Blue and white represents the flexible loops; Yellow represents the structured blades of β – propellers). Image from the RCSB PDB (www.rcsb.org) of PDB ID 6ROG (Sethi, R. et al., 2019).

A) ^{1}H-^{15}N HSQC Spectrum of ^{15}N-labelled Kelch (50 µM)

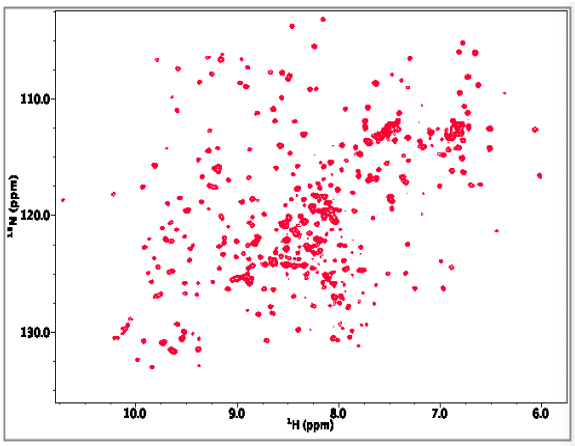

B) ^{1}H-^{15}N HSQC Spectrum of ^{15}N-labelled Kelch (50 µM) with Hsp90 (25 µM)

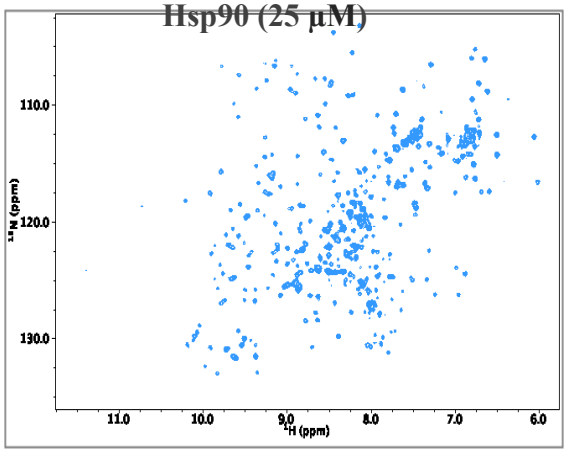

C) ^{1}H-^{15}N HSQC Spectrum of ^{15}N-labelled Kelch (50 µM) with Hsp90 (50 µM)

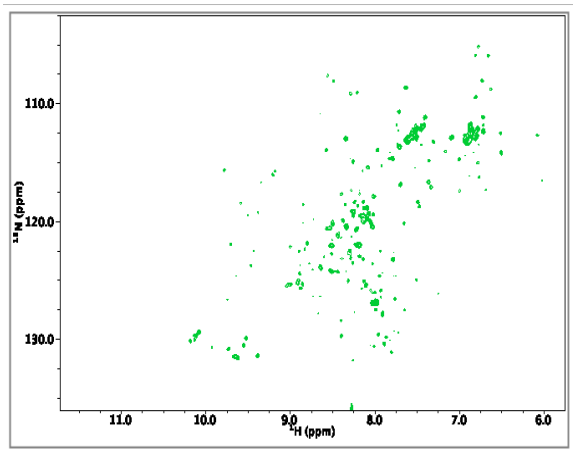

D) ^{1}H-^{15}N HSQC Spectrum of ^{15}N-labelled Kelch (50 µM) with Hsp90 (100 µM)

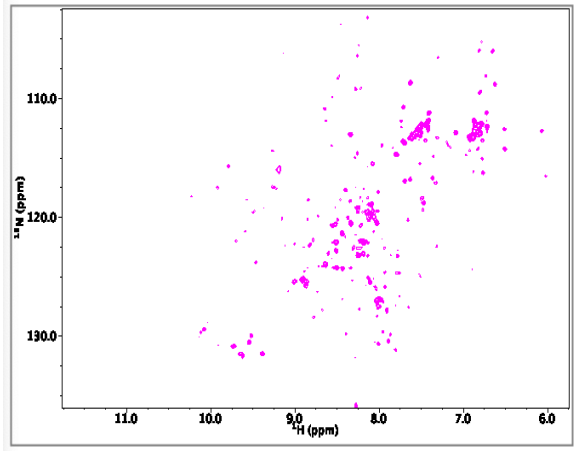

Figure 10

Figure 10. The signal intensity of the ^{15}N-labeled Kelch domain gradually reduces as an increasing amount of Hsp90β is added to the solution. A) the ^{1}H-^{15}N HSQC spectrum of ^{15}N-labeled Kelch domain (50 µM ^{15}N-Kelch, 20 mM Hepes, 150 mM NaCl, pH 7.4, at 25 °C) **B)** the ^{1}H-^{15}N HSQC spectrum of ^{15}N-labeled Kelch domain with partial residues disappeared as they bind to Hsp90β (50 µM ^{15}N-Kelch, 25 µM Hsp90β, 20mM Hepes, 150 mM NaCl, pH 7.4, at 25 °C) **C)** the ^{1}H-^{15}N HSQC spectrum of ^{15}N-labeled Kelch domain with partial residues disappeared as they bind to Hsp90β (50 µM ^{15}N-Kelch, 50 µM Hsp90β, 20 mM Hepes, 150 mM NaCl, pH 7.4, at 25 °C) **D)** the ^{1}H-^{15}N HSQC spectrum of ^{15}N-labeled Kelch domain with partial residues disappeared as they bind to Hsp90β (50 µM ^{15}N-Kelch, 100 µM Hsp90β, 20 mM Hepes, 150 mM NaCl, pH 7.4, at 25 °C) All ^{1}H-^{15}N HSQC spectra were processed and analyzed using NMRpipe, NMRviewJ)

3.2.2 Hsp90β binds to Kelch domain of Keap1 with a weak affinity

Although our NMR data has shown that Hsp90β interacts with the Kelch domain of Keap1 (Figure 10), the binding affinity of Kelch and Hsp90β cannot be determined. Therefore, we attempted to determine the equilibrium dissociation constant (K_d), stoichiometry (n), and enthalpy(ΔH) of the interaction of Kelch and Hsp90β through Isothermal Titration Calorimetry (ITC) experiment.

The experiments were performed with purified Kelch and Hsp90β at 300 μM and 30 μM in 20mM Hepes buffer, respectively. We used the highest concentration of Kelch that allowed it to remained stable in solution. The ITC profile showed in Figure 11 demonstrated that there was a significant amount of heat change when titrating Hsp90β to Kelch, indicating the interactions between these two proteins. However, the binding did not reach saturation.

Therefore, we were not able to determine the K_d, n, or ΔH of their interaction. Nevertheless, the ITC results indicated that Kelch interacted with Hsp90β with a weak affinity.

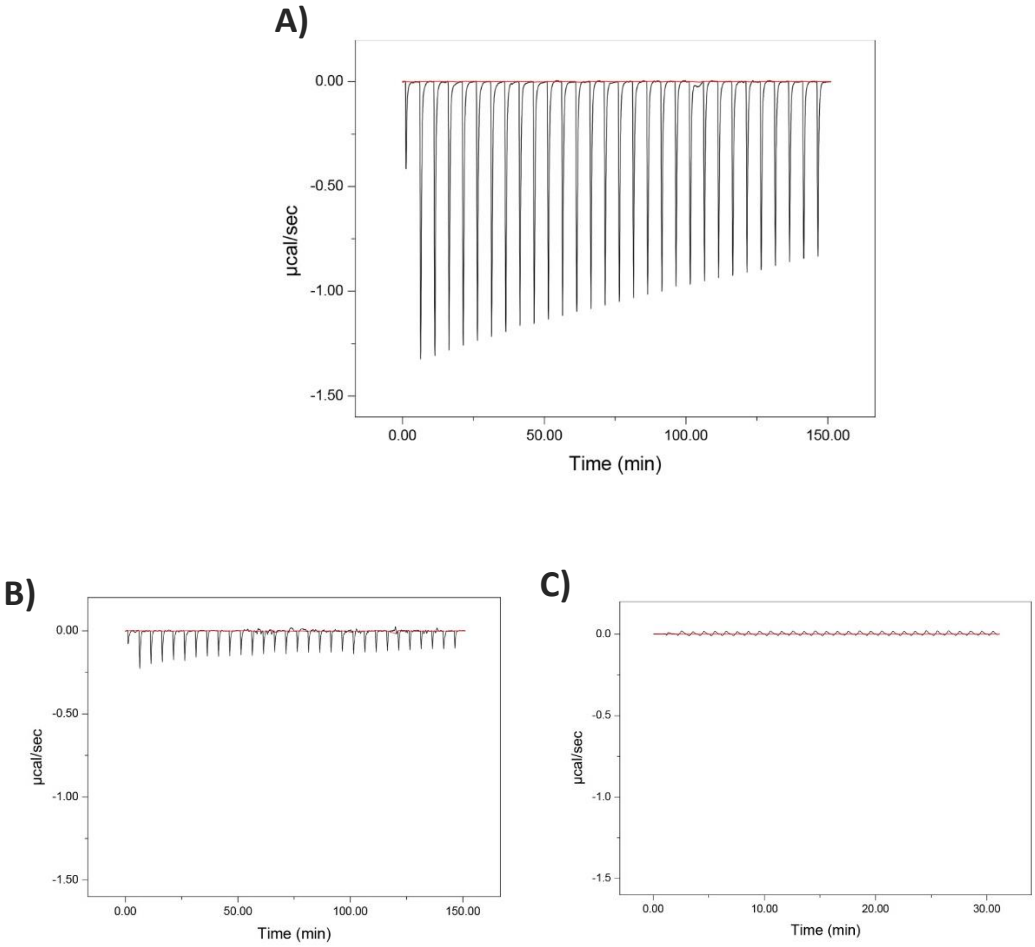

Figure 11

Figure 11. Kelch domain of Keap1 binds to Hsp90β weakly. A) ITC titration profile of Kelch domain with Hsp90β (10:1 mixture Kelch to Hsp90β at 300 µM & 30 µM in 20 mM Hepes, 100 mM NaCl, 1 mM $MgCl_2$ buffer, pH 7.4, respectively). **B)** ITC titration profile of Kelch domain with Buffer (300 µM Kelch combined with 20 mM Hepes, 100 mM NaCl, 1 mM $MgCl_2$ buffer, pH 7.4). **C)** ITC titration profile of buffer with Hsp90β (30 µM Hsp90β combined with 20 mM Hepes, 100 mM NaCl, 1 mM $MgCl_2$ buffer, pH 7.4).

3.2.3 Estimation of the binding affinity between Hsp90β and Kelch domain of Keap1 using the protein-binding assay

Even though the ITC experiments indicated that Kelch binds to Hsp90β at a weak affinity, the information we could obtain was limited through ITC. Therefore, we turned to the protein-binding plate assay, a modified enzyme-linked immunosorbent assay (ELISA). This method required a shorter experimental time and lower quantities of protein; thus, it is more suitable to be used for unstable proteins such as Hsp90β, Keap1, and Nrf2. As shown in Figure 12 A, after 16 μg Hsp90β was immobilized in the plate well surface, increasing quantities of the Fluoresceine-5-Melamide labeled Kelch protein (800 ng, 1.6 μg, 4.8 μg, 9.6 μg, 16 μg, 48 μg, 96 μg) were added to bind with the available Hsp90β. The fluorescence signal was measured at the excitation/emission wavelengths of 485/535 nm, allowing us to quantitively measure the amount of fluorescently labeled Kelch that was bound to Hsp90β. The results (Figure 12 A) showed that as an increasing amount of fluorescently labeled Kelch was added, there was an increasing amount of Kelch binding to the available Hsp90β. On the other hand, as a negative control, the gelatin showed no patterns of increasing quantities of Kelch binding (Figure 12 B).

However, the saturation of binding between fluorescently labeled Kelch and Hsp90β was not reached with the concentrations of proteins used, which made it difficult to estimate their equilibrium-

binding affinity. Therefore, we have repeated the protein binding assay with higher concentrations of fluorescently labeled Kelch. Specifically, the quantities of Kelch that were utilized were 32 μg, 64μg, 128 μg, 256 μg, 320 μg, 512 μg, 640 μg, 768 μg, 896 μg, 1.02 mg, 1.15 mg, 1.28 mg, and 1.6 mg. As shown in Figure 13 A, at ~240 μM (1.15 mg), the fluorescently labeled Kelch was able to saturate the binding with 2 μM (16μg) Hsp90β.

Assume that Kelch and Hsp90β has a 1:1 stoichiometric interaction. According to the data analysis in Section 2.5 of Chapter 2, K_d ~ [Kelch] when Hsp90β was half-saturated. Consequently, we estimated that the K_d of Kelch binding to Hsp90β was 130 μM.

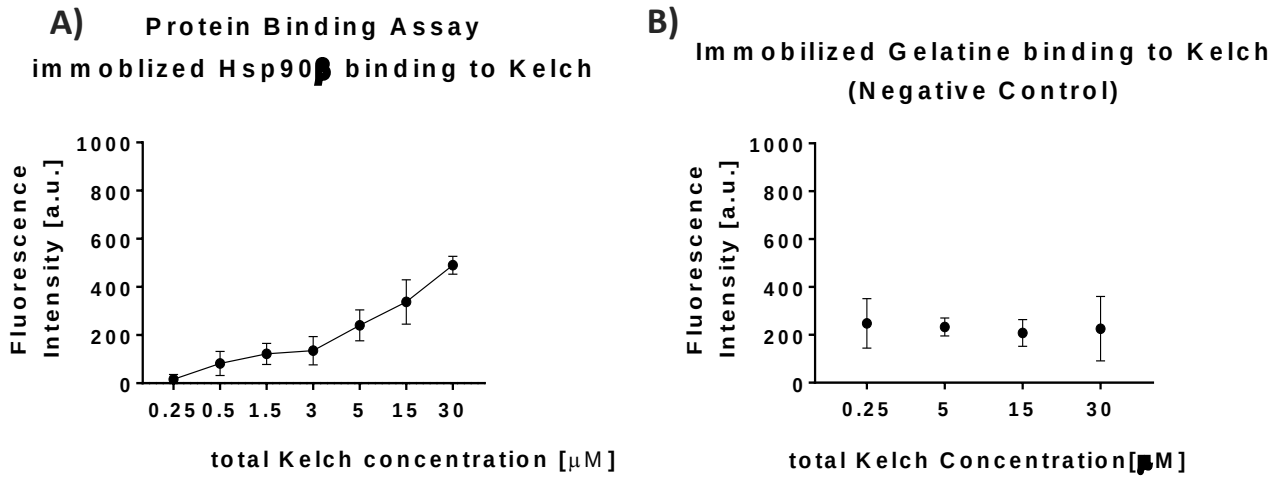

Figure 12

Figure 12. Plate binding assay of fluorescently labeled Kelch binding to Hsp90β weakly. (Fluorescence labeling efficiency for Kelch is 20 %) **A)** The plate assay of Kelch binding to Hsp90. The fluorescence intensity of fluorescently labeled Kelch (concentration range 0.25 μM to 30 μM) as they bind to immobilized Hsp90β (2 μM). **B)** The Negative control of plate assay for Kelch binding to Hsp90β. The fluorescence intensity of fluorescently labeled Kelch (concentration range 0.25 μM to 30 μM) binding to immobilized blocking buffer Gelatine (4 %).

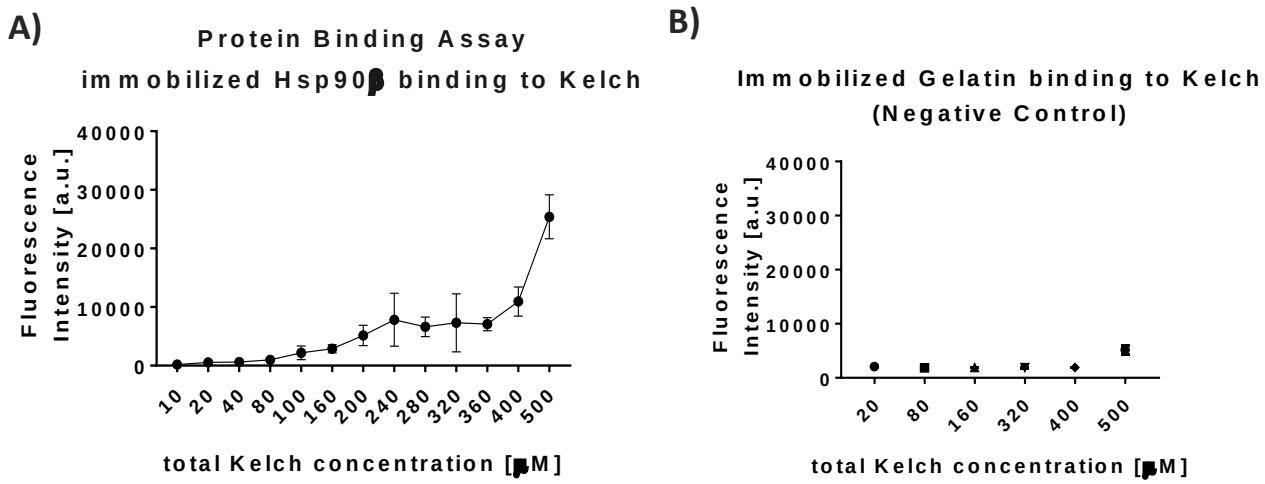

Figure 13

Figure 13. Plate binding assay of fluorescently labeled Kelch at high concentration binds to Hsp90β weakly. (Fluorescence labeling efficiency for Kelch is 20 %) **A)** The plate assay of Kelch binding to Hsp90. The fluorescence intensity of fluorescently labeled Kelch (concentration range 10 µM to 360 µM) as they bind to immobilized Hsp90β (2 µM). **B)** The Negative control of plate assay for Kelch binding to Hsp90β. The fluorescence intensity of fluorescently labeled Kelch (concentration range 10 µM to 360 µM) binding to immobilized blocking buffer Gelatine (4 %).

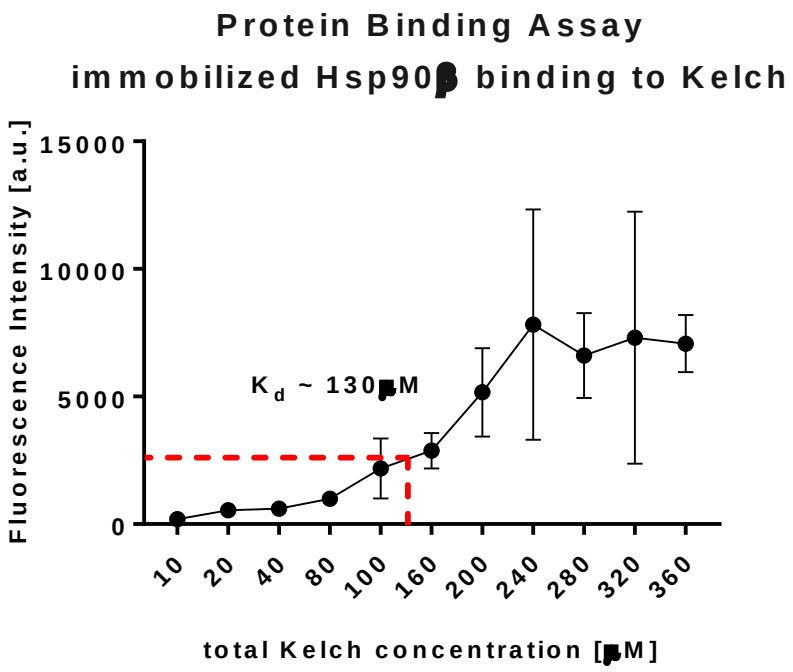

Figure 14

Figure 14. Plate binding assay of fluorescently labeled Kelch at high concentration binds to Hsp90β. (Fluorescence labeling efficiency for Kelch is 20 %) The fluorescence intensity of fluorescently labeled Kelch (concentration range 10 μM to 360 μM) as they bind to immobilized Hsp90β (2 μM). This binding pattern resembles a sigmoidal binding curve of varying concentrations of Kelch as ligand binding to the immobilized Hsp90β on plate well surface. We estimated that the K_d of Kelch binding to Hsp90β was ~ 130 μM.

3.3 Keap1 as a potential client of Hsp90β

3.3.1 Endogenous Keap1 protein expression showed patterns like Hsp90 client protein levels

The NMR, ITC, and protein-binding assay results presented above clearly showed that the Kelch domain of Keap1 is capable of interacting with Hsp90. Our next step was to investigate the biological relevance of this protein-protein interaction. In particular, we want to determine whether Keap1 is a client of Hsp90 *in vivo*. As mentioned in Section 1.4 in Chapter 1, STIP1 is an Hsp90 co-chaperone, which plays a critical role in transferring client proteins from Hsp70 onto Hsp90. Lackie et al. (in preparation) have demonstrated that many of the Hsp70/Hsp90 cochaperones (FKBP51, CHIP, PPIase and CypA) and client proteins (glucocorticoid receptor, tau, and GRK2) all have reduced levels of protein expression in *STIP1*$^{\Delta TPR1}$ (a mouse model with the TPR1 domain of STIP1 deleted) mouse brain tissues compared to Wild Type (WT) brain tissues. Following these findings, we tested whether the Keap1 protein level was affected in the *STIP1*$^{\Delta TPR1}$ mice.

The protein expression of Keap1 in both *STIP1*$^{\Delta TPR1}$ and WT mouse brain tissues were determined by western blotting. Figure 15 D shows the representative blot, and panels B and D represent the quantification of the western blots. Interestingly, in *STIP1*$^{\Delta TPR1}$ brain tissues, there was no significant difference in the expression of endogenous Keap1 between the WT and the *STIP1*$^{\Delta TPR1}$ mouse line (P-

value = 0.7044).

Next, we investigated the Keap1 expression in SN56-STIP1-KO cells, a neuronal cell line with STIP1 deleted. Similar to the effects of ΔTPR1, Lackie et al. had demonstrated that the protein levels of client and co-chaperone proteins, including CypA, Pin1, TDP-43, Glucocorticoid receptor, showed a reduction by approximately 50% when STIP1 was eliminated from the SN56 cells (Lackie et al., in preparation). We also observed the reduction of Keap1 protein expression in SN56-STIP1-KO compared to control cells. Figure 15 D showed the protein expression of endogenous Keap1 reduced by ~50% as STIP1 was absent in SN56 cells, indicating that Keap1 behaved in the same pattern as many client proteins of Hsp90β (P-value = 0.0280).

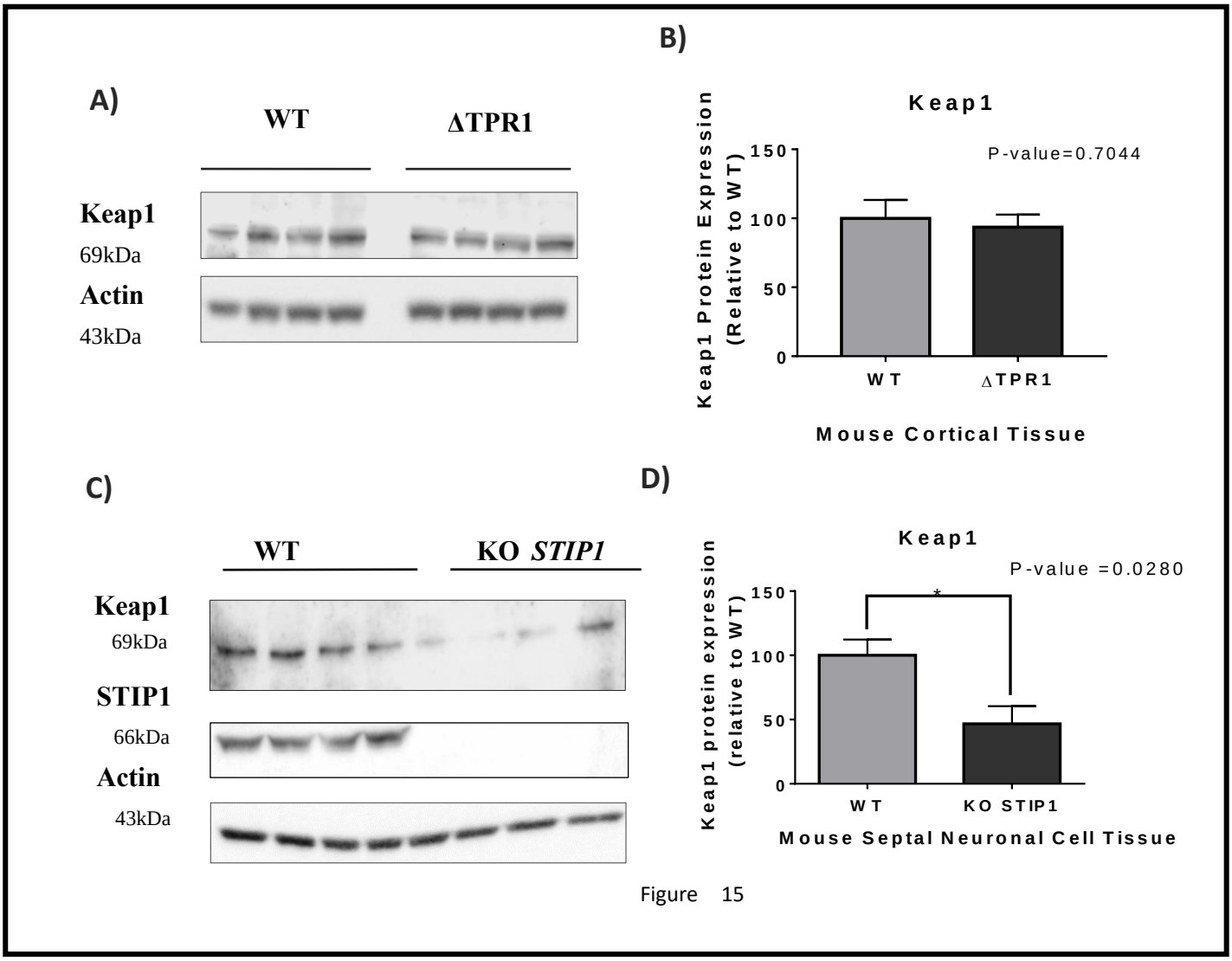

Figure 15. Protein expression of Keap1 in *STIP1*$^{\Delta TPR1}$ mouse line & STIP1 SN56 KO cells. A) Immunoblots showed a similar level of Keap1 in the *STIP1*$^{\Delta TPR1}$ mouse line. **B)** Quantification of Keap1 revealed similar protein levels in WT and *STIP1*$^{\Delta TPR1}$ mouse line (p=0.7044). **C)** Immunoblots showed a decrease in the level of Keap1 in SN56-STIP1-KO cells compared to SN56-WT cells. **D)** Quantification of Keap1 showed a 50% reduction of protein levels in SN56- STIP1-KO cells (p=0.0280). (All quantification had one-way ANOVA & T-tests performed.)

3.3.2 Endogenous Keap1 requires functional co-chaperone STIP1 to maintain protein stability

As we observed, Keap1 protein expression reduced in SN56 cells with STIP1 eliminated, we want to investigate further if the change in protein expression was due to the reduction of mRNA expression. To this end, we performed real-time quantitative polymerase chain reaction (RT-qPCR) experiments to determine the mRNA expression of Keap1 in *STIP1*$^{\Delta TPR1}$ and WT mice as well as SN56-STIP1-KO and SN56-WT cells (Figure 16). Our data showed that Keap1 mRNA expression remained similar between *STIP1*$^{\Delta TPR1}$ and WT mice (P-value = 0.4680), as well as between SN56-STIP1-KO and SN56-WT cells (P-value = 0.2091). The results suggest that the reduction of Keap1 protein levels in the SN56-STIP1-KO was not due to a decrease in mRNA expression, but instead, Keap1 requires functional STIP1 to maintain its protein stability in cells.

A)

Primer	Sequence (5'-3')
Keap1-193F	GGATGGCAACACTGACTCCA
Keap1-193R	GTCCCGCTCTGGCTCATATC

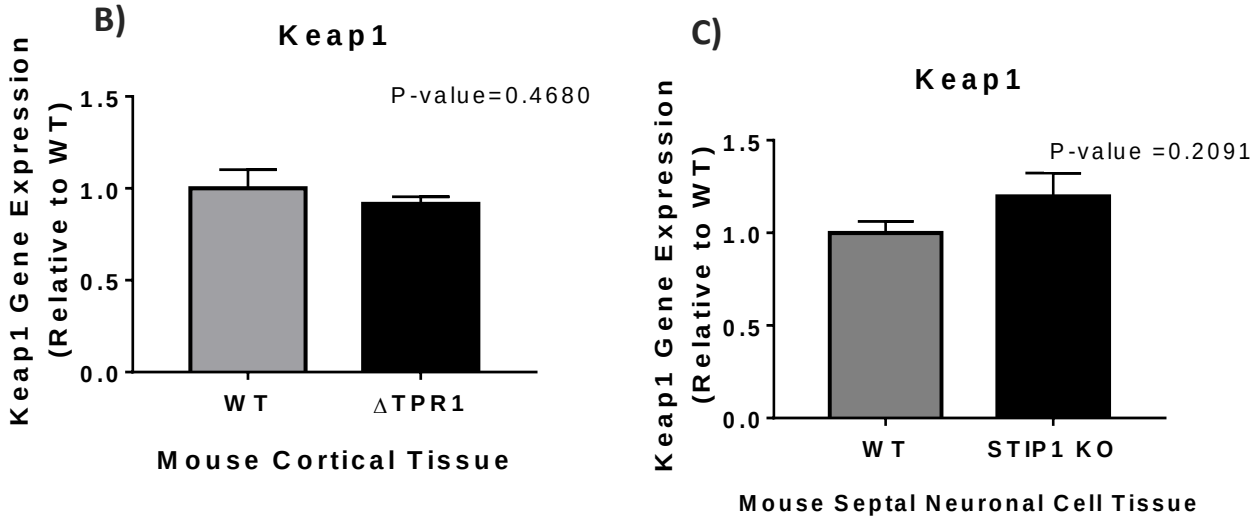

Figure 16

Figure 16. mRNA expression of Keap1 in *STIP1*$^{\Delta TPR1}$ mouse line & STIP1 SN56 KO cells. A) Primer Design for Keap1 **B)** RT-qPCR showed that Keap1 has similar gene expression in WT and *STIP1*$^{\Delta TPR1}$ mouse cortical tissue, Sample size (n) =5, Cycle threshold (Ct) =24~25, p = 0.4680. **C)** RT-qPCR showed that Keap1 has similar gene expression in SN56-WT and SN56-STIP1-KO cells, n=5, Ct = 27~29, p = 0.2091.

3.4 Keap1 interacting with both Hsp90β and STIP1

3.4.1 Recombinant Human Keap1 interacts to recombinant Human Hsp90β

Inspired by our results on protein and mRNA expression of Keap1 in SN56-STIP1-KO cells, we perform protein-binding assays to investigate the binding mechanisms of full-length Keap1 with Hsp90β and STIP1. Similar to the protein-binding assay performed on Hsp90β and the fluorescently labeled Kelch domain of Keap1, after ~20 μg of Hsp90β was immobilized in the plate well surface, increasing quantities of the fluorescently labeled full-length Keap1 were added to bind with the available Hsp90β. As illustrated in Figure 17, Keap1 showed binding activity with Hsp90β at a concentration as low as at 1 μM. Therefore, we learned that the interaction of Hsp90β with fluorescently labeled Keap1 was able to be detected even at low concentrations of Keap1. Unfortunately, Keap1 became unstable at a concentration higher than 6 μM. This was likely to be caused by the high number of cysteines in Keap1, making the protein sensitive to oxidation and prone to precipitate at high concentration. Because of this limitation, we were not able to estimate the binding affinity between full-length Keap1 and Hsp90.

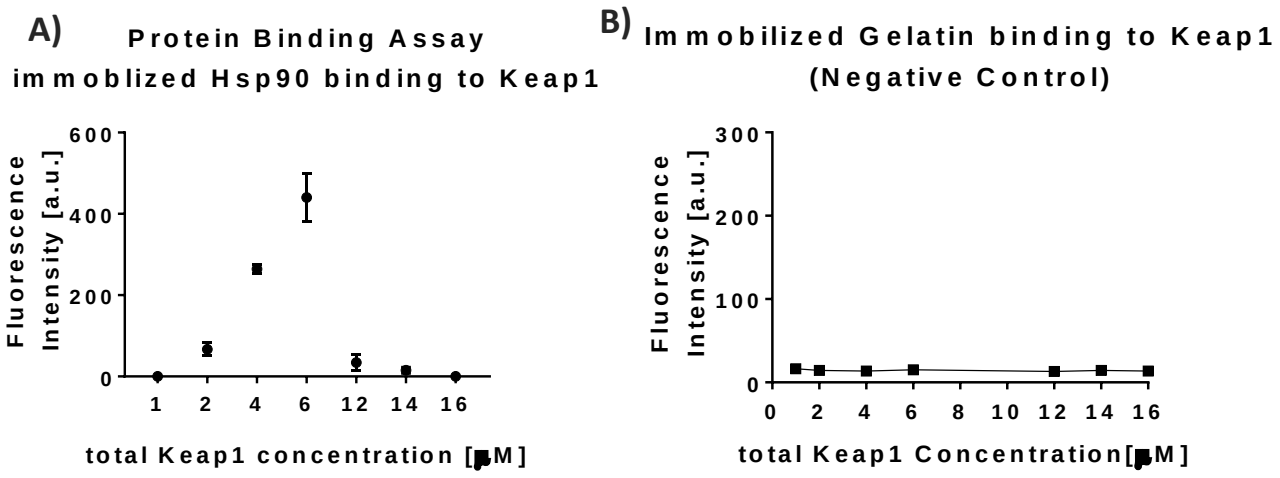

Figure 17

Figure 17. Plate binding assay of fluorescently labeled Keap1 binds to Hsp90β weakly. (Fluorescence labeling efficiency for Keap1 was 100 %) A) The plate assay of Keap1 binding to Hsp90β. The fluorescence intensity of fluorescently labeled Keap1 (concentration range 1 μM to 16 μM) as they bind to immobilized Hsp90β (2 μM). **B)** The Negative control of plate assay for Keap1 binding to Hsp90β. The fluorescence intensity of fluorescently labeled Keap1 (concentration range 1 μM to 16 μM) binding to immobilized blocking buffer Gelatin (4 %).

3.4.2 Estimation of the binding affinity between Keap1 and fluorescently labeled STIP1 using the protein-binding assay

We have performed the protein-binding assays on full-length Keap1 and STIP1. Since Keap1 was found to become unstable at higher concentrations, we decided to immobilize recombinant human Keap1 to the wells of the 96-well plate, which can avoid having Keap1 at high concentration for the experiment. We then probe the binding by adding increasing amounts of Fluorescein-5-Melamide labeled STIP1 to the immobilized Keap1. Specifically, we probed 20 μg unlabeled recombinant human Keap1 with fluorescently labeled recombinant mouse STIP1 in the following quantities: 26.4 μg, 52.8 μg, 79.2 μg, 105.6 μg, 132 μg, 158.4 μg, 184.8 μg, 211.2 μg, 237 μg, 264 μg, 290.4 μg, 316.8 μg, 343.2 μg, 396 μg, 528 μg, and 594 μg. Figure 18 showed that the fluorescent signal as an increasing amount of fluorescently labeled STIP1 was added to Keap1, indicating that STIP1 interacts with Keap1.

As shown in Figure 18 A, at 80~90 μM (528 - 594 μg), the fluorescently labeled STIP1 was likely to saturate the binding with 2 μM (13.8 μg) Keap1. As previously mentioned in Section 2.5 of Chapter 2, the K_d of STIP1 binding with Keap1 could be estimated from the midpoint of the binding curve. Assuming that STIP1 and Keap1 bound at a 1:1 stoichiometric ratio, we estimated that the K_d of STIP1 binding to Keap1 was ~ 44 μM (Figure 19).

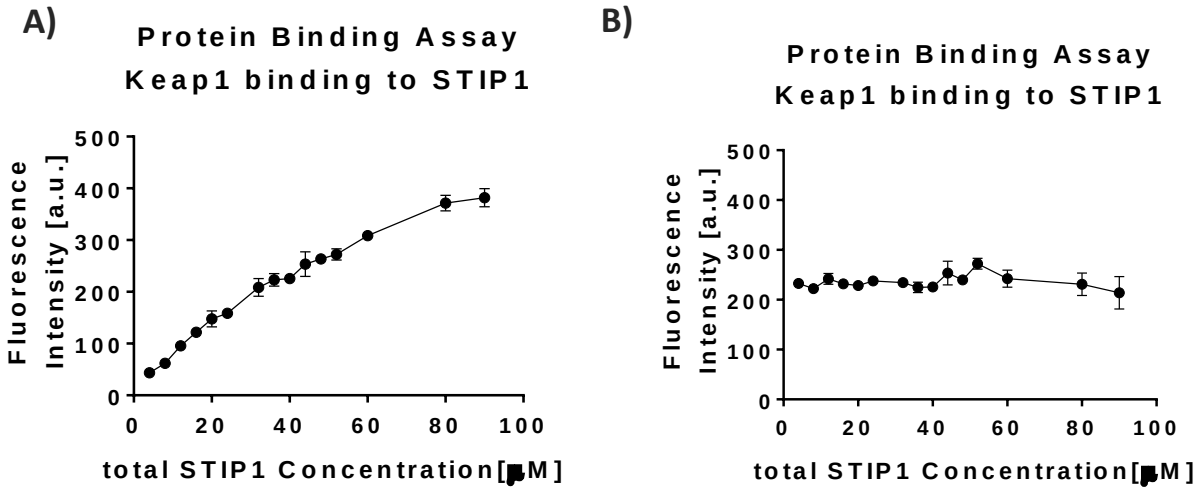

Figure 18

Figure 18. Plate binding assay of fluorescently labeled STIP1 binds to Keap1 with high affinity. (Fluorescence labeling efficiency for STIP1 is 100 %) A) The plate assay of Keap1 binding to fluorescently labeled STIP1. The fluorescence intensity of fluorescently labeled STIP1 (concentration range 2 µM to 90 µM) as they bind to immobilized Keap1 (2 µM). **B)** The Negative control of plate assay for fluorescently labeled STIP1 binding to Gelatine. The fluorescence intensity of fluorescently labeled STIP1 (concentration range 2 µM to 90 µM) binding to immobilized blocking buffer Gelatine (4 %).

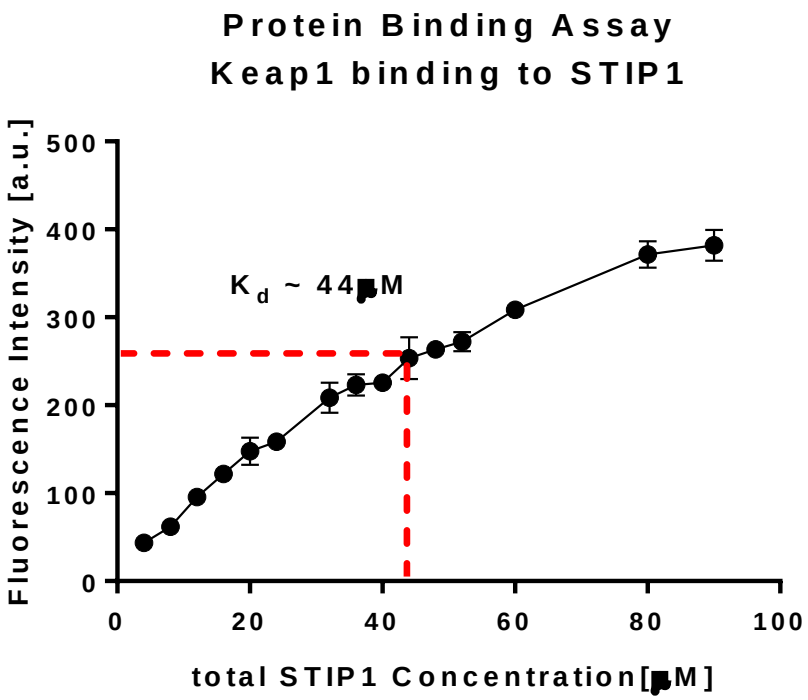

Figure 19

Figure 19. Plate binding assay of fluorescently labeled STIP1 at high concentration binds to Keap1. (Fluorescence labeling efficiency for Keap1 is 100 %) The fluorescence intensity of fluorescently labeled STIP1 (concentration range 4 μM to 90 μM) as they bind to immobilized Keap1 (2 μM). This binding pattern showed a pattern of binding saturation at 80-90 μM. As STIP1 being the ligand and Keap1 being the receptor in the case of our experiment, the middle point of the binding curve before reaching binding equilibrium saturation was about 44 μM, and we estimated that the K_d of STIP1 binding to STIP1 was ~ 44 μM.

3.5 Nrf2 as a potential client of Hsp90β

3.5.1 Endogenous Nrf2 protein expression showed patterns like Hsp90 client protein levels

While the focus of my work was on the interaction between Keap1 and the Hsp90-STIP1 chaperone system, some preliminary data on Nrf2 have been collected. In particular, we have investigated the changes in protein level and mRNA expression of Nrf2 in *STIP1*$^{\Delta TPR1}$ mice and SN56-STIP1-KO cells. The protein expression levels of Nrf2 in both *STIP1*$^{\Delta TPR1}$ and WT mouse brain tissues were determined through western blotting. Figure 20 shows the representative blot and panels. B - D present the quantification of Western blots. This experiment demonstrated that Nrf2 protein level decreases as the TPR1 domain of STIP1 were deleted in mouse brain tissue. The experiment was repeated for more than three times. In *STIP1*$^{\Delta TPR1}$ brain tissues, the expression of endogenous Nrf2 decreased by ~ 40% as the TPR1 domain in STIP1 was deleted (P-value = 0.0394). Similarly, we observed a ~50% reduction of endogenous Nrf2 protein expression as STIP1 was knocked out from the SN56 cells (P-value = 0.0091). These experiment results indicated that endogenous Nrf2 behaved in the same pattern as many client proteins of Hsp90.

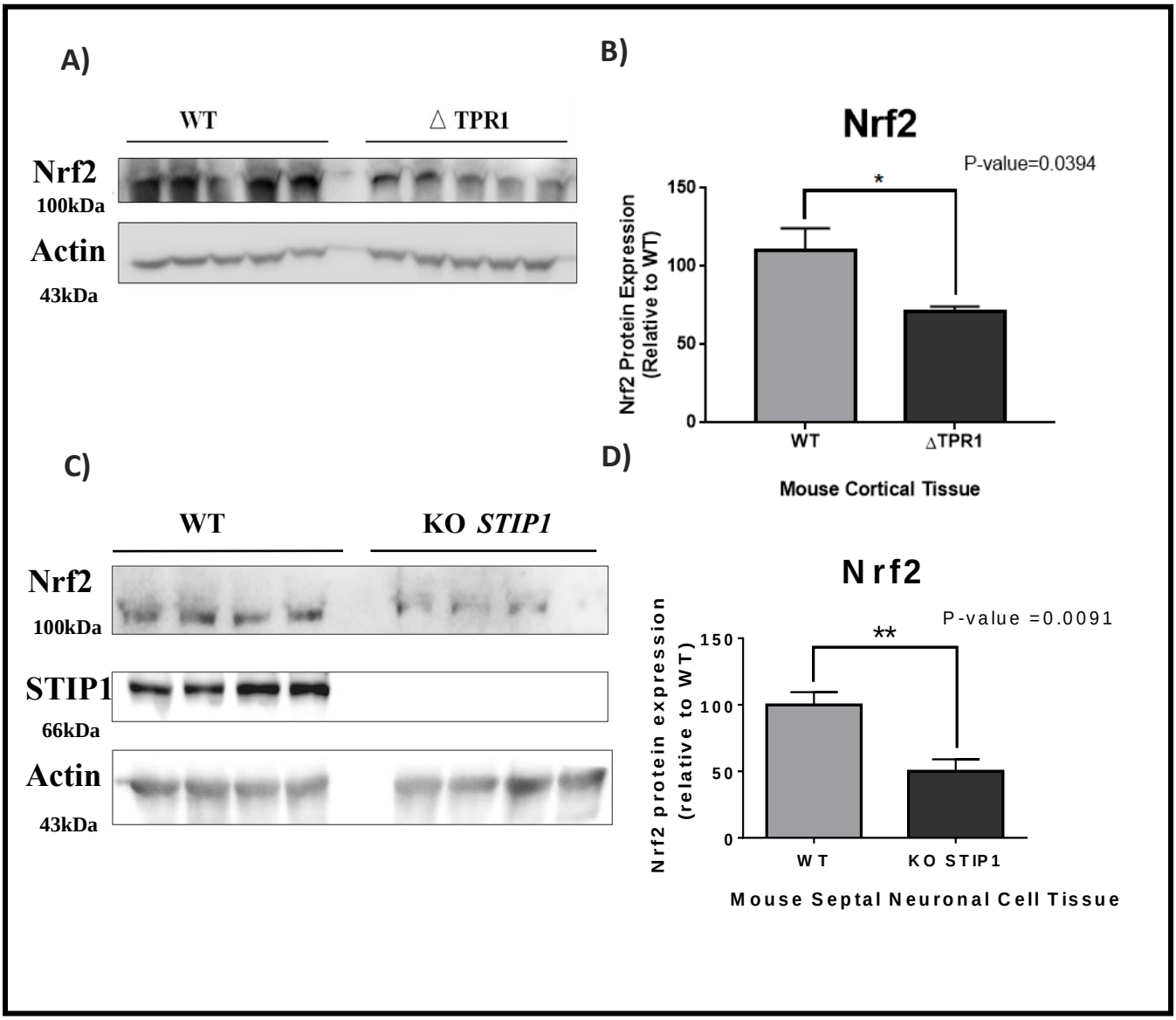

Figure 20. Protein expression of Nrf2 in *STIP1*$^{\Delta TPR1}$ mouse line & SN56-STIP1-KO cells. A) Immunoblots showed a decrease in the level of Nrf2 protein in the *STIP1*$^{\Delta TPR1}$ mouse line. **B)** Quantification of Nrf2 showed a 40 % reduction in *STIP1*$^{\Delta TPR1}$ mice (p=0.0394). **C)** Immunoblots showed a decrease in the level of Nrf2 in SN56-STIP1-KO cells compared to SN56-WT cells. **D)** Quantification of Nrf2 showed a 50 % reduction of protein level (p=0.0091). (All quantification had one-way ANOVA & T-tests performed.)

3.5.2 Endogenous Nrf2 requires functional endogenous co-chaperone STIP1 to maintain protein stability

We have also performed RT-qPCR experiments to check whether the decreases of Nrf2 levels in *STIP1*$^{\Delta TPR1}$ brain tissues and SN56-STIP1-KO cells were caused by the reduction of mRNA expression (Figure 21). The result showed that Nrf2 mRNA expression remained similar between *STIP1*$^{\Delta TPR1}$ and WT mouse lines (P-value = 0.6269). Interestingly, the mRNA expression of Nrf2 in SN56-STIP1-KO cells was elevated compared to SN56-WT cells (P-value = 0.0178). This may suggest that the SN56-STIP1-KO cells were under oxidative stress, causing an increase in Nrf2 mRNA expression. However, functional STIP1 is required to facilitate Hsp90 to maintain Nrf2 protein stability.

A)

Primer	Sequence (5'-3')
Nrf2-164F	GGACATGGAGCAAGTTTGGC
Nrf2-164R	CCAGCGAGGAGATCGATGAG

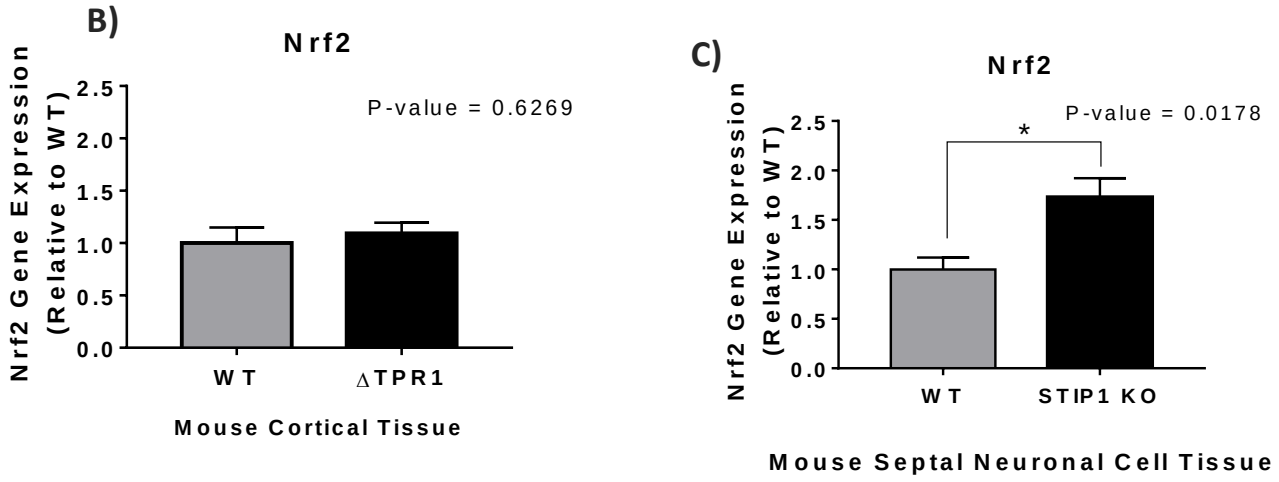

Figure 21

Figure 21. mRNA expression of Nrf2 in *STIP1*$^{\Delta TPR1}$ mouse line & SN56-STIP1-KO cells. A) Primer Design for Nrf2. **B)** RT-qPCR showed that Nrf2 has a similar gene expression in WT and *STIP1*$^{\Delta TPR1}$ mouse cortical tissue, n = 5, Ct = 22~23, p = 0.6269. **C)** RT-qPCR showed that Nrf2 has similar gene expression in SN56-WT and SN56-STIP1-KO cells, n = 5, Ct = 23~25, p = 0.0178.

3.6 Preliminary NMR data on the interaction of Nrf2 with Hsp90β

To probe the physical interaction between recombinant Nrf2 and Hsp90β ^{1}H-^{15}N HSQC NMR experiments were performed on ^{15}N-labeled Nrf2 in the absence and presence of unlabeled FL-Hsp90β. Upon the addition of Hsp90β, the signals of Nrf2 showed minor chemical shifts, which did not provide a conclusive result. This data was difficult to obtain due to the unstable nature of Nrf2 at high concentrations. Repeating the experiments with a higher concentration of Nrf2 and Hsp90β is challenging due to the low solubility of these two proteins.

Moreover, as an intrinsically disordered protein (IDP), Nrf2 possesses a protein architecture that lacks a stable tertiary structure. The NMR analysis of IDPs is extremely challenging because IDPs present a small chemical shift dispersion in NMR spectra (Gibbs et al., 2017). As shown in Figure 22, proton-detected ^{1}H, ^{15}N-HSQC spectra of Nrf2 exhibited clustered residue dispersion, which made it difficult to observe the residue chemical shift changes upon Nrf2-Hsp90β interaction.

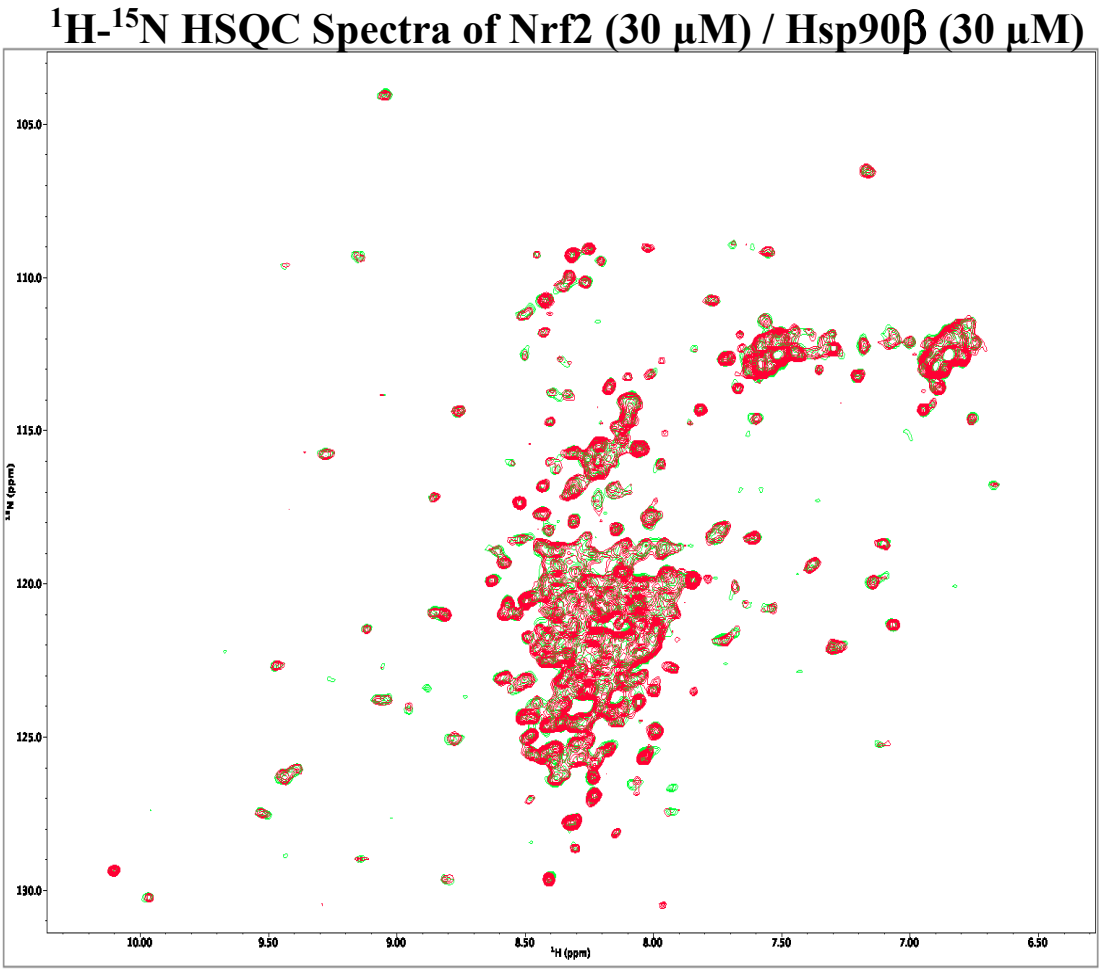

Figure 22

Figure 22. The signal intensity of ^{15}N-labeled Nrf2 showed mild residue chemical shift as Hsp90β is added to the solution. The overlay ^{1}H-^{15}N HSQC spectrum of ^{15}N-labeled Nrf2 by itself and with Hsp90β (Green: 30 µM ^{15}N-Nrf2; Red: 30 µM ^{15}N-Nrf2 combined with 30 µM Hsp90β in 20 mM Hepes, 100 mM NaCl, 1 mM $MgCl_2$ buffer, pH 7.4, at 25 °C; ^{1}H-^{15}N HSQC spectra were processed and analyzed using NMRpipe, NMRviewJ)

CHAPTER 4: DISCUSSION

Neurodegenerative diseases cause devastating effects on patients' health and affect millions of people worldwide. The prevalence of neurodegenerative disorders is expected to increase as the population ages, which leads to a considerable increase in the associated socioeconomic impact on society. Current treatment towards neurodegenerative disease focuses on treating the symptoms but offers no cure.

The heat shock proteins are known as direct activators of transcription factors that upregulate the expression of protein chaperones in response to protein misfolding. For example, the Hsp70 and Hsp90 can promote the proper folding and functional activation of proteins as well as targeting misfolded or aggregated proteins for refolding or degradation (Lackie et al., 2017). Moreover, the HSF1 activity modulated by Hsp70 and Hsp90 can protect cells from proteotoxicity, and cell death was found to be impaired in neurodegenerative diseases (Gomez-Pastor et al., 2017). Recently, Heat shock proteins are also found to interact with crucial proteins such as Tau and Aβ, which are potential targets for neurodegenerative diseases (Karagoz et al., 2014; Willhelmus et al., 2007). Nrf2, whose activation is mainly dependent on Keap1 modulation, is shown to have valuable neuroprotective potential through multiple neurodegenerative disease mouse models (Dinkova-Kostova & Kazantsev, 2017). Recent studies have demonstrated that Keap1 interacts with Hsp90 (Prince et al., 2015; Taipale et al., 2014). However, the molecular mechanism and the function of their interactions remain unknown. Preliminary

yeast-two hybrid experiments performed by Dr. Duennwald and his co-workers have suggested that Nrf2 and Keap1 can both interact with Hsp90. In our study, we focused on studying Hsp90β based on previous research data, which utilized Hsp90β.

Here we demonstrate that Hsp90 indeed interacts with Keap1 and modulates its protein stability in both neuronal cell cultures and mouse models. Moreover, this modulation mechanism depends on a crucial co-chaperone, STIP1. Our data also indicate that Hsp90-STIP1 modulates the protein stability of Nrf2. All these findings show possible underlying crosstalk between the Keap1/Nrf2-mediated antioxidative pathway and the Hsp90/HSF1-mediated heat shock response pathway.

4.1 Keap1 as a client of Hsp90

Hsp70/Hsp90 chaperone machinery plays an essential role in maintaining proteostasis (Lackie et al., 2017). The ATP-dependent Hsp70 can promiscuously bind to unfolded, misfolded, or aggregated proteins (Mayer, 2013). This ability to interact with a wide range of polypeptides allows Hsp70 to facilitate polypeptide to fold at the early stage of protein-folding processes and helps them to maintain their native conformations (Mayer, 2013). Moreover, Hsp70 can help the refolding of denatured and aggregated proteins to prevent proteotoxicity (Mayer, 2013).

On the other hand, Hsp90 facilitates protein maturation, stabilizes the proteins that tend to aggregate and helps to activate proteins at the later stage of the protein-folding process (Lackie et al., 2017; Picard, 2006; Taipale et al., 2012). These cellular events are crucial for stress regulation, cellular

development, DNA repair, neuronal signaling, and the maintenance of protein quality (Schopf et al., 2017; Zuehlke et al., 2017). The Hsp70/Hsp90 chaperone machinery has a large pool of protein substrates (or clients) (Schopf et al., 2017). Moreover, many of the clients chaperoned by Hsp70/Hsp90 chaperone machinery play essential roles in neurodegenerative diseases (Karagoz et al., 2014; Wilhelmus et al., 2007; Zhang et al., 2010). For example, the microtubule-associated protein tau, one of the clients of Hsp90, is known to be associated with Alzheimer's diseases.

Recent studies have shown about 30 % of human E3 ubiquitin ligases were able to bind to Hsp90 (Taipale et al., 2012). For example, the ubiquitin-like PHD and RING finger domain-containing protein 1 (UHRF1) E3 ubiquitin ligases that were discovered to be Hsp90 clients (Ding et al., 2016). PHD and RING were essential for the maintenance of DNA methylation and were targeted for degradation by Hsp90 (Ding et al., 2016). Another E3 ubiquitin ligase called CHIP was found to be a co-chaperone of Hsp70/Hsp90 chaperone machinery and facilitate the degradation of clients through binding with both Hsp70 and Hsp90 (Connell et al., 2001; Xu et al., 2002; Kundrat & Regan, 2010). Moreover, an E3 ubiquitin ligase, the Cullin 5 (CUL5) was also found to interact with both Hsp70 and Hsp90 and are involved in client degradation of Hsp90 (Ehrlich et al., 2009). These pieces of evidence indicated that many E3 ligases were likely to be involved in Hsp70/Hsp90 chaperone machinery interaction and facilitate the degradation of Hsp90 clients.

A recent discovery made by Dr. Duennawald showed that Keap1, an E3 ubiquitin ligase that

functions primarily in inhibiting the activation of Nrf2, was able to interact with Hsp90β through Yeast Two-Hybrid experiments transiently. Through performing western blotting and co-immunoprecipitation experiments using the HEK293 cells with transfected HA-Keap1 and FLAG-Hsp90 constructs, Prince et al. also demonstrated that Keap1 was an interactor of both Hsp90 isoforms, Hsp90α, and Hsp90β (Prince, 2015).

Our physiological data suggested that Keap1 behaves like a client of Hsp90 in mammalian cells. The *STIP1*$^{\Delta TPR1}$ developed by the Prado lab is a mouse line that expresses hypomorphic STIP1 lacking the TPR1 domain (Lackie et al., in preparation). The deletion of the TPR1 domain led a significant reduction in levels of several Hsp90 co-chaperones and STIP1/Hsp90 client-proteins, providing a suitable tool for us to monitor the behaviors of clients of Hsp90 that requires the STIP1-mediated regulation. Moreover, the murine Septal Neuronal cell (SN56) provided by Bruce Wainer (Emory University) was used to generate STIP1 knockouts (Lackie et al., in preparation). Using both mouse tissues, we found that endogenous Keap1 expression was significantly reduced in SN56-STIP1-KO cells but remained unchanged in *STIP1*$^{\Delta TPR1}$ mice. The level of Keap1 decreased when STIP1 loss the ability to transfer clients to Hsp90, which indicated that Keap1 is likely to be clients of Hsp90 and requires STIP1 to be stabilized by Hsp90. However, the level of Keap1 remained similar in *STIP1*$^{\Delta TPR1}$ mice, and WT mice indicated that the transfer of Keap1 to Hsp90 might be achieved through regions other than the TPR1 domain in STIP1. Furthermore, we determined that the gene expression of Keap1

was the same in *STIP1*$^{\Delta TPR1}$ mice and SN56-STIP1-KO cells when compared with wild types. This result indicated that the protein expression change found in Keap1 was due to protein stability instead of low mRNA production.

In agreement with the data from mice model and cell line, our biophysical data also indicated that purified recombinant human Keap1 could interact with purified recombinant human Hsp90. Since the abundance of cysteines in the Keap1 protein structure caused it to be highly unstable, we could not utilize Keap1 at higher concentrations to examine the binding affinity between Keap1 and Hsp90β. However, the binding between Keap1 and Hsp90β indeed indicated that Keap1 directly interacts with Hsp90β. Since the interaction between Keap1 and Hsp90β plays an important role in maintaining Keap1 protein stability, it could directly contribute to the modulation of Nrf2-mediated antioxidative response.

4.1.1 Keap1 interacts with Hsp90 through the Kelch domain

The quantitative high-throughput assessment of Hsp90 client interactions performed by Taipale et al. has demonstrated that E3 ligases with Kelch domains showed a highly significant trend in interacting with Hsp90 (Taipale et al., 2014). We performed NMR Spectroscopy, ITC, and protein binding assay to characterize the interaction between the recombinant Kelch domain of human Keap1 and human Hsp90β. Upon binding with Hsp90, the NMR spectra of the Kelch domain of Keap1 showed diminished peak intensity, minor chemical shift changes, and signal disappearance. The combination of complex signal changes indicated that indeed, Kelch was interacting with Hsp90. Notably, NMR spectroscopy studies of larger protein (300-1000 residues) are especially challenging (Frueh, 2014; Jiang & Kalodimos, 2017). This is because large proteins consist of a larger number of residues tend to display loss of signals in NMR spectroscopy spectra caused by the broaden signal and lower signal-to-noise ratios (Frueh, 2014). Therefore, we expected Kelch, the protein with a smaller size, to exhibit a reduction in signal intensity as it increasingly bound to Hsp90β, the larger protein. Our data showed that signals from the Kelch domain diminished as an increasing amount of Kelch entered the bound form with Hsp90β and existed as a large protein complex. This result revealed that human Keap1 could interact with human Hsp90β through the Kelch domain.

Also, we observed that the signal intensity reduction in NMR spectra was minor even when Kelch domain monomer and Hsp90β dimer were combined at a monomeric ratio of 1:2. This revealed that a

Kelch domain was not binding with all the available Hsp90β, which indicated that they interacted at a weak affinity. This result was consistent with the pattern of client-Hsp90 interaction because Hsp90 has the nature of interacting with its clients transiently (Taipale et al., 2014).

Furthermore, the residues that showed diminishments in signal intensity, as well as minor changes in chemical shifts, were found in regions of the Kelch domain that were structurally well-folded. As a 32-kDa protein, the Kelch domain has a highly symmetrical six-bladed β-propeller conformation formed by β-sheet and flexible loops that remained flexible between β-strands. The loop region of the Kelch domain appeared to remain flexible upon binding Hsp90β, thus with a signal intensity not changing as much (Figure 9B). Meanwhile, the intensity of the signals from the structured six-bladed β-propeller showed gradual reduction as more Hsp90β bound with Kelch to become a large protein-complex. This indicated that Hsp90β was likely to be interacting with Kelch at the well-folded six-bladed β-propeller region.

In agreement with the NMR results, out ITC data indicated that the Kelch domain interacts with Hsp90 at a weak affinity. Upon combining purified recombinant Kelch domain of human Keap1 with purified recombinant Hsp90β to achieve a final approximately 10:1 (monomeric Kelch: monomeric Hsp90β) molar ratio, there was significant heat change in the solution caused by protein-protein interaction. However, the binding curve of ITC titration indicated that the binding of Kelch with Hsp90β did not reach saturation, revealing that the Kelch domain of Keap1 interacted with Hsp90β at a weak

affinity.

Our protein-binding assay was designed and optimized for studying protein-protein interaction using a small quantity of protein while allowing us to achieve a high protein-protein ratio difference. Our data allowed the estimation of K_d being ~ 130 μM. This confirmed that the Kelch domain interacts with Hsp90β transiently at weak affinity.

4.1.2 Keap1 might bind with Hsp90 through other domains

We compared the binding affinity observed when Kelch domain of Keap1 binding with Hsp90β to when full-length Keap1 binding with Hsp90β. The unstable precipitation-prone nature of purified Keap1 caused difficulty for us to estimate the binding affinity between Keap1 and Hsp90β. However, we were able to obtain the unsaturated binding curve of Keap1 interacting with Hsp90β, and the result showed that full-length Keap1 gave strong fluorescence signal upon binding with Hsp90β. The reason for the stronger signal may be caused by higher fluorescence labeling efficiency of full-length Keap1 (100 % labeling efficiency) or that full-length Keap1 interacted with Hsp90β with higher affinity than Kelch domain itself. As Keap1 exists as a homodimer in the native state, the signals could be stronger because there were two Kelch domains involved in binding with Hsp90β. However, we also suspected that Keap1 bound to Hsp90β with higher affinity. This is because Keap1 may bind to Hsp90β through domains other than Kelch. Through literature, we found that Broad-Complex-Tramtrack-Bric-a-Brac (BTB) domain, a highly conserved domain that could be found in different proteins, was able to bind

to Hsp90 through pull-down assay and co-immunoprecipitation (Cai et al., 2014; Manjarrez et al., 2014). A BTB domain is also found in Keap1. Therefore, we speculate that Keap1 can interact with Hsp90β through both the Kelch domain and the BTB domain. However, further investigation would be required to confirm and understand the binding mechanism between the BTB domain and Hsp90β.

4.2 Nrf2 as a client of Hsp90

The identification of clients of Hsp90 through binding sites has been challenging (Schopf et al., 2017). The structural and functional characteristics of Hsp90 clients encompassed large varieties and were found to follow nonspecific patterns (Schopf et al., 2017). Moreover, Hsp90-client complexes have transient and dynamic nature, which had made the journey of identifying Hsp90 clients and understanding Hsp90-client interaction difficult (Taipale et al., 2014). In addition, the large size of complexes formed by Hsp90 with clients made NMR studies tough. Therefore, the conventional method of studying Hsp90-client complexes such as crystallization and NMR spectroscopy are not available methods for all kinds of clients.

Previous studies suggested that E3 ubiquitin ligases that interact with Hsp90 are involved in the degradation of Hsp90 clients (Taipale et al., 2014; Schopf et al., 2017). Our data reveal that Keap1, an adaptor protein of the Cul3-based E3 ubiquitin ligase, interacts and behaves as a client of Hsp90. Since Keap1 is the primary negative regulator of anti-oxidative stress response transcription factor Nrf2, we speculated that Nrf2, an intrinsically disordered protein, is also a client of Hsp90. Our collaborator Dr.

Duennawald found that Nrf2 was also able to transiently interact with Hsp90 through Yeast Two-Hybrid experiment.

Our data from western blotting utilized the *STIP1*$^{\Delta TPR1}$ mice model, and the SN56-STIP1-KO cell line reveals that Nrf2 indeed behaves like other clients of Hsp90. The protein expression level of Nrf2 was reduced significantly in both the *STIP1*$^{\Delta TPR1}$ mice model and SN56-STIP1-KO cell line. This suggests that Nrf2 protein stability maintenance depends on the proper functional Hsp70/Hsp90 chaperone machinery. As STIP1 was deleted in SN56-STIP1-KO cell tissue, the transfer of clients from Hsp70 to Hsp90 was disrupted, leading to a reduction of protein expression of Hsp90 clients (Lackie et al., 2017). Moreover, the absence of the TPR1 domain in STIP1 also led to decreased protein expression of client that required the TPR1 domain to be transferred to Hsp90. Furthermore, we determined that the gene expression of Nrf2 was the same in *STIP1*$^{\Delta TPR1}$ mice and elevated in SN56-STIP1-KO cells when compared with wild types. This result indicated that the protein expression change found in Nrf2 was caused by loss of protein stability instead of transcriptome modulation. Our findings revealed that Nrf2 required the transfer of STIP1 through the TPR1 domain to Hsp90 to maintain protein stability.

We attempted to use NMR spectroscopy to probe the interaction between Nrf2 and Hsp90b. However, the spectral changes of Nrf2 upon addition of Hsp90β was minor. The intrinsically disorder nature of Nrf2, as well as the large size of both Nrf2 and Hsp90β, made observing structural changes upon binding challenging. Further investigation would be required to understand the molecular

mechanism of Nrf2 interacting with Hsp90β.

4.3 STIP1 is critical for modulating Keap1 and Nrf2 protein stability

Co-chaperones are essential regulators of Hsp90 (Schopf et al., 2017). They can bind to Hsp90 and compete with other co-chaperones or bind to Hsp90 simultaneously and facilitate client recruitment, client structural stabilization, client folding process, and client functional activation (Schopf et al., 2017). Several co-chaperones recognize the Met-Glu-Glu-Val-Asp (MEEVD) motif in the CTD of Hsp90 through the TPR domains (Lackie et al., 2017). One of the crucial co-chaperones that facilitates the stabilization and maturation of client proteins of Hsp90 is the TPR domain-containing protein STIP1 (Lackie et al., 2017). STIP1 binds to both Hsp70 and Hsp90, allowing the client to transfer between the two chaperones (Lackie et al., 2017; Schopf et al., 2017).

STIP1 contains three TPR domains and two DP domains, in which the TPR2A-TPR2B is the minimal fragment that is required to bind both Hsp70 and Hsp90 (Lackie et al., 2017; Schmid et al., 2012). STIP1 was shown to be crucial for the activation of clients (Beraldo et al., 2013; Chang et al., 1997). The lack of STIP1 in mice model was shown to be embryonically lethal indicating the importance of STIP1 in embryonic development and survival (Chang et al., 1997; Beraldo et al., 2013; Lackie et al., 2017). Specifically, STIP1's crucial activity is involved in the maintenance of the functionality of chaperone networks and modulation of apoptosis as well as cellular resilience (Beraldo et al., 2013; Lackie et al., 2017).

Previous studies done by Lackie et al. revealed that STIP1 was a master controller of the chaperone network that maintained the stability of Hsp90 client proteins through proteostasis instead of transcriptome modulation (Lackie et al., 2017). We took advantage of the recently generated SN56-STIP1-KO cell line as well as the △TPR1 STIP1 mice model to understand the role of Hsp70/Hsp90 chaperone machinery in modulating Keap1 and Nrf2 protein maturation and stability. Our results revealed that not only the protein stability of Keap1 and Nrf2 was dependent on their interaction with Hsp90, but also, they required STIP1 activity to modulate their protein stability. Based on these observations, we speculate that the Hsp90-STIP1 chaperone system modulates the binding of Nrf2 through STIP1. Plate binding assay using Nrf2 with STIP1 will be performed to test this hypothesis.

4.4 Significance

The understanding of Hsp90-client interaction has been challenging so far (Lackie et al., 2017; Schopf et al., 2017; Taipale et al., 2012; 2014). This study has established that Keap1 and Nrf2 are likely to be clients of Hsp70/Hsp90 chaperone machinery that required STIP1 to maintain protein stability. Moreover, previous research provided evidence that the HSF1 and Nrf2 both mediate cytoprotective pathways that shared common transcriptional targets, compensatory to each in mammalian, played essential roles in cellular redox metabolism and modulating mitochondrial structure and functions (Naidu et al., 2015). These two pathways can be activated by the same inducers, simultaneously indicating possible crosstalk in their molecular mechanism and functions (Naidu et al., 2015). Our study provides valuable insight into how Hsp90 and STIP1 proteostasis modulation of Keap1 and Nrf2 may bridge the Keap1/Nrf2 antioxidative response pathway with the Hsp90/HSF1 heat shock response pathway. The potential in co-modulating these two pathways could provide benefits in advancing therapeutic treatments and pharmaceutical drug development to treat neurodisorders.

CHAPTER 5: CONCLUSION

5.1 Conclusion

Recent studies increasingly suggested that the Keap1/Nrf2-mediated antioxidative response pathway played an essential role in protecting neurons against pathological symptoms such as exacerbated oxidative stress, mitochondrial dysfunction, and chronic neuroinflammation, which were commonly found in neurodegenerative diseases (Browne et al., 2006; Deshmukh et al., 2017; Dinkova-Kostova & Kanzatsev, 2017; Johnson et al., 2010; 2015; Neymotin et al., 2011; Ramsey et al., 2007). Moreover, crosstalk between the Keap1/Nrf2-mediated pathway and Hsp90/HSF1-mediated heat shock response pathway was proposed based on indirect evidence such as they shared transcriptional targets, combated cellular oxidative stress, maintain mitochondrial structure and functions (Baird et al., 2011; Naidu et al., 2015). Both cytoprotective pathways are essential targets for neurodegenerative disease prevention and treatment-related treatments.

The results of our works suggest that Keap1 and Nrf2 are both clients of Hsp90. Through studies using mouse brain tissues and neuronal tissue cell culture, we revealed that the protein stability of Keap1 and Nrf2 rely on functional Hsp70/Hsp90 chaperone machinery and the client transfer co-chaperone STIP1. Moreover, we identified that Keap1 interacts transiently with Hsp90 through the Kelch domain. We have also shown that Keap1 directly interacts with STIP1. Future studies should

evaluate the molecular mechanism of interaction between Keap1-Hsp90, Keap1-STIP1, Nrf2-Hsp90, and Nrf2-STIP1.

Overall, our findings proposed Keap1 and Nrf2 as novel Hsp90 clients, which confirmed the crosstalk between Keap1/Nrf2-mediated pathway and Hsp90/HSF1-mediated pathway. These findings could provide valuable information for developing effective treatments for neurodegenerative diseases.

5.2 Limitation & Future Directions

5.2.1 Molecular mechanism of Keap1-Hsp90 and Nrf2-Hsp90 interaction

Through our research, we elucidated that Keap1 and Nrf2 are likely to be clients of Hsp70/Hsp90 chaperone machinery, and their protein stability required the involvement of co-chaperone STIP1. Further experiments involving co-immunoprecipitating Keap1 and Nrf2 with Hsp90 in neuronal cell tissues would provide strong evidence that they form endogenous client-chaperone complex.

Additionally, the Kelch domain was Keap1 was determined as the region where Hsp90 bound. However, our data also indicates that Keap1 may bind Hsp90 with a stronger affinity than the Kelch

domain alone. Therefore, further investigations should be dedicated to understanding how other domains of Keap1, such as the BTB domain, interact with Hsp90.

We performed a protein-binding assay using fluorescent dye to elucidate the binding affinity between proteins. This method depended on cysteines in protein to react with the dye, which can produce proteins that were not uniformly labeled or has low labeling efficiency. A better fluorescent labeling method could be helpful for a precise future calculation of binding affinity between proteins. Further experiments should use individual domains of Keap1, Nrf2, and Hsp90 to understand their involvement in the binding interface as well as their affinity.

Figures 23, 24, and 25 (Section Supplementary) showed the current progress in purifying truncated Middle and C-terminal domains of Hsp90β. However, the current protocol encountered difficulties in separating GST-tag from the purified individual MD and CTD of Hsp90β because GST-tag unspecifically binds strongly with MD and CTD of Hsp90β. Thus, further optimization would be required for using them in future experiments.

5.2.2 The role of STIP1 in transferring Keap1 and Nrf2 to Hsp90

By using protein-binding assays with fluorescently labeled proteins, we were able to show that Keap1 interacts directly with STIP1. However, the instability nature of full-length Keap1 caused difficulties in studying Keap1-STIP1 binding using NMR spectroscopy and ITC. To overcome this barrier, individual domains of Keap1, which may have higher stability and solubility than the full-length protein, could be used to dissect the molecular basis of the Keap1-STIP1 interaction further.

Even though results suggest that Nrf2 is also a client of the Hsp90-STIP1 chaperone system, physical interactions of Nrf2 with STIP1 and Hsp90 have yet to be determined. Therefore, future experiments need to purify individual domains of Nrf2 and using them for protein-protein interaction studies with STIP1 and Hsp90.

SUPPLEMENTARY

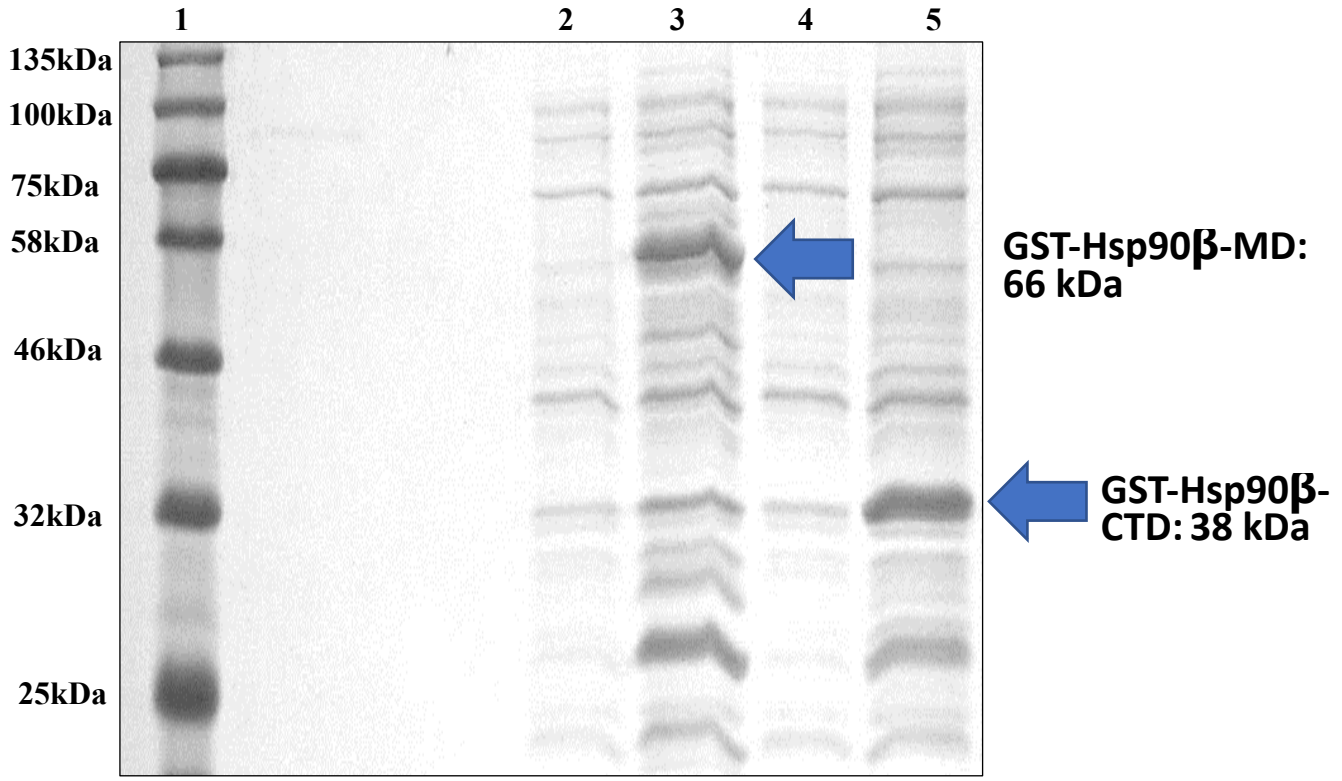

Figure 23

Figure 23. The overexpression of the Middle domain (MD) and the C-terminal domain (CTD) of recombinant human Hsp90β. 12 % SDS-PAGE Analysis of overexpression of GST-tagged MD and CTD of Hsp90β: Lane 1- Protein molecular weight ladder; Lane 2-total protein from pre-induced *E. coli* for overexpressing GST-tagged MD of Hsp90β; Lane 3-total protein from post-induced *E. coli* for overexpressing GST-tagged MD of Hsp90β; Lane 4-total protein from pre-induced *E. coli* for overexpressing GST-tagged CTD of Hsp90β; Lane 5- total protein from post-induced *E. coli* for overexpressing GST-tagged CTD of Hsp90β

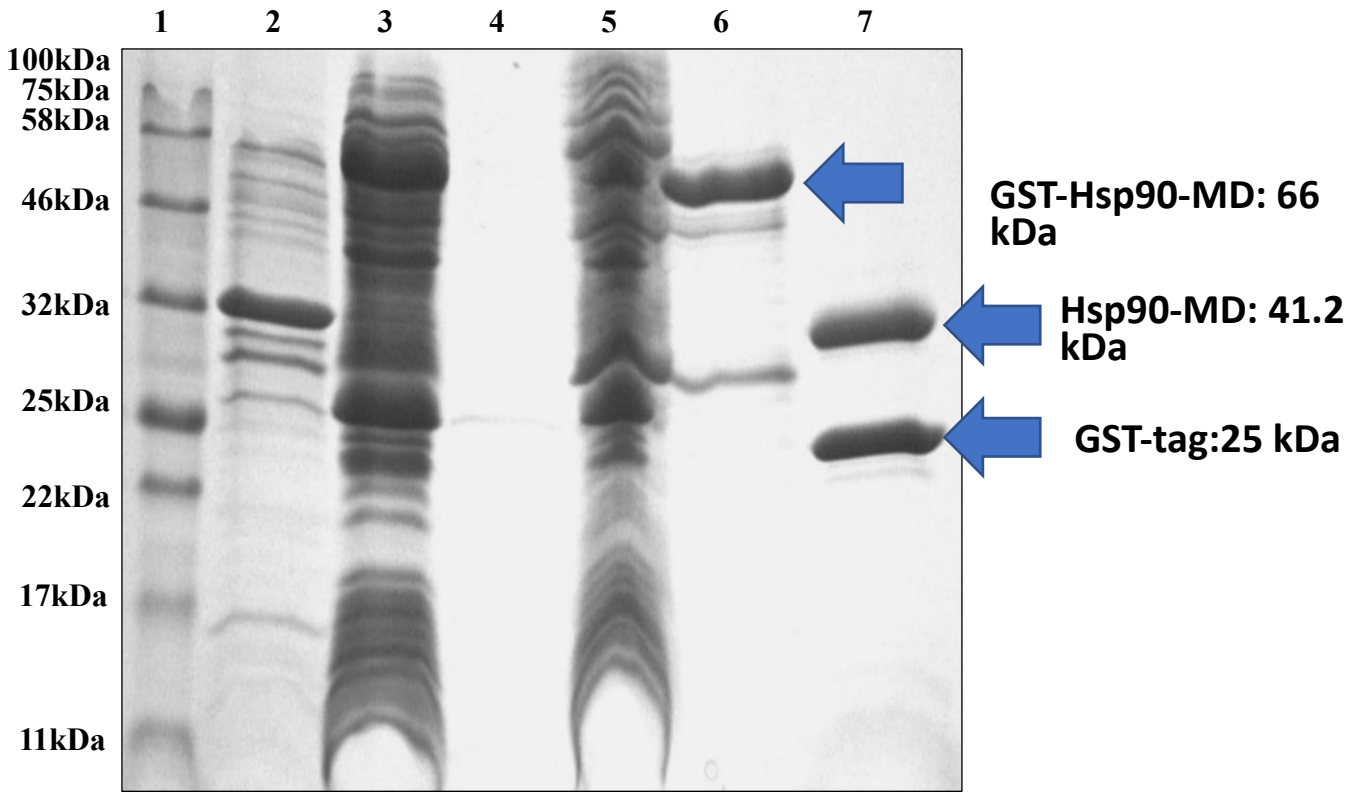

Figure 24

Figure 24. The purification of the Middle domain (MD) of recombinant human Hsp90β. 16 % SDS-PAGE Analysis of overexpression of GST-tagged MD of Hsp90β: Lane 1- Protein molecular weight ladder; Lane 2-total protein from insoluble *E. coli*; Lane 3-total protein from soluble *E. coli*; Lane 4-total protein from unbound; Lane 5-total protein from first wash; Lane 6- total protein eluted; Lane 7- the final protein after thrombin cleavage.

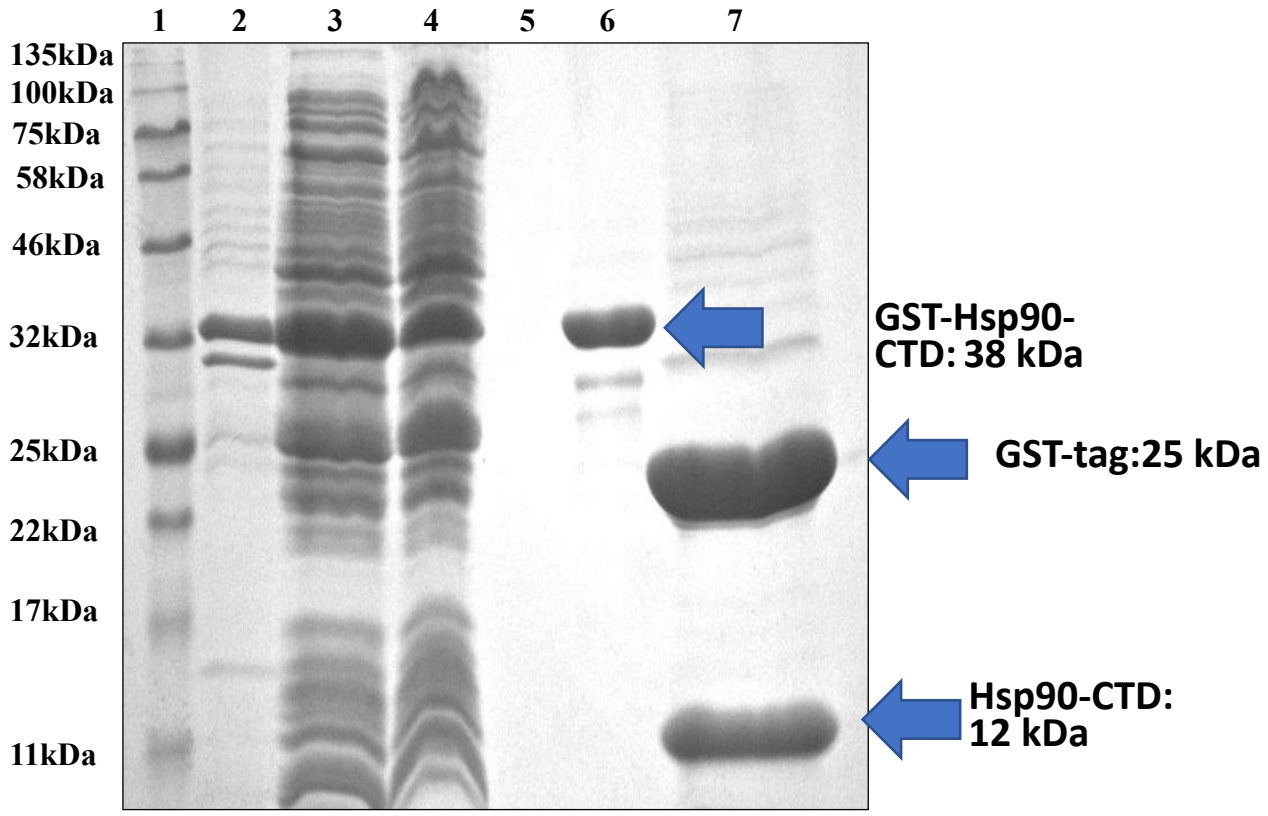

Figure 25

Figure 25. The purification of the C-terminal domain (CTD) of recombinant human Hsp90β. 16% SDS-PAGE Analysis of overexpression of GST-tagged CTD of Hsp90β: Lane 1- Protein molecular weight ladder; Lane 2-total protein from insoluble *E. coli*; Lane 3-total protein from soluble *E. coli*; Lane 4-total protein from unbound; Lane 5-total protein from first wash; Lane 6- total protein eluted; Lane 7- the final protein after thrombin cleavage.

BIBLIOGRAPHY

- Akerfelt, M., Morimoto, R. I., & Sistonen, L. (2010). Heat shock factors: integrators of cell stress, development, and lifespan. Nat Rev Mol Cell Biol, 11(8), 545-555. doi:10.1038/nrm2938
- Akerfelt, M., Vihervaara, A., Laiho, A., Conter, A., Christians, E. S., Sistonen, L., & Henriksson, E. (2010). Heat shock transcription factor 1 localizes to sex chromatin during meiotic repression. J Biol Chem, 285(45), 34469-34476. doi:10.1074/jbc.M110.157552
- Ali, A., Bharadwaj, S., O'Carroll, R., & Ovsenek, N. (1998). HSP90 interacts with and regulates the activity of heat shock factor 1 in Xenopus oocytes. Mol Cell Biol, 18(9), 4949-4960. doi:10.1128/mcb.18.9.4949
- Ali, M. M., Roe, S. M., Vaughan, C. K., Meyer, P., Panaretou, B., Piper, P. W., . . . Pearl, L. H. (2006). Crystal structure of an Hsp90-nucleotide-p23/Sba1 closed chaperone complex. Nature, 440(7087), 1013-1017. doi:10.1038/nature04716
- Alvira, S., Cuéllar, J., Röhl, A., Yamamoto, S., Itoh, H., Alfonso, C., . . . Valpuesta, J. M. (2014). Structural characterization of the substrate transfer mechanism in Hsp70/Hsp90 folding machinery mediated by Hop. Nat Commun, 5, 5484. doi:10.1038/ncomms6484
- Aoki, Y., Sato, H., Nishimura, N., Takahashi, S., Itoh, K., & Yamamoto, M. (2001). Accelerated DNA adduct formation in the lung of the Nrf2 knockout mouse exposed to diesel exhaust. Toxicol Appl Pharmacol, 173(3), 154-160. doi:10.1006/taap.2001.9176

- Baird, L., & Dinkova-Kostova, A. T. (2011). The cytoprotective role of the Keap1-Nrf2 pathway. Arch Toxicol, 85(4), 241-272. doi:10.1007/s00204-011-0674-5
- Baird, L., Swift, S., Llères, D., & Dinkova-Kostova, A. T. (2014). Monitoring Keap1-Nrf2 interactions in single live cells. Biotechnol Adv, 32(6), 1133-1144. doi:10.1016/j.biotechadv.2014.03.004
- Balch, W. E., Morimoto, R. I., Dillin, A., & Kelly, J. W. (2008). Adapting proteostasis for disease intervention. Science, 319(5865), 916-919. doi:10.1126/science.1141448
- Benedict, R. H., & Zivadinov, R. (2011). Risk factors for and management of cognitive dysfunction in multiple sclerosis. Nat Rev Neurol, 7(6), 332-342. doi:10.1038/nrneurol.2011.61
- Beraldo, F. H., Soares, I. N., Goncalves, D. F., Fan, J., Thomas, A. A., Santos, T. G., . . . Prado, M. A. (2013). Stress-inducible phosphoprotein 1 has unique cochaperone activity during development and regulates cellular response to ischemia via the prion protein. FASEB J, 27(9), 3594-3607. doi:10.1096/fj.13-232280
- Berson, S. A., & Yalow, R. S. (1959). Quantitative aspects of the reaction between insulin and insulin-binding antibody. J Clin Invest, 38, 1996-2016. doi:10.1172/JCI103979
- Bharadwaj, S., Ali, A., & Ovsenek, N. (1999). Multiple components of the HSP90 chaperone complex function in regulation of heat shock factor 1 In vivo. Mol Cell Biol, 19(12), 8033-8041. doi:10.1128/mcb.19.12.8033

- Browne, S. E., & Beal, M. F. (2006). Oxidative damage in Huntington's disease pathogenesis. Antioxid Redox Signal, 8(11-12), 2061-2073. doi:10.1089/ars.2006.8.2061
- Browne, S. E., Yang, L., DiMauro, J. P., Fuller, S. W., Licata, S. C., & Beal, M. F. (2006). Bioenergetic abnormalities in discrete cerebral motor pathways presage spinal cord pathology in the G93A SOD1 mouse model of ALS. Neurobiol Dis, 22(3), 599-610. doi:10.1016/j.nbd.2006.01.001
- Bryan, H. K., Olayanju, A., Goldring, C. E., & Park, B. K. (2013). The Nrf2 cell defence pathway: Keap1-dependent and -independent mechanisms of regulation. Biochem Pharmacol, 85(6), 705-717. doi:10.1016/j.bcp.2012.11.016
- Cai, M. J., Li, X. R., Pei, X. Y., Liu, W., Wang, J. X., & Zhao, X. F. (2014). Heat shock protein 90 maintains the stability and function of transcription factor Broad Z7 by interacting with its Broad-Complex-Tramtrack-Bric-a-brac domain. Insect Mol Biol, 23(6), 720-732. doi:10.1111/imb.12118
- Cala, O., Guillière, F., & Krimm, I. (2014). NMR-based analysis of protein-ligand interactions. Anal Bioanal Chem, 406(4), 943-956. doi:10.1007/s00216-013-6931-0
- Calkins, M. J., Jakel, R. J., Johnson, D. A., Chan, K., Kan, Y. W., & Johnson, J. A. (2005). Protection from mitochondrial complex II inhibition in vitro and in vivo by Nrf2-mediated transcription. Proc Natl Acad Sci U S A, 102(1), 244-249. doi:10.1073/pnas.0408487101
- Canning, P., Sorrell, F. J., & Bullock, A. N. (2015). Structural basis of Keap1 interactions with Nrf2. Free Radic Biol Med, 88(Pt B), 101-107. doi:10.1016/j.freeradbiomed.2015.05.034

- Chan, K., & Kan, Y. W. (1999). Nrf2 is essential for protection against acute pulmonary injury in mice. Proc Natl Acad Sci U S A, 96(22), 12731-12736. doi:10.1073/pnas.96.22.12731
- Chang, H. C., Nathan, D. F., & Lindquist, S. (1997). In vivo analysis of the Hsp90 cochaperone Sti1 (p60). Mol Cell Biol, 17(1), 318-325. doi:10.1128/mcb.17.1.318
- Chang, H. C., Tang, Y. C., Hayer-Hartl, M., & Hartl, F. U. (2007). SnapShot: molecular chaperones, Part I. Cell, 128(1), 212. doi:10.1016/j.cell.2007.01.001
- Chiti, F., & Dobson, C. M. (2006). Protein misfolding, functional amyloid, and human disease. Annu Rev Biochem, 75, 333-366. doi:10.1146/annurev.biochem.75.101304.123901
- Chiti, F., & Dobson, C. M. (2017). Protein Misfolding, Amyloid Formation, and Human Disease: A Summary of Progress Over the Last Decade. Annu Rev Biochem, 86, 27-68. doi:10.1146/annurev-biochem-061516-045115
- Clerico, E. M., Tilitsky, J. M., Meng, W., & Gierasch, L. M. (2015). How hsp70 molecular machines interact with their substrates to mediate diverse physiological functions. J Mol Biol, 427(7), 1575-1588. doi:10.1016/j.jmb.2015.02.004
- Connell, P., Ballinger, C. A., Jiang, J., Wu, Y., Thompson, L. J., Höhfeld, J., & Patterson, C. (2001). The co-chaperone CHIP regulates protein triage decisions mediated by heat-shock proteins. Nat Cell Biol, 3(1), 93-96. doi:10.1038/35050618
- Dayalan Naidu, S., Kostov, R. V., & Dinkova-Kostova, A. T. (2015). Transcription factors Hsf1 and

Nrf2 engage in crosstalk for cytoprotection. Trends Pharmacol Sci, 36(1), 6-14. doi:10.1016/j.tips.2014.10.011

- Delaglio, F., Grzesiek, S., Vuister, G. W., Zhu, G., Pfeifer, J., & Bax, A. (1995). NMRPipe: a multidimensional spectral processing system based on UNIX pipes. J Biomol NMR, 6(3), 277-293.
- Derjuga, A., Gourley, T. S., Holm, T. M., Heng, H. H., Shivdasani, R. A., Ahmed, R., . . . Blank, V. (2004). Complexity of CNC transcription factors as revealed by gene targeting of the Nrf3 locus. Mol Cell Biol, 24(8), 3286-3294. doi:10.1128/mcb.24.8.3286-3294.2004
- Deshmukh, P., Unni, S., Krishnappa, G., & Padmanabhan, B. (2017). The Keap1-Nrf2 pathway: promising therapeutic target to counteract ROS-mediated damage in cancers and neurodegenerative diseases. Biophys Rev, 9(1), 41-56. doi:10.1007/s12551-016-0244-4
- Dickey, C. A., Kamal, A., Lundgren, K., Klosak, N., Bailey, R. M., Dunmore, J., . . . Petrucelli, L. (2007). The high-affinity HSP90-CHIP complex recognizes and selectively degrades phosphorylated tau client proteins. J Clin Invest, 117(3), 648-658. doi:10.1172/JCI29715
- Ding, G., Chen, P., Zhang, H., Huang, X., Zang, Y., Li, J., & Wong, J. (2016). Regulation of Ubiquitin-like with Plant Homeodomain and RING Finger Domain 1 (UHRF1) Protein Stability by Heat Shock Protein 90 Chaperone Machinery. J Biol Chem, 291(38), 20125-20135. doi:10.1074/jbc.M116.727214
- Dinkova-Kostova, A. T., Fahey, J. W., Kostov, R. V., & Kensler, T. W. (2017). KEAP1 and Done?

Targeting the NRF2 Pathway with Sulforaphane. Trends Food Sci Technol, 69(Pt B), 257-269. doi:10.1016/j.tifs.2017.02.002

- Dinkova-Kostova, A. T., & Kazantsev, A. G. (2017). Activation of Nrf2 signaling as a common treatment of neurodegenerative diseases. Neurodegener Dis Manag, 7(2), 97-100. doi:10.2217/nmt-2017-0011
- Eggler, A. L., Liu, G., Pezzuto, J. M., van Breemen, R. B., & Mesecar, A. D. (2005). Modifying specific cysteines of the electrophile-sensing human Keap1 protein is insufficient to disrupt binding to the Nrf2 domain Neh2. Proc Natl Acad Sci U S A, 102(29), 10070-10075. doi:10.1073/pnas.0502402102
- Ehrlich, E. S., Wang, T., Luo, K., Xiao, Z., Niewiadomska, A. M., Martinez, T., . . . Yu, X. F. (2009). Regulation of Hsp90 client proteins by a Cullin5-RING E3 ubiquitin ligase. Proc Natl Acad Sci U S A, 106(48), 20330-20335. doi:10.1073/pnas.0810571106
- Enomoto, A., Itoh, K., Nagayoshi, E., Haruta, J., Kimura, T., O'Connor, T., . . . Yamamoto, M. (2001). High sensitivity of Nrf2 knockout mice to acetaminophen hepatotoxicity associated with decreased expression of ARE-regulated drug metabolizing enzymes and antioxidant genes. Toxicol Sci, 59(1), 169-177. doi:10.1093/toxsci/59.1.169
- Feldman, J. D., Tubergen, D. G., Pollock, E. M., & Unanue, E. R. (1972). Distribution of a macrophage-specific antigen. Cell Immunol, 5(2), 325-337. doi:10.1016/0008-8749(72)90058-5

- Frueh, D. P. (2014). Practical aspects of NMR signal assignment in larger and challenging proteins. Prog Nucl Magn Reson Spectrosc, 78, 47-75. doi:10.1016/j.pnmrs.2013.12.001
- Furukawa, M., & Xiong, Y. (2005). BTB protein Keap1 targets antioxidant transcription factor Nrf2 for ubiquitination by the Cullin 3-Roc1 ligase. Mol Cell Biol, 25(1), 162-171. doi:10.1128/MCB.25.1.162-171.2005
- Gell, D. A., Grant, R. P., & Mackay, J. P. (2012). The detection and quantitation of protein oligomerization. Adv Exp Med Biol, 747, 19-41. doi:10.1007/978-1-4614-3229-6_2
- Genest, O., Wickner, S., & Doyle, S. M. (2019). Hsp90 and Hsp70 chaperones: Collaborators in protein remodeling. J Biol Chem, 294(6), 2109-2120. doi:10.1074/jbc.REV118.002806
- Gibbs, E. B., Cook, E. C., & Showalter, S. A. (2017). Application of NMR to studies of intrinsically disordered proteins. Arch Biochem Biophys, 628, 57-70. doi:10.1016/j.abb.2017.05.008
- Gomez-Pastor, R., Burchfiel, E. T., & Thiele, D. J. (2018). Regulation of heat shock transcription factors and their roles in physiology and disease. Nat Rev Mol Cell Biol, 19(1), 4-19. doi:10.1038/nrm.2017.73
- Gonsalves, S. E., Moses, A. M., Razak, Z., Robert, F., & Westwood, J. T. (2011). Whole-genome analysis reveals that active heat shock factor binding sites are mostly associated with non-heat shock genes in Drosophila melanogaster. PLoS One, 6(1), e15934. doi:10.1371/journal.pone.0015934

- Guo, Y., Guettouche, T., Fenna, M., Boellmann, F., Pratt, W. B., Toft, D. O., . . . Voellmy, R. (2001). Evidence for a mechanism of repression of heat shock factor 1 transcriptional activity by a multichaperone complex. J Biol Chem, 276(49), 45791-45799. doi:10.1074/jbc.M105931200
- Hahn, J. S., Hu, Z., Thiele, D. J., & Iyer, V. R. (2004). Genome-wide analysis of the biology of stress responses through heat shock transcription factor. Mol Cell Biol, 24(12), 5249-5256. doi:10.1128/MCB.24.12.5249-5256.2004
- Hainzl, O., Lapina, M. C., Buchner, J., & Richter, K. (2009). The charged linker region is an important regulator of Hsp90 function. J Biol Chem, 284(34), 22559-22567. doi:10.1074/jbc.M109.031658
- Hartl, F. U., Bracher, A., & Hayer-Hartl, M. (2011). Molecular chaperones in protein folding and proteostasis. Nature, 475(7356), 324-332. doi:10.1038/nature10317
- Hartl, F. U., & Hayer-Hartl, M. (2009). Converging concepts of protein folding in vitro and in vivo. Nat Struct Mol Biol, 16(6), 574-581. doi:10.1038/nsmb.1591
- Hernández, M. P., Sullivan, W. P., & Toft, D. O. (2002). The assembly and intermolecular properties of the hsp70-Hop-hsp90 molecular chaperone complex. J Biol Chem, 277(41), 38294-38304. doi:10.1074/jbc.M206566200
- H.M. Berman, J. Westbrook, Z. Feng, G. Gilliland, T.N. Bhat, H. Weissig, I.N. Shindyalov, P.E. Bourne. (2000) The Protein Data Bank *Nucleic Acids Research*, 28: 235-242.

- Hulme, E. C., & Trevethick, M. A. (2010). Ligand binding assays at equilibrium: validation and interpretation. Br J Pharmacol, 161(6), 1219-1237. doi:10.1111/j.1476-5381.2009.00604.x
- Hunter, S. A., & Cochran, J. R. (2016). Cell-Binding Assays for Determining the Affinity of Protein-Protein Interactions: Technologies and Considerations. Methods Enzymol, 580, 21-44. doi:10.1016/bs.mie.2016.05.002
- Itoh, K., Wakabayashi, N., Katoh, Y., Ishii, T., Igarashi, K., Engel, J. D., & Yamamoto, M. (1999). Keap1 represses nuclear activation of antioxidant responsive elements by Nrf2 through binding to the amino-terminal Neh2 domain. Genes Dev, 13(1), 76-86. doi:10.1101/gad.13.1.76
- Jahn, M., Rehn, A., Pelz, B., Hellenkamp, B., Richter, K., Rief, M., . . . Hugel, T. (2014). The charged linker of the molecular chaperone Hsp90 modulates domain contacts and biological function. Proc Natl Acad Sci U S A, 111(50), 17881-17886. doi:10.1073/pnas.1414073111
- Jahn, M., Tych, K., Girstmair, H., Steinmaßl, M., Hugel, T., Buchner, J., & Rief, M. (2018). Folding and Domain Interactions of Three Orthologs of Hsp90 Studied by Single-Molecule Force Spectroscopy. Structure, 26(1), 96-105.e104. doi:10.1016/j.str.2017.11.023
- Jellinger, K. A. (2003). General aspects of neurodegeneration. J Neural Transm Suppl(65), 101-144.
- Jellinger, K. A. (2010). Basic mechanisms of neurodegeneration: a critical update. J Cell Mol Med, 14(3), 457-487. doi:10.1111/j.1582-4934.2010.01010.x
- Jiang, Y., & Kalodimos, C. G. (2017). NMR Studies of Large Proteins. J Mol Biol, 429(17), 2667-

2676. doi:10.1016/j.jmb.2017.07.007

- Johnson, B. A. (2018). From Raw Data to Protein Backbone Chemical Shifts Using NMRFx Processing and NMRViewJ Analysis. Methods Mol Biol, 1688, 257-310. doi:10.1007/978-1-4939-7386-6_13
- Johnson, D. A., Amirahmadi, S., Ward, C., Fabry, Z., & Johnson, J. A. (2010). The absence of the pro-antioxidant transcription factor Nrf2 exacerbates experimental autoimmune encephalomyelitis. Toxicol Sci, 114(2), 237-246. doi:10.1093/toxsci/kfp274
- Johnson, D. A., & Johnson, J. A. (2015). Nrf2--a therapeutic target for the treatment of neurodegenerative diseases. Free Radic Biol Med, 88(Pt B), 253-267. doi:10.1016/j.freeradbiomed.2015.07.147
- Joshi, G., Gan, K. A., Johnson, D. A., & Johnson, J. A. (2015). Increased Alzheimer's disease-like pathology in the APP/ PS1ΔE9 mouse model lacking Nrf2 through modulation of autophagy. Neurobiol Aging, 36(2), 664-679. doi:10.1016/j.neurobiolaging.2014.09.004
- Kaiser, C. M., Chang, H. C., Agashe, V. R., Lakshmipathy, S. K., Etchells, S. A., Hayer-Hartl, M., . . . Barral, J. M. (2006). Real-time observation of trigger factor function on translating ribosomes. Nature, 444(7118), 455-460. doi:10.1038/nature05225
- Kang, M. I., Kobayashi, A., Wakabayashi, N., Kim, S. G., & Yamamoto, M. (2004). Scaffolding of Keap1 to the actin cytoskeleton controls the function of Nrf2 as key regulator of cytoprotective

phase 2 genes. Proc Natl Acad Sci U S A, 101(7), 2046-2051. doi:10.1073/pnas.0308347100

- Kanninen, K., Malm, T. M., Jyrkkänen, H. K., Goldsteins, G., Keksa-Goldsteine, V., Tanila, H., . . . Koistinaho, J. (2008). Nuclear factor erythroid 2-related factor 2 protects against beta amyloid. Mol Cell Neurosci, 39(3), 302-313. doi:10.1016/j.mcn.2008.07.010
- Karagöz, G. E., Duarte, A. M., Akoury, E., Ippel, H., Biernat, J., Morán Luengo, T., . . . Rüdiger, S. G. (2014). Hsp90-Tau complex reveals molecular basis for specificity in chaperone action. Cell, 156(5), 963-974. doi:10.1016/j.cell.2014.01.037
- Kensler, T. W., & Wakabayashi, N. (2010). Nrf2: friend or foe for chemoprevention? Carcinogenesis, 31(1), 90-99. doi:10.1093/carcin/bgp231
- Kerr, J. S., Adriaanse, B. A., Greig, N. H., Mattson, M. P., Cader, M. Z., Bohr, V. A., & Fang, E. F. (2017). Mitophagy and Alzheimer's Disease: Cellular and Molecular Mechanisms. Trends Neurosci, 40(3), 151-166. doi:10.1016/j.tins.2017.01.002
- Khan, H., Cino, E. A., Brickenden, A., Fan, J., Yang, D., & Choy, W. Y. (2013). Fuzzy complex formation between the intrinsically disordered prothymosin α and the Kelch domain of Keap1 involved in the oxidative stress response. J Mol Biol, 425(6), 1011-1027. doi:10.1016/j.jmb.2013.01.005
- Khan, H., Killoran, R. C., Brickenden, A., Fan, J., Yang, D., & Choy, W. Y. (2015). Molecular effects of cancer-associated somatic mutations on the structural and target recognition properties of

Keap1. Biochem J, 467(1), 141-151. doi:10.1042/BJ20140761

- Khanam, H., Ali, A., Asif, M., & Shamsuzzaman. (2016). Neurodegenerative diseases linked to misfolded proteins and their therapeutic approaches: A review. Eur J Med Chem, 124, 1121-1141. doi:10.1016/j.ejmech.2016.08.006
- Khor, T. O., Huang, M. T., Kwon, K. H., Chan, J. Y., Reddy, B. S., & Kong, A. N. (2006). Nrf2-deficient mice have an increased susceptibility to dextran sulfate sodium-induced colitis. Cancer Res, 66(24), 11580-11584. doi:10.1158/0008-5472.CAN-06-3562
- Kim, Y. E., Hipp, M. S., Bracher, A., Hayer-Hartl, M., & Hartl, F. U. (2013). Molecular chaperone functions in protein folding and proteostasis. Annu Rev Biochem, 82, 323-355. doi:10.1146/annurev-biochem-060208-092442
- Kirschke, E., Goswami, D., Southworth, D., Griffin, P. R., & Agard, D. A. (2014). Glucocorticoid receptor function regulated by coordinated action of the Hsp90 and Hsp70 chaperone cycles. Cell, 157(7), 1685-1697. doi:10.1016/j.cell.2014.04.038
- Kobayashi, A., Kang, M. I., Okawa, H., Ohtsuji, M., Zenke, Y., Chiba, T., . . . Yamamoto, M. (2004). Oxidative stress sensor Keap1 functions as an adaptor for Cul3-based E3 ligase to regulate proteasomal degradation of Nrf2. Mol Cell Biol, 24(16), 7130-7139. doi:10.1128/MCB.24.16.7130-7139.2004
- Kobayashi, A., Ohta, T., & Yamamoto, M. (2004). Unique function of the Nrf2-Keap1 pathway in

the inducible expression of antioxidant and detoxifying enzymes. Methods Enzymol, 378, 273-286. doi:10.1016/S0076-6879(04)78021-0

- Kobayashi, M., & Yamamoto, M. (2006). Nrf2-Keap1 regulation of cellular defense mechanisms against electrophiles and reactive oxygen species. Adv Enzyme Regul, 46, 113-140. doi:10.1016/j.advenzreg.2006.01.007
- Koh, J. Y., Yang, L. L., & Cotman, C. W. (1990). Beta-amyloid protein increases the vulnerability of cultured cortical neurons to excitotoxic damage. Brain Res, 533(2), 315-320. doi:10.1016/0006-8993(90)91355-k
- Kraft, A. D., Johnson, D. A., & Johnson, J. A. (2004). Nuclear factor E2-related factor 2-dependent antioxidant response element activation by tert-butylhydroquinone and sulforaphane occurring preferentially in astrocytes conditions neurons against oxidative insult. J Neurosci, 24(5), 1101-1112. doi:10.1523/JNEUROSCI.3817-03.2004
- Kundrat, L., & Regan, L. (2010). Balance between folding and degradation for Hsp90-dependent client proteins: a key role for CHIP. Biochemistry, 49(35), 7428-7438. doi:10.1021/bi100386w
- Lackie, R. E., Maciejewski, A., Ostapchenko, V. G., Marques-Lopes, J., Choy, W. Y., Duennwald, M. L., . . . Prado, M. A. M. (2017). The Hsp70/Hsp90 Chaperone Machinery in Neurodegenerative Diseases. Front Neurosci, 11, 254. doi:10.3389/fnins.2017.00254
- Lakshmipathy, S. K., Tomic, S., Kaiser, C. M., Chang, H. C., Genevaux, P., Georgopoulos, C., . . .

Etchells, S. A. (2007). Identification of nascent chain interaction sites on trigger factor. J Biol Chem, 282(16), 12186-12193. doi:10.1074/jbc.M609871200

- Laskey, R. A., Honda, B. M., Mills, A. D., & Finch, J. T. (1978). Nucleosomes are assembled by an acidic protein which binds histones and transfers them to DNA. Nature, 275(5679), 416-420. doi:10.1038/275416a0
- Lau, A., Villeneuve, N. F., Sun, Z., Wong, P. K., & Zhang, D. D. (2008). Dual roles of Nrf2 in cancer. Pharmacol Res, 58(5-6), 262-270. doi:10.1016/j.phrs.2008.09.003
- Lavery, L. A., Partridge, J. R., Ramelot, T. A., Elnatan, D., Kennedy, M. A., & Agard, D. A. (2014). Structural asymmetry in the closed state of mitochondrial Hsp90 (TRAP1) supports a two-step ATP hydrolysis mechanism. Mol Cell, 53(2), 330-343. doi:10.1016/j.molcel.2013.12.023
- Li, J., & Buchner, J. (2013). Structure, function and regulation of the hsp90 machinery. Biomed J, 36(3), 106-117. doi:10.4103/2319-4170.113230
- Linker, R. A., Lee, D. H., Ryan, S., van Dam, A. M., Conrad, R., Bista, P., . . . Gold, R. (2011). Fumaric acid esters exert neuroprotective effects in neuroinflammation via activation of the Nrf2 antioxidant pathway. Brain, 134(Pt 3), 678-692. doi:10.1093/brain/awq386
- Longshaw, V. M., Chapple, J. P., Balda, M. S., Cheetham, M. E., & Blatch, G. L. (2004). Nuclear translocation of the Hsp70/Hsp90 organizing protein mSTI1 is regulated by cell cycle kinases. J Cell Sci, 117(Pt 5), 701-710. doi:10.1242/jcs.00905

- Lorenz, O. R., Freiburger, L., Rutz, D. A., Krause, M., Zierer, B. K., Alvira, S., . . . Buchner, J. (2014). Modulation of the Hsp90 chaperone cycle by a stringent client protein. Mol Cell, 53(6), 941-953. doi:10.1016/j.molcel.2014.02.003
- Maciejewski, A., Ostapchenko, V. G., Beraldo, F. H., Prado, V. F., Prado, M. A., & Choy, W. Y. (2016). Domains of STIP1 responsible for regulating PrPC-dependent amyloid-β oligomer toxicity. Biochem J, 473(14), 2119-2130. doi:10.1042/BCJ20160087
- Maciejewski, A., Prado, M. A., & Choy, W. Y. (2013). ^{1}H, ^{15}N and ^{13}C backbone resonance assignments of the TPR1 and TPR2A domains of mouse STI1. Biomol NMR Assign, 7(2), 305-310. doi:10.1007/s12104-012-9433-7
- Maciejewski, A., Prado, V. F., Prado, M. A. M., & Choy, W. Y. (2017). Molecular basis for the interaction between stress-inducible phosphoprotein 1 (STIP1) and S100A1. Biochem J, 474(11), 1853-1866. doi:10.1042/BCJ20161055
- Manjarrez, J. R., Sun, L., Prince, T., & Matts, R. L. (2014). Hsp90-dependent assembly of the DBC2/RhoBTB2-Cullin3 E3-ligase complex. PLoS One, 9(3), e90054. doi:10.1371/journal.pone.0090054
- Martins-Silva, C., De Jaeger, X., Guzman, M. S., Lima, R. D., Santos, M. S., Kushmerick, C., . . . Prado, V. F. (2011). Novel strains of mice deficient for the vesicular acetylcholine transporter: insights on transcriptional regulation and control of locomotor behavior. PLoS One, 6(3), e17611.

doi:10.1371/journal.pone.0017611

- Mayer, M. P. (2013). Hsp70 chaperone dynamics and molecular mechanism. Trends Biochem Sci, 38(10), 507-514. doi:10.1016/j.tibs.2013.08.001
- Mayer, M. P., Rüdiger, S., & Bukau, B. (2000). Molecular basis for interactions of the DnaK chaperone with substrates. Biol Chem, 381(9-10), 877-885. doi:10.1515/BC.2000.109
- McMahon, M., Thomas, N., Itoh, K., Yamamoto, M., & Hayes, J. D. (2004). Redox-regulated turnover of Nrf2 is determined by at least two separate protein domains, the redox-sensitive Neh2 degron and the redox-insensitive Neh6 degron. J Biol Chem, 279(30), 31556-31567. doi:10.1074/jbc.M403061200
- Merz, F., Boehringer, D., Schaffitzel, C., Preissler, S., Hoffmann, A., Maier, T., . . . Deuerling, E. (2008). Molecular mechanism and structure of Trigger Factor bound to the translating ribosome. EMBO J, 27(11), 1622-1632. doi:10.1038/emboj.2008.89
- Merz, F., Hoffmann, A., Rutkowska, A., Zachmann-Brand, B., Bukau, B., & Deuerling, E. (2006). The C-terminal domain of Escherichia coli trigger factor represents the central module of its chaperone activity. J Biol Chem, 281(42), 31963-31971. doi:10.1074/jbc.M605164200
- Meyer, B., & Peters, T. (2003). NMR spectroscopy techniques for screening and identifying ligand binding to protein receptors. Angew Chem Int Ed Engl, 42(8), 864-890. doi:10.1002/anie.200390233

- Miller, K. P., & Ramos, K. S. (2005). DNA sequence determinants of nuclear protein binding to the c-Ha-ras antioxidant/electrophile response element in vascular smooth muscle cells: identification of Nrf2 and heat shock protein 90 beta as heterocomplex components. Cell Stress Chaperones, 10(2), 114-125. doi:10.1379/csc-73r.1
- Mitsuishi, Y., Motohashi, H., & Yamamoto, M. (2012). The Keap1-Nrf2 system in cancers: stress response and anabolic metabolism. Front Oncol, 2, 200. doi:10.3389/fonc.2012.00200
- Moi, P., Chan, K., Asunis, I., Cao, A., & Kan, Y. W. (1994). Isolation of NF-E2-related factor 2 (Nrf2), a NF-E2-like basic leucine zipper transcriptional activator that binds to the tandem NF-E2/AP1 repeat of the beta-globin locus control region. Proc Natl Acad Sci U S A, 91(21), 9926-9930. doi:10.1073/pnas.91.21.9926
- Motohashi, H., O'Connor, T., Katsuoka, F., Engel, J. D., & Yamamoto, M. (2002). Integration and diversity of the regulatory network composed of Maf and CNC families of transcription factors. Gene, 294(1-2), 1-12. doi:10.1016/s0378-1119(02)00788-6
- Muchowski, P. J., Schaffar, G., Sittler, A., Wanker, E. E., Hayer-Hartl, M. K., & Hartl, F. U. (2000). Hsp70 and hsp40 chaperones can inhibit self-assembly of polyglutamine proteins into amyloid-like fibrils. Proc Natl Acad Sci U S A, 97(14), 7841-7846. doi:10.1073/pnas.140202897
- Neef, D. W., Turski, M. L., & Thiele, D. J. (2010). Modulation of heat shock transcription factor 1 as a therapeutic target for small molecule intervention in neurodegenerative disease. PLoS Biol,

8(1), e1000291. doi:10.1371/journal.pbio.1000291

- Neymotin, A., Calingasan, N. Y., Wille, E., Naseri, N., Petri, S., Damiano, M., . . . Kiaei, M. (2011). Neuroprotective effect of Nrf2/ARE activators, CDDO ethylamide and CDDO trifluoroethylamide, in a mouse model of amyotrophic lateral sclerosis. Free Radic Biol Med, 51(1), 88-96. doi:10.1016/j.freeradbiomed.2011.03.027
- Nioi, P., Nguyen, T., Sherratt, P. J., & Pickett, C. B. (2005). The carboxy-terminal Neh3 domain of Nrf2 is required for transcriptional activation. Mol Cell Biol, 25(24), 10895-10906. doi:10.1128/MCB.25.24.10895-10906.2005
- Nollen, E. A., Garcia, S. M., van Haaften, G., Kim, S., Chavez, A., Morimoto, R. I., & Plasterk, R. H. (2004). Genome-wide RNA interference screen identifies previously undescribed regulators of polyglutamine aggregation. Proc Natl Acad Sci U S A, 101(17), 6403-6408. doi:10.1073/pnas.0307697101
- Ogura, T., Tong, K. I., Mio, K., Maruyama, Y., Kurokawa, H., Sato, C., & Yamamoto, M. (2010). Keap1 is a forked-stem dimer structure with two large spheres enclosing the intervening, double glycine repeat, and C-terminal domains. Proc Natl Acad Sci U S A, 107(7), 2842-2847. doi:10.1073/pnas.0914036107
- Ostapchenko, V. G., Beraldo, F. H., Mohammad, A. H., Xie, Y. F., Hirata, P. H., Magalhaes, A. C., . . . Prado, M. A. (2013). The prion protein ligand, stress-inducible phosphoprotein 1, regulates

amyloid-β oligomer toxicity. J Neurosci, 33(42), 16552-16564. doi:10.1523/JNEUROSCI.3214-13.2013

- Pareek, T. K., Belkadi, A., Kesavapany, S., Zaremba, A., Loh, S. L., Bai, L., . . . Letterio, J. J. (2011). Triterpenoid modulation of IL-17 and Nrf-2 expression ameliorates neuroinflammation and promotes remyelination in autoimmune encephalomyelitis. Sci Rep, 1, 201. doi:10.1038/srep00201
- Pehar, M., Vargas, M. R., Robinson, K. M., Cassina, P., Díaz-Amarilla, P. J., Hagen, T. M., . . . Beckman, J. S. (2007). Mitochondrial superoxide production and nuclear factor erythroid 2-related factor 2 activation in p75 neurotrophin receptor-induced motor neuron apoptosis. J Neurosci, 27(29), 7777-7785. doi:10.1523/JNEUROSCI.0823-07.2007
- Picard, D. (2006). Intracellular dynamics of the Hsp90 co-chaperone p23 is dictated by Hsp90. Exp Cell Res, 312(2), 198-204. doi:10.1016/j.yexcr.2005.10.009
- Pike, C. J., Walencewicz, A. J., Glabe, C. G., & Cotman, C. W. (1991). In vitro aging of beta-amyloid protein causes peptide aggregation and neurotoxicity. Brain Res, 563(1-2), 311-314. doi:10.1016/0006-8993(91)91553-d
- Pratt, W. B., Gestwicki, J. E., Osawa, Y., & Lieberman, A. P. (2015). Targeting Hsp90/Hsp70-based protein quality control for treatment of adult onset neurodegenerative diseases. Annu Rev Pharmacol Toxicol, 55, 353-371. doi:10.1146/annurev-pharmtox-010814-124332
- Prince, T. L., Kijima, T., Tatokoro, M., Lee, S., Tsutsumi, S., Yim, K., . . . Neckers, L. (2015).

Client Proteins and Small Molecule Inhibitors Display Distinct Binding Preferences for Constitutive and Stress-Induced HSP90 Isoforms and Their Conformationally Restricted Mutants. PLoS One, 10(10), e0141786. doi:10.1371/journal.pone.0141786

- Prodromou, C. (2017). Regulatory Mechanisms of Hsp90. Biochem Mol Biol J, 3(1), 2. doi:10.21767/2471-8084.100030
- Quinti, L., Dayalan Naidu, S., Träger, U., Chen, X., Kegel-Gleason, K., Llères, D., . . . Kazantsev, A. G. (2017). KEAP1-modifying small molecule reveals muted NRF2 signaling responses in neural stem cells from Huntington's disease patients. Proc Natl Acad Sci U S A, 114(23), E4676-E4685. doi:10.1073/pnas.1614943114
- Radli, M., Veprintsev, D. B., & Rüdiger, S. G. D. (2017). Production and purification of human Hsp90β in Escherichia coli. PLoS One, 12(6), e0180047. doi:10.1371/journal.pone.0180047
- Ramsey, C. P., Glass, C. A., Montgomery, M. B., Lindl, K. A., Ritson, G. P., Chia, L. A., . . . Jordan-Sciutto, K. L. (2007). Expression of Nrf2 in neurodegenerative diseases. J Neuropathol Exp Neurol, 66(1), 75-85. doi:10.1097/nen.0b013e31802d6da9
- Razzaq, Abdul (2018). Role of STIP1 in TDP-43 Mediated Toxicity and Proteinopathy in Neurodegenerative Disorders . *Electronic Thesis and Dissertation Repository*. 5442. https://ir.lib.uwo.ca/etd/5442
- Reis, S. D., Pinho, B. R., & Oliveira, J. M. A. (2017). Modulation of Molecular Chaperones in

Huntington's Disease and Other Polyglutamine Disorders. Mol Neurobiol, 54(8), 5829-5854. doi:10.1007/s12035-016-0120-z

- Rosenthal, H. E. (1967). A graphic method for the determination and presentation of binding parameters in a complex system. Anal Biochem, 20(3), 525-532. doi:10.1016/0003-2697(67)90297-7
- Rushmore, T. H., Morton, M. R., & Pickett, C. B. (1991). The antioxidant responsive element. Activation by oxidative stress and identification of the DNA consensus sequence required for functional activity. J Biol Chem, 266(18), 11632-11639.
- Rushmore, T. H., & Pickett, C. B. (1990). Transcriptional regulation of the rat glutathione S-transferase Ya subunit gene. Characterization of a xenobiotic-responsive element controlling inducible expression by phenolic antioxidants. J Biol Chem, 265(24), 14648-14653.
- Röhl, A., Wengler, D., Madl, T., Lagleder, S., Tippel, F., Herrmann, M., . . . Buchner, J. (2015). Hsp90 regulates the dynamics of its cochaperone Sti1 and the transfer of Hsp70 between modules. Nat Commun, 6, 6655. doi:10.1038/ncomms7655
- Saibil, H. (2013). Chaperone machines for protein folding, unfolding and disaggregation. Nat Rev Mol Cell Biol, 14(10), 630-642. doi:10.1038/nrm3658
- Saito, R., Suzuki, T., Hiramoto, K., Asami, S., Naganuma, E., Suda, H., . . . Yamamoto, M. (2016). Characterizations of Three Major Cysteine Sensors of Keap1 in Stress Response. Mol Cell Biol,

36(2), 271-284. doi:10.1128/MCB.00868-15

- Sambrook, J., & Russell, D. W. (2006). Preparation and Transformation of Competent E. coli Using Calcium Chloride. CSH Protoc, 2006(1). doi:10.1101/pdb.prot3932
- Satoh, T., Rezaie, T., Seki, M., Sunico, C. R., Tabuchi, T., Kitagawa, T., . . . Lipton, S. A. (2011). Dual neuroprotective pathways of a pro-electrophilic compound via HSF-1-activated heat-shock proteins and Nrf2-activated phase 2 antioxidant response enzymes. J Neurochem, 119(3), 569-578. doi:10.1111/j.1471-4159.2011.07449.x
- Scheufler, C., Brinker, A., Bourenkov, G., Pegoraro, S., Moroder, L., Bartunik, H., . . . Moarefi, I. (2000). Structure of TPR domain-peptide complexes: critical elements in the assembly of the Hsp70-Hsp90 multichaperone machine. Cell, 101(2), 199-210. doi:10.1016/S0092-8674(00)80830-2.
- Schopf, F. H., Biebl, M. M., & Buchner, J. (2017). The HSP90 chaperone machinery. Nat Rev Mol Cell Biol, 18(6), 345-360. doi:10.1038/nrm.2017.20
- Sekhar, K. R., Yan, X. X., & Freeman, M. L. (2002). Nrf2 degradation by the ubiquitin proteasome pathway is inhibited by KIAA0132, the human homolog to INrf2. Oncogene, 21(44), 6829-6834. doi:10.1038/sj.onc.1205905
- Sethi, R., Krojer, T., Bountra, C., Arrowsmith, C.H., Edwards, A.M., Bullock, A.N., von Delft, F., Structural Genomics Consortium (SGC)) (2019). Crystal Structure of the KELCH domain of

human KEAP1. TO BE PUBLISHED. 10.2210/PDB6ROG/PDB

- Shiau, A. K., Harris, S. F., Southworth, D. R., & Agard, D. A. (2006). Structural Analysis of E. coli hsp90 reveals dramatic nucleotide-dependent conformational rearrangements. Cell, 127(2), 329-340. doi:10.1016/j.cell.2006.09.027
- Sittler, A., Lurz, R., Lueder, G., Priller, J., Lehrach, H., Hayer-Hartl, M. K., . . . Wanker, E. E. (2001). Geldanamycin activates a heat shock response and inhibits huntingtin aggregation in a cell culture model of Huntington's disease. Hum Mol Genet, 10(12), 1307-1315. doi:10.1093/hmg/10.12.1307
- Soares, I. N., Caetano, F. A., Pinder, J., Rodrigues, B. R., Beraldo, F. H., Ostapchenko, V. G., . . . Prado, M. A. (2013). Regulation of stress-inducible phosphoprotein 1 nuclear retention by protein inhibitor of activated STAT PIAS1. Mol Cell Proteomics, 12(11), 3253-3270. doi:10.1074/mcp.M113.031005
- Sreedhar, A. S., Kalmár, E., Csermely, P., & Shen, Y. F. (2004). Hsp90 isoforms: functions, expression and clinical importance. FEBS Lett, 562(1-3), 11-15. doi:10.1016/s0014-5793(04)00229-7
- Stack, C., Ho, D., Wille, E., Calingasan, N. Y., Williams, C., Liby, K., . . . Beal, M. F. (2010). Triterpenoids CDDO-ethyl amide and CDDO-trifluoroethyl amide improve the behavioral phenotype and brain pathology in a transgenic mouse model of Huntington's disease. Free Radic

Biol Med, 49(2), 147-158. doi:10.1016/j.freeradbiomed.2010.03.017

- Sun, Z., Wu, T., Zhao, F., Lau, A., Birch, C. M., & Zhang, D. D. (2011). KPNA6 (Importin {alpha}7)-mediated nuclear import of Keap1 represses the Nrf2-dependent antioxidant response. Mol Cell Biol, 31(9), 1800-1811. doi:10.1128/MCB.05036-11
- Sung, N., Lee, J., Kim, J. H., Chang, C., Tsai, F. T., & Lee, S. (2016). 2.4 Å resolution crystal structure of human TRAP1NM, the Hsp90 paralog in the mitochondrial matrix. Acta Crystallogr D Struct Biol, 72(Pt 8), 904-911. doi:10.1107/S2059798316009906
- Taguchi, K., Motohashi, H., & Yamamoto, M. (2011). Molecular mechanisms of the Keap1–Nrf2 pathway in stress response and cancer evolution. Genes Cells, 16(2), 123-140. doi:10.1111/j.1365-2443.2010.01473.x
- Taipale, M., Krykbaeva, I., Koeva, M., Kayatekin, C., Westover, K. D., . . . Lindquist, S. (2012). Quantitative analysis of HSP90 – client interactions reveals principles of substrate recognition. Cell, 150 (5), 987 – 1001. doi: 10.1016/j.cell.2012.06.047
- Taipale, M., Tucker, G., Peng, J., Krykbaeva, I., Lin, Z. Y., Larsen, B., . . . Lindquist, S. (2014). A quantitative chaperone interaction network reveals the architecture of cellular protein homeostasis pathways. Cell, 158(2), 434-448. doi:10.1016/j.cell.2014.05.039
- Takahashi, Y., Kobayashi, Y., Kawata, K., Kawamura, K., Sumiyoshi, S., Noritake, H., . . . Suda, T. (2014). Does hepatic oxidative stress enhance activation of nuclear factor-E2-related factor in

patients with nonalcoholic steatohepatitis? Antioxid Redox Signal, 20(3), 538-543. doi:10.1089/ars.2013.5470

- Tang, Y. C., Chang, H. C., Hayer-Hartl, M., & Hartl, F. U. (2007). SnapShot: molecular chaperones, Part II. Cell, 128(2), 412. doi:10.1016/j.cell.2007.01.013
- Tong, K. I., Katoh, Y., Kusunoki, H., Itoh, K., Tanaka, T., & Yamamoto, M. (2006). Keap1 recruits Neh2 through binding to ETGE and DLG motifs: characterization of the two-site molecular recognition model. Mol Cell Biol, 26(8), 2887-2900. doi:10.1128/MCB.26.8.2887-2900.2006
- Tong, K. I., Kobayashi, A., Katsuoka, F., & Yamamoto, M. (2006). Two-site substrate recognition model for the Keap1-Nrf2 system: a hinge and latch mechanism. Biol Chem, 387(10-11), 1311-1320. doi:10.1515/BC.2006.164
- Trinklein, N. D., Murray, J. I., Hartman, S. J., Botstein, D., & Myers, R. M. (2004). The role of heat shock transcription factor 1 in the genome-wide regulation of the mammalian heat shock response. Mol Biol Cell, 15(3), 1254-1261. doi:10.1091/mbc.e03-10-0738
- Tsutsumi, S., Mollapour, M., Graf, C., Lee, C. T., Scroggins, B. T., Xu, W., . . . Neckers, L. (2009). Hsp90 charged-linker truncation reverses the functional consequences of weakened hydrophobic contacts in the N domain. Nat Struct Mol Biol, 16(11), 1141-1147. doi:10.1038/nsmb.1682
- Tufekci, K. U., Civi Bayin, E., Genc, S., & Genc, K. (2011). The Nrf2/ARE Pathway: A Promising Target to Counteract Mitochondrial Dysfunction in Parkinson's Disease. Parkinsons Dis, 2011,

314082. doi:10.4061/2011/314082

- Verba, K. A., Wang, R. Y., Arakawa, A., Liu, Y., Shirouzu, M., Yokoyama, S., & Agard, D. A. (2016). Atomic structure of Hsp90-Cdc37-Cdk4 reveals that Hsp90 traps and stabilizes an unfolded kinase. Science, 352(6293), 1542-1547. doi:10.1126/science.aaf5023
- Wakabayashi, N., Slocum, S. L., Skoko, J. J., Shin, S., & Kensler, T. W. (2010). When NRF2 talks, who's listening? Antioxid Redox Signal, 13(11), 1649-1663. doi:10.1089/ars.2010.3216
- Walsh, D. M., & Selkoe, D. J. (2007). A beta oligomers - a decade of discovery. J Neurochem, 101(5), 1172-1184. doi:10.1111/j.1471-4159.2006.04426.x
- Wang, H., Liu, K., Geng, M., Gao, P., Wu, X., Hai, Y., . . . Tang, X. (2013). RXRα inhibits the NRF2-ARE signaling pathway through a direct interaction with the Neh7 domain of NRF2. Cancer Res, 73(10), 3097-3108. doi:10.1158/0008-5472.CAN-12-3386
- Wilhelmus, M. M., de Waal, R. M., & Verbeek, M. M. (2007). Heat shock proteins and amateur chaperones in amyloid-Beta accumulation and clearance in Alzheimer's disease. Mol Neurobiol, 35(3), 203-216.
- Winkler, J., Tyedmers, J., Bukau, B., & Mogk, A. (2012a). Chaperone networks in protein disaggregation and prion propagation. J Struct Biol, 179(2), 152-160. doi:10.1016/j.jsb.2012.05.002
- Xu, C., Huang, M. T., Shen, G., Yuan, X., Lin, W., Khor, T. O., . . . Kong, A. N. (2006). Inhibition of 7,12-dimethylbenz(a)anthracene-induced skin tumorigenesis in C57BL/6 mice by sulforaphane

is mediated by nuclear factor E2-related factor 2. Cancer Res, 66(16), 8293-8296. doi:10.1158/0008-5472.CAN-06-0300

- Xu, C., Yuan, X., Pan, Z., Shen, G., Kim, J. H., Yu, S., . . . Kong, A. N. (2006). Mechanism of action of isothiocyanates: the induction of ARE-regulated genes is associated with activation of ERK and JNK and the phosphorylation and nuclear translocation of Nrf2. Mol Cancer Ther, 5(8), 1918-1926. doi:10.1158/1535-7163.MCT-05-0497
- Xu, W., Marcu, M., Yuan, X., Mimnaugh, E., Patterson, C., & Neckers, L. (2002). Chaperone-dependent E3 ubiquitin ligase CHIP mediates a degradative pathway for c-ErbB2/Neu. Proc Natl Acad Sci U S A, 99(20), 12847-12852. doi:10.1073/pnas.202365899
- Yankner, B. A., Dawes, L. R., Fisher, S., Villa-Komaroff, L., Oster-Granite, M. L., & Neve, R. L. (1989). Neurotoxicity of a fragment of the amyloid precursor associated with Alzheimer's disease. Science, 245(4916), 417-420. doi:10.1126/science.2474201
- Youdim, M. B., & Buccafusco, J. J. (2005). Multi-functional drugs for various CNS targets in the treatment of neurodegenerative disorders. Trends Pharmacol Sci, 26(1), 27-35. doi:10.1016/j.tips.2004.11.007
- Zhang, D. D., & Hannink, M. (2003). Distinct cysteine residues in Keap1 are required for Keap1-dependent ubiquitination of Nrf2 and for stabilization of Nrf2 by chemopreventive agents and oxidative stress. Mol Cell Biol, 23(22), 8137-8151. doi:10.1128/mcb.23.22.8137-8151.2003

- Zhang, M., An, C., Gao, Y., Leak, R. K., Chen, J., & Zhang, F. (2013a). Emerging roles of Nrf2 and phase II antioxidant enzymes in neuroprotection. Prog Neurobiol, 100, 30-47. doi:10.1016/j.pneurobio.2012.09.003
- Zhang, M., An, C., Gao, Y., Leak, R. K., Chen, J., & Zhang, F. (2013b). Emerging roles of Nrf2 and phase II antioxidant enzymes in neuroprotection. Prog Neurobiol, 100, 30-47. doi:10.1016/j.pneurobio.2012.09.003
- Zhang, M., An, C., Gao, Y., Leak, R. K., Chen, J., & Zhang, F. (2013c). Emerging roles of Nrf2 and phase II antioxidant enzymes in neuroprotection. Prog Neurobiol, 100, 30-47. doi:10.1016/j.pneurobio.2012.09.003
- Zhang, Q., & Denlinger, D. L. (2010). Molecular characterization of heat shock protein 90, 70 and 70 cognate cDNAs and their expression patterns during thermal stress and pupal diapause in the corn earworm. J Insect Physiol, 56(2), 138-150. doi:10.1016/j.jinsphys.2009.09.013
- Zhang, Y., Dayalan Naidu, S., Samarasinghe, K., Van Hecke, G. C., Pheely, A., Boronina, T. N., . . . Dinkova-Kostova, A. T. (2014). Sulphoxythiocarbamates modify cysteine residues in HSP90 causing degradation of client proteins and inhibition of cancer cell proliferation. Br J Cancer, 110(1), 71-82. doi:10.1038/bjc.2013.710
- Zipper, L. M., & Mulcahy, R. T. (2002). The Keap1 BTB/POZ dimerization function is required to sequester Nrf2 in cytoplasm. J Biol Chem, 277(39), 36544-36552. doi:10.1074/jbc.M206530200

- Zuehlke, A. D., & Neckers, L. (2017). Out with the old: Hsp90 finds amino acid residue more useful than co-chaperone protein. Microb Cell, 4(8), 273-274. doi:10.15698/mic2017.08.586

Curriculum Vitae

Name:	Zheng Song
Post-secondary Education and Degrees:	The University of Toronto Toronto, Ontario, Canada 2012 - 2017 HBSc. Honors Health and Diseases
	The University of Western Ontario London, Ontario, Canada 2017 - 2019 MSc Candidate Biochemistry
Related Work Experience	Research Assistant The University of Toronto 2015 – 2017